Les effets de la répartition non-uniforme des fibres sur la propagation des fissures á l'interface fibre/matrice dans les matériaux composites

Linqi Zhuang

UNIVERSITÉ DE LORRAINE

Ecole doctorale EMMA

THÈSE

Pour l'obtention du titre de:

DOCTEUR de L'UNIVERSITÉ DE LORRAINE

Spécialité: Mécanique des Matériaux (Composites)

Présentée par :

Linqi Zhuang

Les effets de la répartition non-uniforme des fibres sur la propagation des fissures á l'interface fibre/matrice dans les matériaux composites

---

Thèse soutenue publiquement le 24 mai 2017 à Luleå (Suède) devant le jury suivant :

Prof. Paris Federico	University of Seville, Spain	**Rapporteur**
Prof. Yves Berthaud	Université Pierre et Marie Curie, France	**Rapporteur**
Prof. Daghia Federica	Endommagement et rupture des composites sous solicitations mécaniques et environnementale Ecole Normale supérieure de Cachan, France	**Examinateur**
Prof. Zoubir Ayadi	Département Science et Ingénierie des Matériaux et Métallurgie-IJL, Université de Lorraine, Nancy, France	**Directeur de thèse**
Prof. Janis Varna	Department of engineering sciences and mathematics, division of material science, polymeric composite materials, Luleå university of technology, Sweden	**Directeur de thèse**

Institut Jean Lamour –UMR 7198- Département SI2M – Equipe 305
Parc de Saurupt - CS 50840- 54011 NANCY Cedex

Université de Lorraine – Pôle M4 : matière, matériaux, métallurgie, mécanique

Preface

The work presented in this thesis contains five scientific papers that summarize my work performed within the Division of Materials Science in Luleå University of Technology in Sweden and in the Division of Mechanics of Materials (SI2M) in Jean Lamour Institute in France as well as Department of Aerospace Engineering in Texas A&M University in USA during the period from October 2013 to March 2017.

I am very fortunate to have the chance to do my PhD in three different universities of different countries, which I'll forever be grateful about.

I would like to thank my advisor Professor Janis Varna first for giving me the opportunity to do research in the northernmost technical university, and for his straightforward but very helpful advice and guidance. I would also like to thank Professor Ramesh Talreja for bringing me to the world of composite and supporting me through out of my PhD study. I would also like to thank Professor Zoubir AYADI for his support and assistance with my poor French.

Special thanks go to my amazing colleagues in Lulea: Andrejs, Liva, Hana, Newsha, Hiba, Abdelghani, Johanna, Roberts, Lennart for their kind assistance and great sense of humor, which made my adventure in Luleå quite enjoyable.

I would also like to thank the Joint European Doctoral Program in Material Science and Engineering (DocMase) for financing this project.

Finally, I would like to express my greatest gratitude to my family especially my wife Xiaoying, for their unconditional love and supports, this one is for you.

Luleå, May 2017

Linqi Zhuang

Abstract

In the presence thesis, the growth of fiber/matrix interface debond of a UD composite with hexagonal fiber packing under longitudinal and transverse tensile loading was investigated numerically, with the special focus on the influence of neighboring fibers on its growth. In the current study, energy release rate (ERR) is considered as the driving force for debond growth and was calculated based on J Integral and Virtual Crack Closure Technique (VCCT) using finite element software ANSYS. In the present thesis research, we started with investigating the influence of neighboring fibers on ERR of a debond emanating from a fiber break in longitudinal loading condition. In longitudinal loading case, debond growth is mode II dominated. As the starting point for the research, an axisymmetric model consisting 5 concentric cylinders that represent broken fiber with debond, surrounding matrix, neighboring fibers, surrounding matrix and effective composites was generated. It's found that there are two stages of debond growth, the first stage is when debond length is short, the ERR decreases with increasing debond angle, and the presence of neighboring significantly increase the ERR of debond. For relatively long debond, the debond is in a steady state growth region when ERR is almost constant regardless of debond length. In steady state of debond growth, the presence of neighboring fibers has little effect on the ERR. In the later research, a 3-D model was generated with broken fiber and its 6 nearest fibers in a hexagonal packed UD composite were modelled explicitly, surrounded by the homogenized composite. Based on the obtained results, it's shown that ERR is varying along debond front, and has its maximum at the circumferential location where the distance between two fiber centers is the smallest. This indicates the debond front is not a circle. For steady state debond, the presence of fibers has little effect on ERR that averages along debond front. For short debond, the presence of fibers increases the averaged ERRS, and that the increase is more significant when inter-fiber distance are the smallest. When we conclude our investigation on fiber/matrix debonding under longitudinal loading, we began studying the growth of a fiber/matrix debond along fiber circumference under transverse loading. It's found that debond growth is mixed-mode, and both mode I and mode II ERR components increase with increasing debond angle and then decreases. Debond growth is mode I dominated for small debond angle and then switch to mode II dominated. The presence of neighboring fibers have an enhancement effect on debond growth up to certain small debond angle and then

changes to a protective effect. Finally, the interaction between two arc-size debond under transverse loading is investigated. It's found that when two debonds are close to each other, the interaction between two debond becomes much stronger, and that interaction leads to the increase of ERR of each debond significantly, which facilitates further debond growth for both debond.

Résumé

Dans ces travaux, nous avons étudié numériquement la croissance du décollement de l'interface fibre / matrice d' un composite UD avec garnissage hexagonale de fibre sous charge longitudinal et transversal. Nous avons mis l'accent en particulier sur l'influence des fibres voisines sur sa croissance. Dans la présente étude, le taux de libération d'énergie (ERR) est considéré comme la force motrice de la croissance du décollement et a été calculé sur la base de Integral J et de la technique de fermeture virtuelle de fissures (VCCT) à l'aide du logiciel de calcul par éléments finis ANSYS.

Dans la présente recherche de thèse, nous avons étudier d'abord l'influence des fibres voisines sur ERR d'une décohésion émanant d'une rupture de fibre en condition de chargement longitudinal. Dans le cas du chargement longitudinal, la croissance du décollement est gouvernée par le mode II. Comme point de départ l'étude, nous avons mis place un modèle axisymétrique composé de 5 cylindres concentriques représentant la fibre endommagée, la matrice environnante, les fibres voisines, la matrice environnante et le composite effectif généré. On constate qu'il y a deux stades de croissance, la première étape correspond à une longueur courte du décollement, l'ERR diminue à mesure que l'angle du décollement augmente, et la présence de voisins augmente significativement la décohésion de l'ERR. Pour une décohésion relativement longue, le décollement se situ dans une région de croissance en état stationnaire lorsque l'ERR est pratiquement constant quelle que soit la longueur du décollement. A l'état stationnaire de la croissance du défaut, la présence de fibres voisines n'a que peu d'effet sur l'ERR.

Les travails ultérieurs, nous avons mis en place un modèle 3-D (explicite) avec la fibre endommagée et ses 6 fibres les plus proches dans un composite UD compacté hexagonal, entourées par le composite homogénéisé. Sur la base des résultats obtenus, nous avons montré que l'ERR varie le long de la face frontale et a son maximum à l'endroit circonférentiel où la distance entre deux centres de fibre est la plus petite. Cela indique que le front du décollement n'est pas circulaire. Pour l'état stable du décollement, la présence de fibres a peu d'effet sur l'ERR qui progresse le long du front du décollement. Pour un décollement court, la présence de fibres augmente l'ERRS moyenné, et cette augmentation est plus significative lorsque la distance entre fibre est la plus petite. Après l'étude du la décollement fibre / matrice en charge longitudinale, nous avons commencé à étudier la croissance du décollement fibre / matrice le long de

la circonférence de la fibre sous charge transversale. On constate que la croissance de la du décollement est en mode mixte, et les composants ERR du mode I et du mode II augmentent avec l'augmentation de l'angle de déformation puis diminuent. La croissance du décollement démarre principalement en mode I pour les petits angles de décollement et se poursuit en mode II. La présence de fibres voisines a un effet d'accroissement sur la croissance du décollement jusqu'à certains petits angles et change ensuite en effet protecteur.

En fin, nous avons étudié l'interaction entre deux décollement sous chargement transversale. Nous avons constaté que lorsque deux décollements sont proches l'un de l'autre, l'interaction entre devient beaucoup plus forte et conduit à l'augmentation significative de l'ERR de chaque décollement, ce qui facilite la croissance du décollement.

List of appended papers

Paper A

Zhuang, L and Pupurs, A, Effect of neighboring fibers on energy release rate during fiber/matrix debond growth. Proceedings in 16th Eurepean Conference on Composite Materials, 2014, Seville, Spain.

Paper B

Zhuang, L., Pupurs, A., Varna, J., and Ayadi, Z., 2016, "Effect of fiber clustering on debond growth energy release rate in UD composites with hexagonal packing," Engineering Fracture Mechanics, 161, pp. 76-88

Paper C

Zhuang, L., Pupurs, A., Varna, J., and Ayadi, Z., 2016, "Fiber/matrix debond growth from fiber break in unidirectional composite with local hexagonal fiber clustering," Composites Part B: Engineering, 101, pp. 124-131.

Paper D

Zhuang, L., Pupurs, A., Varna, J., Talreja, R. and Ayadi, Z., 2017, “Effects of Inter-Fiber Spacing on Fiber-matrix debond Crack Growth in Unidirectional Composites Under Transverse Loading," Submitted to Composites Part A: Applied Science and Manufacturing.

Paper E

Varna, J., **Zhuang, L.**, Pupurs, A., and Ayadi, Z., 2017, “Growth and interaction of debonds in local clusters of fibers in unidirectional composites during transverse loading," Submitted to Key Engineering Materials

Contents

1. Introduction

Composites have been widely used in engineering industries especially in aerospace industry and wind energy industry due to their unique mechanical properties compared to traditional metal materials. One of most attractive features of composites is their design flexibility, i.e. engineers could design composite structures with desired properties by selecting different lay-up of composite, reinforcement or matrix materials etc. For a composite structure, depending on the design requirements, it usually contains substantial amount of unidirectional (UD) plies with fibers orienting along loading direction (called 0° or longitudinal plies) or perpendicular to the loading direction (called 90° or transverse plies). When subjected to tensile loading, 0° and 90° plies usually fail at different levels of applied load due to the difference in failure mechanisms. For 0° plies, fiber breakages, matrix cracking and fiber/matrix interface debonding are the common damage modes upon loading, due to the complicated nature of composites, those damages could occur at the same time or in a sequence. 0° plies are believed to fail when a critical fracture plane is formed by coalescing of fiber breaks through interface debonds and matrix cracks and propagates unstably. For 90° plies, the most common damages caused by tensile loading perpendicular to the fibers direction are fber/matrix interface debonding and matrix cracking. Transverse cracking is often considered as the first failure event in composite structures and the macro-scaled transverse crack is believed to form by the coalesce of debonds. The increasing structural applications of composites lay heavily on the models that could accurately predict the behaviors of composites under any given loading conditions while the accuracy of such models depends on the thorough understanding of underlying failure mechanisms, especially, the mechanism for damage initiation and final failure. For any given composites, based on the discussion above, the first failure event is usually occur at 90º plies and 0º plies control the strength of the composite. As a result, it is of great importance to investigate the failure mechanism of UD plies under longitudinal or transverse loading condition in order to gain a better understanding of failure of the composite structures.

1.1 Tensile failure of 0° plies

In order to investigate the tensile failure mechanisms of 0° plies, UD composites where a composite contains only 0° plies are commonly adopted. When subjected to increasing or repeated tensile loading, failure of UD composite is governed by different mechanisms, which could be summarized in fatigue life diagram proposed by Talreja [1]. As shown in the Fig.1, fatigue life diagram could be divided into three region. In horizontal region I where applied load is larger than the strength of fiber, fiber breakages is the main failure mechanism. During first cycle of loading, individual fiber with lower strength than maximum stress breaks randomly, upon further application of loading, due to stress concentration causing by the broken fiber, more discrete fiber break occurs until a critical fracture plane is formed where crack propagate unstably and lead to final failure of UD composite. Because fiber is considered not to experience fatigue, that whole process is thus non-progressive and highly statistical. When the applied load is lower than the strength of fiber, during first application, due to the statistical nature of fiber strength, individual fiber break would still occur at their weakest position as well as subsequent fiber/matrix interface debonding and matrix cracking, upon further loading, more fiber break would occur near previous damage region, as well as further growth of previous debond and fiber-bridged matrix cracking, final failure would occur when a critical fracture plane is formed by connecting each individual fiber breaks through debonding and matrix cracking. Finally, if applied load is so low that although certain damage events occur during loading, they will be arrested upon further loading. Then it reached fatigue limit as shown in the Fig.1, where final failure would not occur during cyclic tensile loading. A systematic experimental work to demonstrate fatigue life diagram could be found in [2, 3].

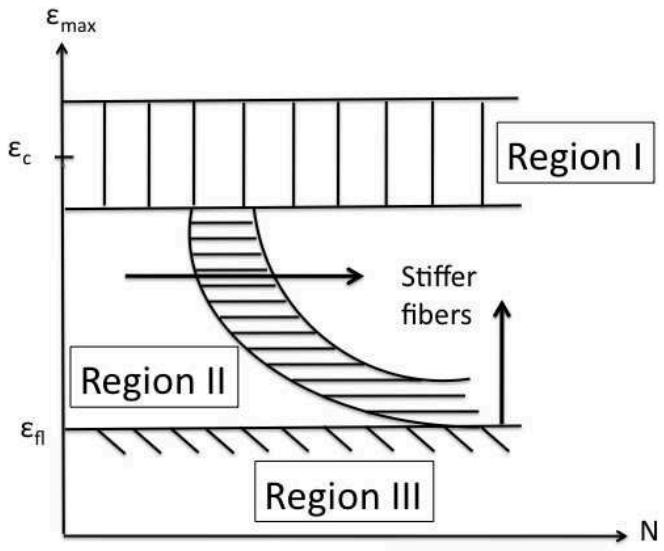

Fig.1. Fatigue life diagram for UD composite under cyclic tensile loading (Courtesy of Prof. Talreja)

It should be noted that the progress failure region (Region II) discussed in fatigue life diagram, although is proposed based on repeated tensile loading condition, it also highlights some very important failure features of UD composite under statically tensile loading: the final failure of the UD composite is also caused by the coalesce of fiber breaks through fiber/matrix debonding and matrix cracking, which forms a critical fracture plane that grows unstably. In the following section we will discuss the exact mechanisms for some of the most important damage modes under tensile loading.

1.11 Fiber breakages in UD composites

When a UD composite is subjected to tensile loading along fiber direction, individual fiber breaks first at its weakest location due to the statistical distribution of fiber strength. The breakage of a fiber causes the axial stress redistribution along fiber axis. As shown in Fig. 2, at the fiber break, fiber no longer carries axial load, and the load carrying ability of broken fiber recovers gradually from fiber break through shear stress carried by matrix. The distance from fiber break to where the axial stress recovered to up to certain level (usually 90%) of the nominal load before fiber breakage is often referred as “effective length” which represents the load transferred ability between fiber and matrix. Since at fiber break, broken fiber does not carry axial loads, this part of load has to be shared by the intact fibers nearby, which leads to the enhancement of local axial stress (or stress concentration) in neighboring fibers. If the

enhanced local axial stress exceeds the fiber strength, a new fiber would break resulting in more significant enhancement of local axial stress in the intact fibers nearby, which leads to the successive breakage of nearby intact fibers simultaneously or with the further increase of applied load. It's expected that a UD composite would eventually fails if substantial amount of fibers break within the composite. Based on this idea, the majority of the UD composites failure models have been developed based on the failure of fibers in order to predict the final failure of UD composites.

In order to be able to predict the fiber breakages, the accurate calculation of stress enhancement in the intact fibers near broken fiber is the key. As a result, numerous research efforts have been devoted to investigating the stress enhancement mechanism in the nearby fibers.

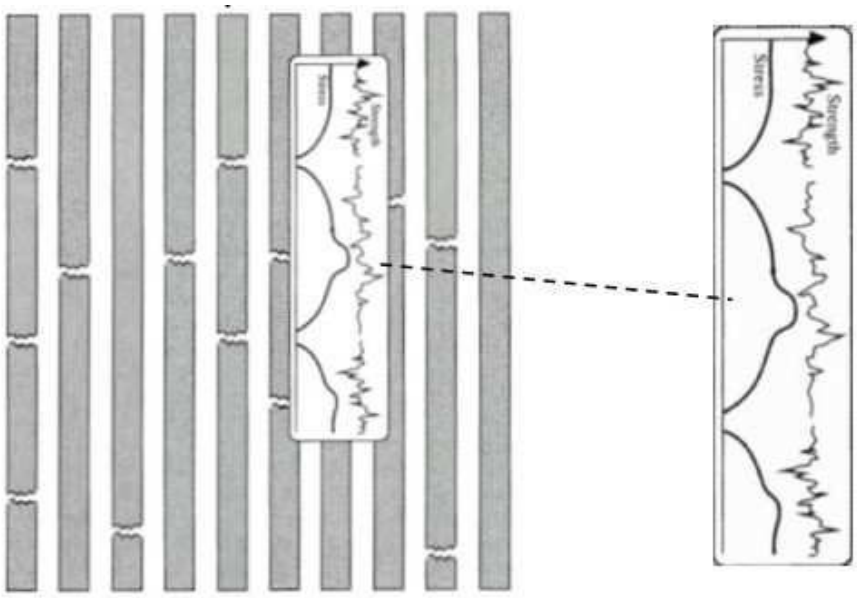

Fig.2 The distribution of axial stress, and of local fiber strength along the fiber length. (Figure adopted from [4] and is originally from [5])

The first attempt to study this stress enhancement in composites was made by Hedgepeth [6] where he investigated the stress concentration in a 2-D filamentary structures. The sheet of parallel filaments is assumed to carry the normal loads and is embedded in a matrix which carries only shear. A stress concentration factor (SCF:

ratio between local axial stress and nominal stress applied at the fiber) of 4/3 was found for an intact fiber near single broken fiber and he also found that the stress concentration factor is larger when dynamic effect was considered. This study was based on the assumption that all the filaments carry the same extra load resulting from fiber breakage, which is considered as so called "global load sharing" theory. This theory has some drawbacks: intuitively, we expect the influence of stress field caused by fiber breakage should be within a local region near broken fiber and the nearest neighborhood should be affected the most. Hedegpeth and Van Dyke [7] then improved the previous theory by assuming only the nearest fibers have to share the extra load caused by fiber breakage and obtained smaller stress concentrator factor based on the 3-D model. These two studies are commonly considered as the first investigations on the stress concentration in the nearby intact fibers cause by fiber breakages, after that, several analytical models were also developed by various researchers [8-11] and obtained similar SCF as that in Hedgepeth's studies [6, 7]. With the help of development of computational abilities, many numerical models were later developed in order to calculate the SCF accurately. The work done by Nedele and Wisnom [12, 13] was considered as one of the first numerical models developed to investigate the SCF. They first developed a 3-D model to account for a UD composite with fibers uniformly distributed in a hexagonal pattern, and found a smaller SCF in the nearest 6 fibers around broken fibers compared to that obtained by Hegepeth and Van Dyke [7]. They then extended their work to an axisymmetric model with broken fiber placed as the central fiber ring, and neighboring fibers were also modeled as a concentric fiber ring near central broken fiber. From the calculation they found that SCF was varying across the cross-section of nearby fibers and has the highest value at the fiber/matrix interface near broken fiber. They then calculated the mean SCF using the axial stress value at the center of nearby fiber's cross section and obtained a smaller SCF compared to that obtained by Hegepeth and Van Dyke [7]. After that, numerous research efforts [14-25] have been done on SCF and majority of those research have been focusing on the effect of matrix yielding and fiber/matrix debonding near fiber break on obtained SCF, and based on the results obtained from those research, it is generally accepted that the presence of matrix yielding or fiber/matrix debonding would reduce the maximum SCF in the nearby fibers.

With the better understanding of the stress enhancement mechanism in the composites, researchers are able to developed different analytical models to predict the final failure of a UD composite. Until now, the majority of models developed to predict the failure of a UD composites are based on the so-called "fiber bundles" model, which assumes only fibers carry the axial loads and a UD composite fails when certain amount of fibers are broken. Based on that argument, the major research focus was on predicting the successive breakages of fibers. Realizing that the strength of a single fiber is not constant along the fiber length, a certain statistical distribution (usually the Weibull distribution) of fiber strength is commonly adopted when developing the composite model. The first comprehensive analytical model to predict the tensile failure of a UD composite was developed by Rosen [26]. In his model, the axial loads are assumed to be carried by fibers only, and the extra load caused by the fiber breakage is shared by all the fibers in a cross-section. The strength of the fibers is assumed to follow Weibull distribution. Based on the "weakest link" theory that fiber fails when the local stress exceeds its lowest strength value, the composite failure occurs when a cross-section fails. Zweben [27], Zweben and Rosen [28] later proposed a statistical model based on the accumulative weaken of fibers that including the stress concentration. The basic of their model lays on the argument that the breakage of a single fiber will cause stress concentration in the nearest fibers in a 2-D fiber array, which will increase the probability of failure of nearest two fibers, the breakage of nearest fibers will cause a higher stress concentration in the surrounding fibers which will further increase the probability of failure of those fibers. The final failure of a composite occurs when a first multi-fractured group of fibers is formed. A few years later Harlow and Phoenix [29, 30] also developed their own statistical model to predict the failure of UD composites. It should be noted that, until now, the analytical models we discussed so far are all considered as the "chain of bundles", that is each fiber is considered as one chain within the bundles, and the weakest fiber fails the first, the composite fails when the fiber bundle fails. The "chain of bundles" model constitute majority of the early years' models to predict the final failure of a UD composite until Batdorf [31] proposed his model concentrating on the formation and growth of multiple fiber fractures. In his work, he also adopted weakest link theory to predict the isolated single fiber breakage (singlet), double fractures (doublet) and multiplets with respect to applied load, a UD composite is considered failed when a Griffith-type instability occurs which

corresponding to a certain number of broken fibers at the same location. This approaches significantly simplify the procedures in previous “chain of bundles” models and he and his co-worker [32] as well as other research [33] found that the amount of broken fibers at the same location that could results in the beginning of instability most often varies from 6-14 fibers, this also supported by the fractography investigation conducted by Purslow [34], as he found the numbers of broken fibers within a bundle in the fracture surface of a UD composite fell within that range of numbers, as shown in Fig. 3. Besides those analytical models discussed, numerous numerical models were also develop to predict the failure of UD composite with the focus devoted on the fiber fractures, for example, in [35-40]. Those models, although can agree relatively well with the experimentally obtained failure strain of a UD composite, they are all focused only on the fiber breakages, which do not capture the exact failure mechanism of the UD composite, as we’ll shown later, which put its real accuracy in doubt.

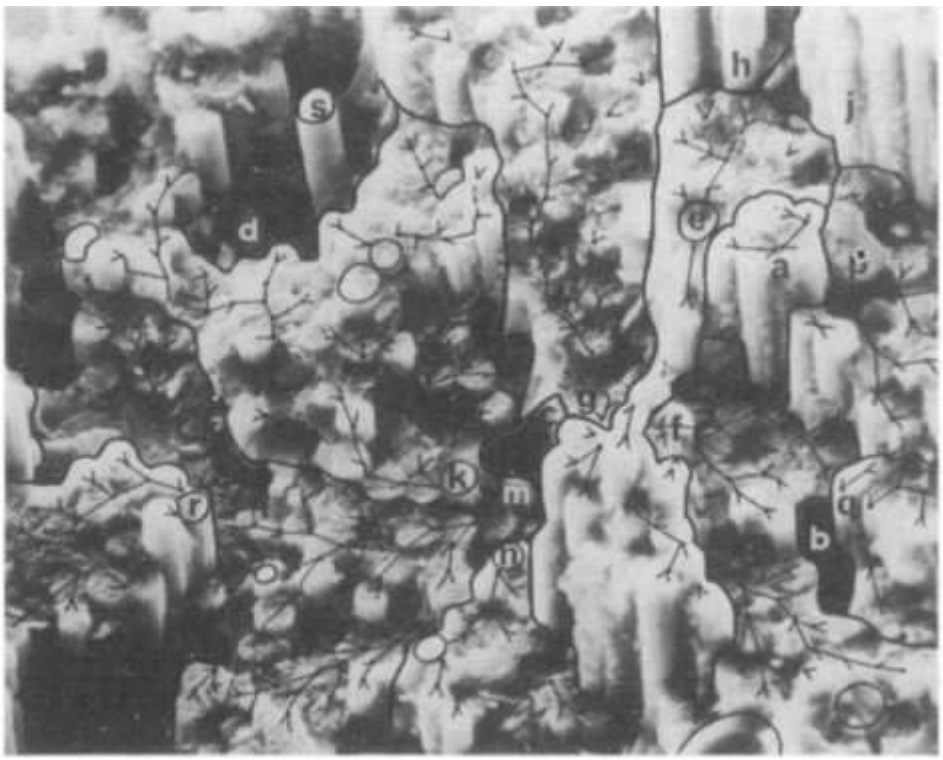

Fig.3 Fracture surface of a UD composite. Figure adopted from [34]

In a synchrotron X-ray microtomography study conducted by Aroush et al [41], the whole process of growth of single fiber fracture (singlet) to multi-fiber fractures

(multiplets) and the final failure as a result of instability occurs was clearly demonstrated, as shown in Fig. 4. A more clear picture of cluster of broken fibers was captured by Garcea et al [42], as shown in Fig.5, a fracture plane containing clusters of broken fibers are displayed. A closer look at these two figure reveals that the fracture plane is not strictly planar, i.e., fibers did not break at an exact same plane and was connected by the means of fiber/matrix debonding and matrix cracking. Although the effect of matrix cracking on the stress enhancement of neighboring fibers are relatively small, as discussed by Swolfs et al [43], it plays a very important role, together with fiber/matrix debonding, in connecting individual broken fiber and forming the fracture plane, as found by the current author [44]. As a result, a more accurate model to predict the failure of a UD composite through unstable growth of the fracture plane has to be able to account for the effects of matrix cracking and fiber /matrix debonding in order to capture the correct failure mechanism. In the following section, we will specially focus on fiber/matrix longitudinal debonding mechanism.

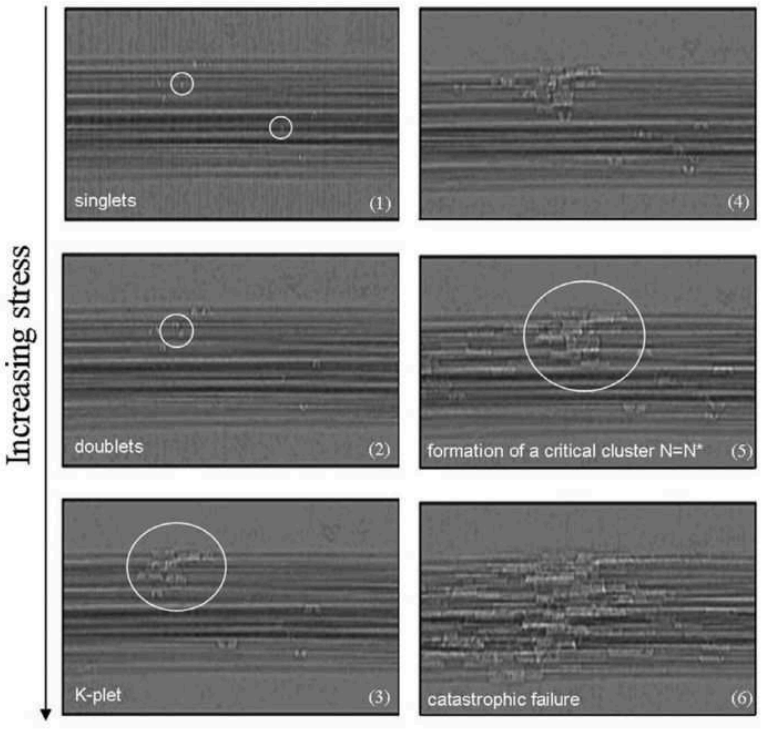

Fig. 4 Sequence of damage evolution in a UD composite subjected to longitudinal tension. Figure adopted from [41]

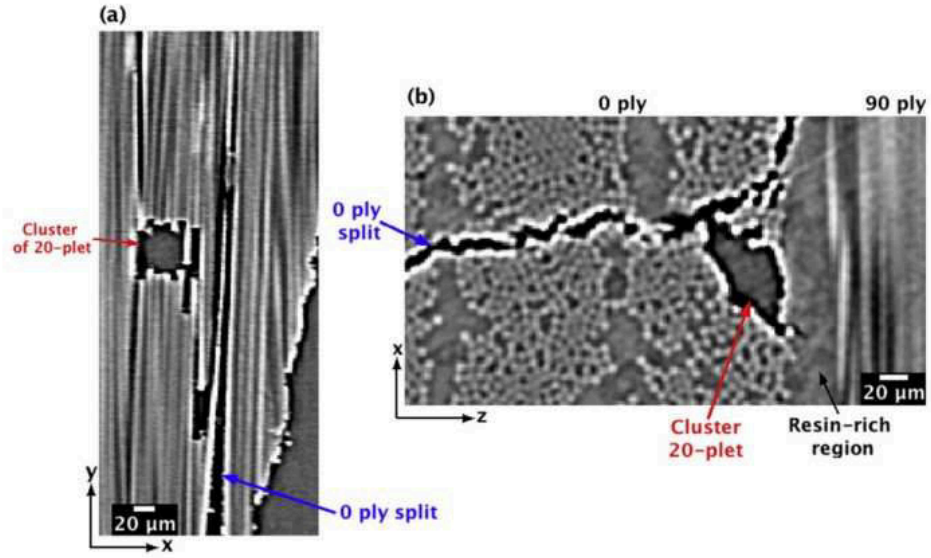

Fig. 5 Illustration of clusters of fiber breaks. Figures adopted from [42]

1.12 Fiber/matrix interfacial debonding in UD composites.

It is clear that for a UD composite subjected to longitudinally tensile loading, fiber/matrix debonding is a very important sub-damage mode, although it will not directly lead to the final failure of the UD composite.

It has been shown that interfacial debonding would deflect original propagating brittle crack and thus increase the overall fracture toughness of composites [45, 46]. Although the concept of fiber/matrix interface it is widely accepted nowadays [47-49], the exact properties of interface is still unknown. In order to characterize the interface properties, single fiber fragmentation test has been widely adopted due to its experimental simplicity [50-55]. At the same time, it could also be used to calculate statistical parameters for fiber strength [56-59]. The idea of fiber fragmentation was first described by Kelly and Tyson [60] where they studied the interface strength of fiber-reinforced metal by assuming a linear stress build up from fiber break end. Based on shear-lag typed analysis that tensile stress is transferred back to fiber through shear stress transforms along fiber/matrix interface from fiber break, they proposed that critical length of fiber l_c is related to the yield strength of fiber/matrix interface by Eqn.1, where σ_f the fiber breaking strength, r is is the fiber radius and τ_y is the yielding strength of the interface, which could also be characterized as fiber/matrix interfacial

strength in literature published later on although the expression would be different based on the methods, for example, in [50, 51, 61]. In the single fiber fragmentation test, a continuous single fiber is usually embedded in a dog bone shape matrix subjected to tensile loading along fiber direction. Upon loading, fiber breaks at its weakest position, with increase of applied load, more fiber breaks occur until it reach saturation state where the distance between two fiber break is not long enough for the tensile stress to recover to induce further fiber break. During single fiber fragmentation, it is found that based on the fiber/matrix interfacial properties, fiber radius as well as other factors, both fiber/matrix debonding, matrix cracking and matrix shear yielding would occur after initial fiber break [62-64]. Optical method is commonly used to observe stress state near fiber break. Fig.6 shows the typical birefringence pattern at fiber break for carbon/epoxy composites, due to the high shear stress concentration near fiber break, fiber/matrix interface failure could be found (sheath region), as reported in [51, 53], and symmetric birefringence is usually found on both side of fiber beak. Based on the experimental finding from single fiber fragmentation test, several analytical work and numerical work have been carried out to study the stress transfer between fiber/matrix interface as well as fiber/matrix debond growth from fiber break [55, 62, 65-68]

$$l_c = \frac{\sigma_f r}{\tau_y} \tag{1}$$

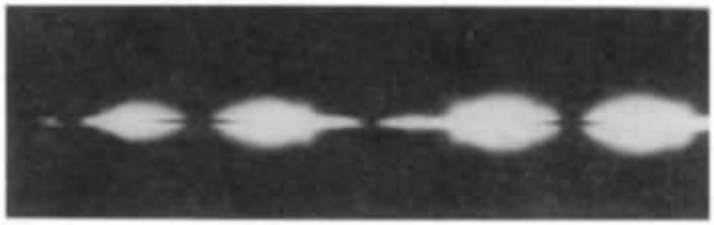

Fig.6 Birefringence pattern at fiber break (Figure adopted from [51])

As useful as it is, however, in single fiber composite model, it does not account for the effect of surrounding constituents, which would affect the obtained results as stress field near certain fiber is closely related to its surrounding medium. Previous research [12-21, 33, 69, 70] adopted multiple fibers in the specimen in order to investigate the

influence of neighboring fiber on Stress Intensity Factor (SCF) and subsequent fiber breakage process. However, the effects of neighboring fibers on longitudinal debond growth is less understood. As an improvement of single fiber composite model, several numerical and analytical investigations [71-75] on debond growth from single fiber break have been conduct recently. The whole model was constructed based on three-phase concentric cylinders, with initial broken fiber and surrounding matrix to be the first two rings and neighboring substituents around them to be smeared into an effective composite phase with homogenized composite properties, as shown in Fig. 7. ERR is calculated as driving force to debond growth. It's found that two distinct region existing during debond growth, first one is when debond length is relatively short and there will be interaction between debond tip and fiber break, which would affect obtained ERR; The other region is when debond length is long enough such that there is no interaction between debond tip and fiber break, debond would grow steadily with ERR being constant with increasing debond length. In this steady-state region, an analytical model is able to obtain and good agreements were reached between numerical results and analytical model.

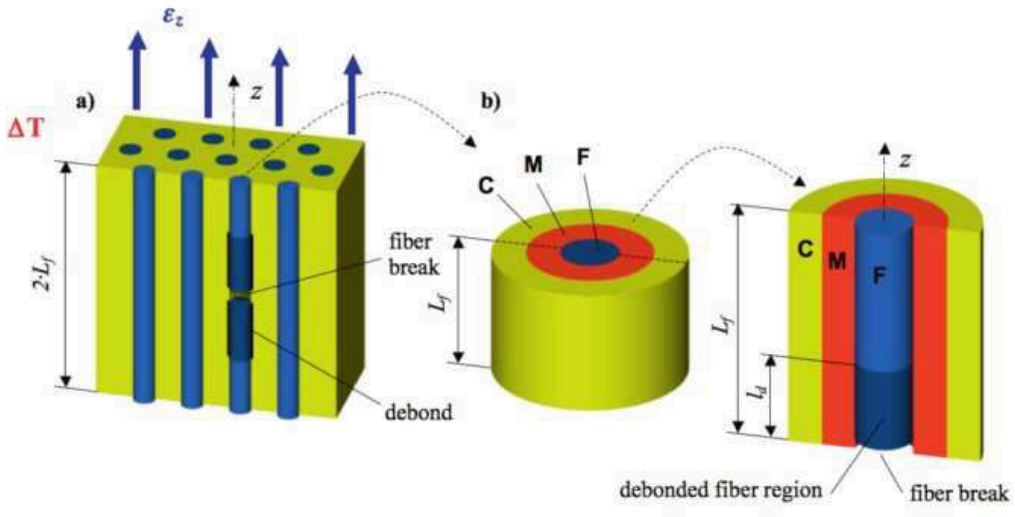

Fig.7 Illustration of three-phases concentric cylinder models (Figure adopted from [4]

Despite the accuracy of previous models described above, they have analyzed an idealized geometry without taking into account the possible non-uniformity of the local fiber arrangement which is present in most of the real cases. It can be expected that the local microstructure would also affect the stress state around the broken fiber and hence

it can affect the debond growth rate. As a result, in the present thesis, we will specifically investigate the effects of local fiber arrangement on debond growth. Before we proceed to the numerical models, we will give a comprehensive overview of transverse failures of 90° plies.

1.2 Transverse cracking of UD plies.

1.2.1 Experimental findings

Previously we have focused our discussion on the tensile failure of 0° plies, in majority of the composite structures, when subjected to longitudinally tensile loading, 0° plies are the major load bearing plies, and failure of 0° plies often leads to the final failure of the composite. In real practice, it is also of great importance for researchers to understand the failure initiation of composites. For composites containing off-axial plies, especially 90° plies, when subjected to longitudinal tensile loading, the first failure event has been commonly found as transverse matrix crack propagating through the thickness in 90° plies, as shown in Fig. 8. A closer look at these transverse matrix crack (Fig. 8(b)) reveal that the observed macro-scaled matrix crack actually results from the coalesce of individual fiber/matrix debond. After the first transverse matrix crack is formed, the number of transverse crack increases with increasing applied load, as shown in Fig. 9.

Similar to fiber/matrix longitudinal debonding discussed above, the multiplication of transverse cracks does not directly lead to the final failure of composites. However, it has been proven [76-80] that multiple transverse cracking will lead to degradation of composite stiffness and strength. Due to its importance in determining the integrity of composites, the mechanism of multiple transverse cracking has been studied by numerous researchers. In the following paragraph let's first focus on some experimental findings to have a better idea of the whole process.

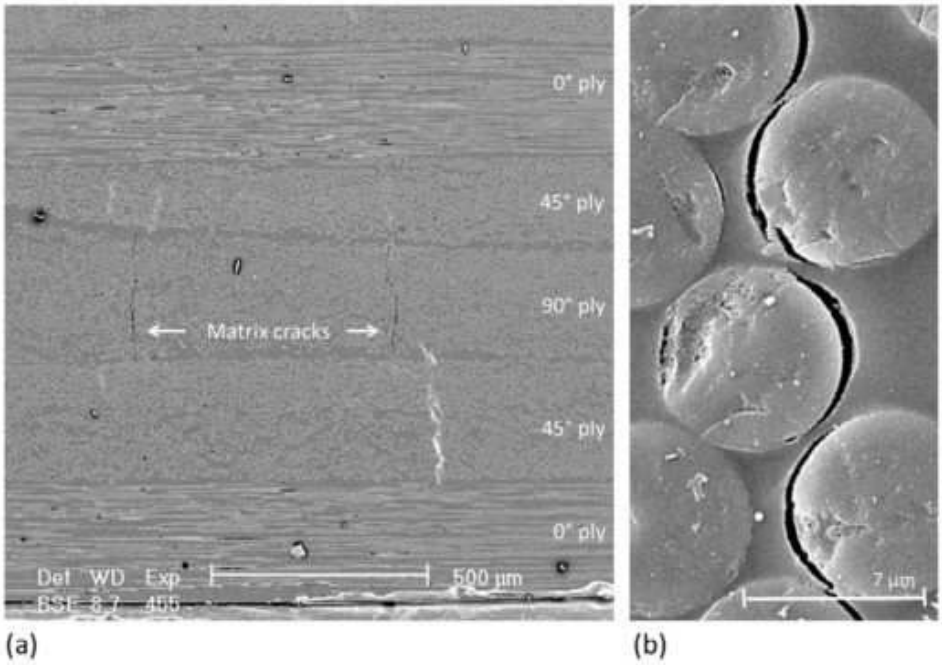

Fig.8 Illustrations of (a). transverse matrix crack in 90° plies, (b) Zoom in on a matrix crack revealing debonding at fiber/matrix interface. (Figure adopted from [81])

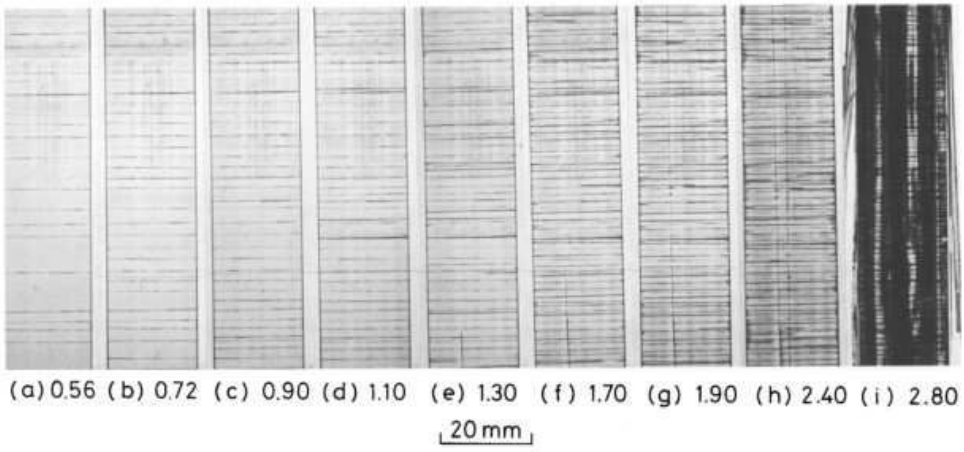

Fig. 9 Development of transverse cracking with increasing applied load in glass-fiber cross ply laminate. (Figure adopted from [78]

Early work done by Garrett and Bailey [82] found that for different lay-ups of cross-ply laminates, transverse crack initiates at around 0.4% of the strain, however, the spacing between transverse cracks depends on the thickness of transverse plies. As shown in Fig. 10, the transverse crack spacing decreases with increasing thickness of

transverse plies. The so-call “constraint effects” by the longitudinal plies was later investigated by Parvizi et al [83, 84] where they found the transverse cracking process changed significantly in cross-ply laminates with different transverse and longitudinal plies ratio. For cross-ply laminates with high percentage of transverse plies, fully developed multiple transverse cracking is the main mechanism, with the decrease of transverse ply thickness, edge cracks are most commonly found and slowly propagate across the specimen width, and for a much smaller transverse ply thickness, the transverse cracking process was completely compressed. This “constraint effect” is demonstrated in Fig.11. As it could be seen from Fig.11, the number of transverse crack decreases as the thickness of the transverse plies reduced. The constraint effect of neighboring plies could be explained in terms of stress recovery within transverse plies. Once a fully propagated transverse crack is formed within transverse plies, the normal stress of the transverse plies at cracking plane is zero, and that normal stress has to be transferred back to transverse plies and fully recovered at certain distance from the cracking plane through shear stress within the interface between transverse plies and neighboring plies. Once the normal stress is fully recovered, another transverse crack is considered to form, and this same process results in the multiple transverse cracking process. Depending on the material properties and the lay-up of composite laminates, the ability of normal stress recovery through shearing varied, which result in the different spacing between transverse cracks. It is expected that as the transverse crack spacing reduced, the ability of normal stress recovery through shearing decreases and there will be a certain transverse cracking spacing below which normal stress will never be fully recovered, and thus no more transverse crack is formed after that. This is so-called “Characteristics Damage State” (CDS) which is first discovered by Reisfnider and his co-workers [85-87]. The CDS was first found [85] to be a state where the number of transverse cracks saturated, i.e., transverse crack spacing remain constant with increasing cycles in fatigue loading or increasing applied load in quasi-static loading. Later the same author and his co-worker found [87] that the residual strength, stiffness of the composites also influenced significantly by CDS.

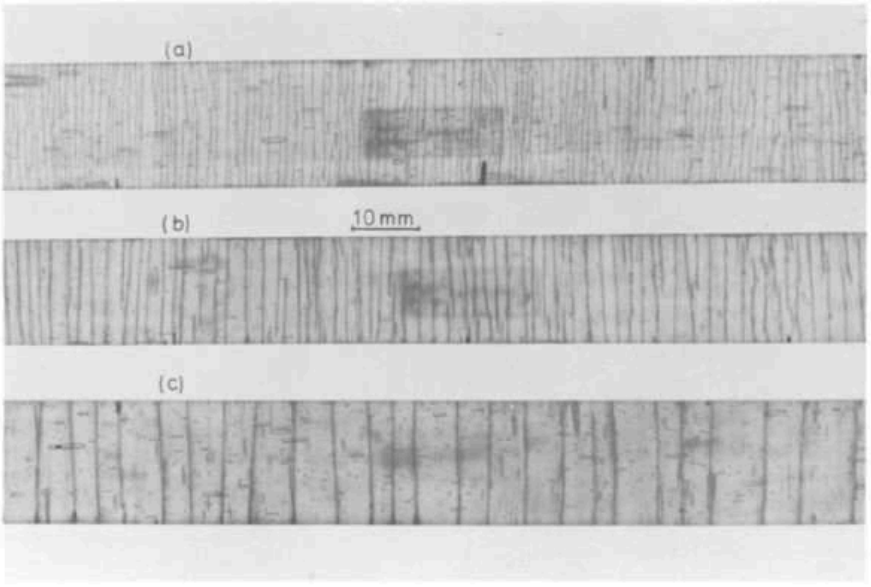

Fig.10 Transverse cracking in specimens with different transverse-ply thickness (a). 0.75mm, (b). 1.5mm, (c). 2.6mm. (Figure adopted from [82])

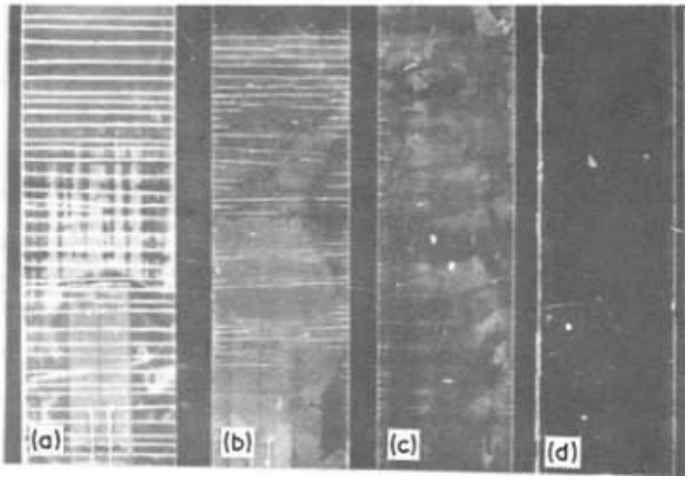

Fig.11 Illustration of the "constraint effect" in cross-ply laminates. The transverse ply thickness is reduced from a to d as the thickness of the transverse plies reduced. Figure adopted from [84]

1.2.2 Analytical and numerical findings

The experimental findings on transverse cracking in UD plies have been briefly summarized in the previous section. Multiple transverse cracking is found to be the main mechanism for UD plies subjected to transverse tension. The presence of multiple

transverse cracks also reduce composite stiffness, as a result, researchers are interested in developing analytical and numerical models in order to predict the corresponding multiple transverse cracking and resulting stiffness degradation of composites. Some of the milestones in this area include the "ACK" method developed by Aveston et al [88] which was able to predict whether it is a single facture or multiple transverse cracking in composite based on a simple strength argument where stress analysis was carried out using shear-lag type analysis. In that study, normal stress originally carried by matrix was assumed to be transferred back to matrix at certain distance away from matrix crack plane through friction between matrix and fiber interface. The appearance of the next matrix crack was predicted based on an energy balance method. The crack spacing was able to be predicted then. However, one of the major limitations is that this approach assumes constant shear stress which due to friction in normal stress recovery process. This approach was later extended by some of the same authors [89] to account for fully bonded and partially bonded composites. In order to predict the stiffness degradation of composite due to multiple transverse cracking, Hashin [90] adopted variational approach to investigate the stress distribution and stiffness degradation in a cracked cross-ply laminate. In his work, the local tensile stress is assumed to be constant through thickness and the stress field in the cracked laminate was represented by the original uncracked stress field plus the stress perturbation caused by transverse cracks, and the solution of the stress field is later solved by minimized the complementary energy of the composite. Similar variational approach was later adopted by other researchers [e.g[80, 91]] to investigate transverse cracking in the cross-ply laminates to account for the strain energy release rate of the matrix crack and variation of local tensile stress across thickness. Talreja [79] adopted a continuum damage theory to study the multiple cracking and stiffness degradation problem by using vector field to characterize the damage (matrix cracks) for various lay-up of laminated composites. The material constants in this work have to be determined experimentally. Recently Huang et al [92] was able to adopted a statistically analysis to investigate the multiple cracking process which also be able to account for the effect of manufacturing defects.

The analytical models we discussed all investigated the crack initiation and multiple cracking based on the assumption that plies are homogenous solid. With the development of computational mechanics, more numerical models were developed that

could study the transverse cracking mechanism in a constituent level. For example, Asp et al [93-96] found the stress field within epoxy matrix near fiber/matrix interface to be almost equally tri-axial, which is a preferred condition for matrix cavitation process. They argued that as cavitation grows and reaches its criticality based on dilatational energy density, it bursts open and propagates towards fiber/matrix interface leading to the initiation of fiber/matrix debonding, which is also the initiation of transverse cracking as macro-size transverse crack would eventually occur by the coalesce of debonds. They also conducted the "poker chip" typed experiment [95] of commonly used epoxy materials and found out the critical dilatational energy densities are not very sensitive to difference of epoxy materials. Fiedler et al [97-99] conducted several FE analysis of composite transverse failure and found that hydrostatic tensile stress is responsible for relatively low transverse failure strain and thermal stress and fiber volume fraction is found to influence of transverse failure process.

1.2.3 Fiber/matrix interface crack growth under transverse loading

We have discussed multiple transverse cracking in UD plies, which is the main failure mechanism for composites subjected to transverse tension. However, in many applications of composite materials, design is based on the threshold for first crack formation, which is usually found to be transverse cracking in 90° plies. As shown in Fig.8, the macro-sized transverse crack is formed by the coalesce of debonds. As a result, understanding individual debond growth under transverse loading is the key to investigate the first macro-sized transverse crack growth.

Similar to the case for the study on longitudinal fiber/matrix debonding, single fiber composite models were widely adopted at the beginning due to its simplicity. Fig 12 shows the experimental set-up of a single fiber composite subjected to transverse tensile loading. In this composite, single fiber is placed at the center of matrix materials, and the whole specimen is subjected to transverse tension. During the test, fiber/matrix interface first debonds due to existing flaws, upon further loading, for relatively weak fiber/matrix interfacial bonding, it's found by Zhang et al [100] that debond first grows along arc direction, and then propagates along fiber direction, however, for composites with good fiber/matrix interfacial bonding, it's found that once initiated, debond growth along arc and fiber direction almost simultaneously and the debond angle decreases

with increasing distance from initial defect site. The whole process of interfacial transversely debonding is sketched in Fig.13.

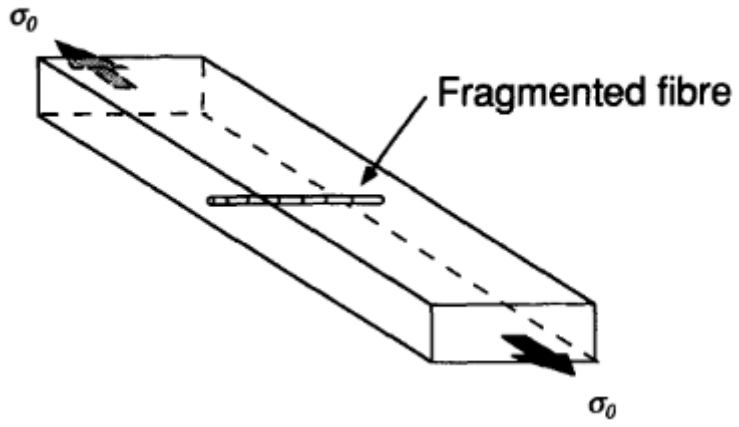

Fig.12 Illustration of single fiber composite test. The specimen is subjected to transverse tensile loading. (Figure adopted from [100])

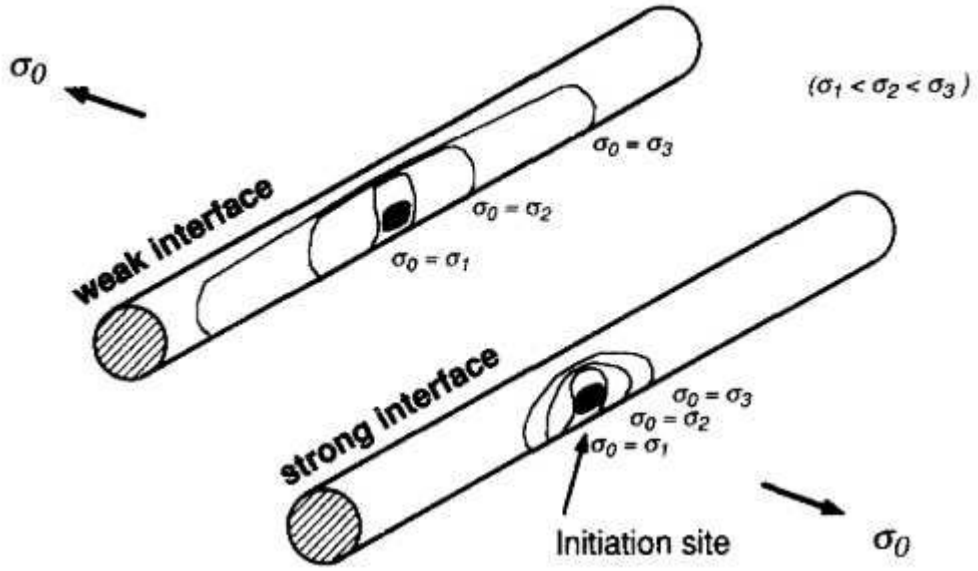

Fig.13 Interfacial debonding processes for a single fiber composite. Figure adopted from [100]

When it comes to study fiber/matrix interface crack (debond) growth, energy release rate (ERR) is usually investigated as the driving force. The general trend for ERR (Fig.15) of a transverse debond in a single fiber composite could be found in a

numerical study conducted by Paris et al [101] for the model shown in Fig.14. As shown in Fig.15, for each material system, debond growth is mixed-mode. Both mode I ERR component (G_I) and mode II ERR component (G_{II}) increases first with increasing debond angle and then decreases. For relatively small debond angle, debond growth is mode I dominated and then switches to mode II dominated growth for larger debond anlge. With the further increasing of debond angle, the crack faces come into contact and debond growth is pure mode II. One of the first studies to investigate the ERR of debond under transverse tension was conducted by Toya [102] analytically where he considered single fiber was embedded in the infinite matrix material and derived the expression for the ERR of different debond angle. The similar fiber/matrix interfacial problem was later investigated by Paris et al [103] numerically using Boundary Elements Method (BEM). This is also one of the first numerical studies on fiber/matrix interface crack growth under transverse loading. This study, together with investigation performed by Varna et al [104] clearly demonstrate the a physical relevant crack face contact zone developed for relatively large debond angle and that contact zone increases with keep increasing of debond size. Paris and his co-workers later published a series of paper to clarify the unknown aspect of transverse debond growth for a single fiber composite. For example, when dealing with potential debond crack kinking out of interface toward matrix in a single fiber composite, Paris et al [101] found that the debond is most likely to kink out of interface between $60^o \sim 70^o$ of semi-debond angle, that's when the ERR of kinked crack is the largest. Regarding to the effect of thermal stress, Correa et al [105] found that thermal stress has a protective effect on debond growth due to the compression nature of thermal stress in single fiber composite. A common question when modeling the debond in a single fiber composite is whether it should be a symmetric debond from both side of the fiber or there is only one debond? García et al [106] conduct the relevant study and conclude that based on the amount of energy required, single debond requires less energy and thus would be the most likely scenario. The discussions we have so far mainly focus on the debond growth in a single fiber composite under uniaxial tension along transverse direction. Some researchers also developed failure criterion to predict the onset of fiber/matrix interface debond under biaxial tension, for example work done by Carraro et al [107] and Mantič et al [108].

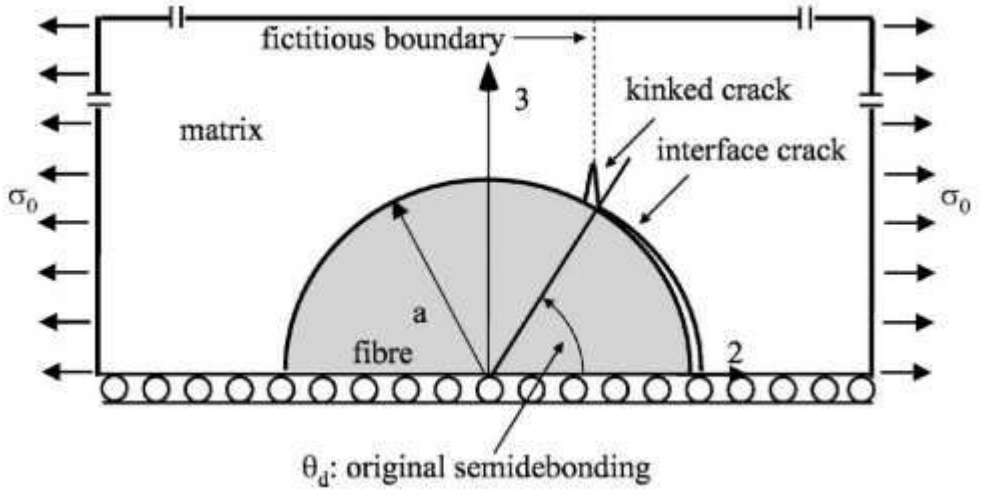

Fig.14 Illustration of the numerical model for single fiber composite. Figure adopted from [101]

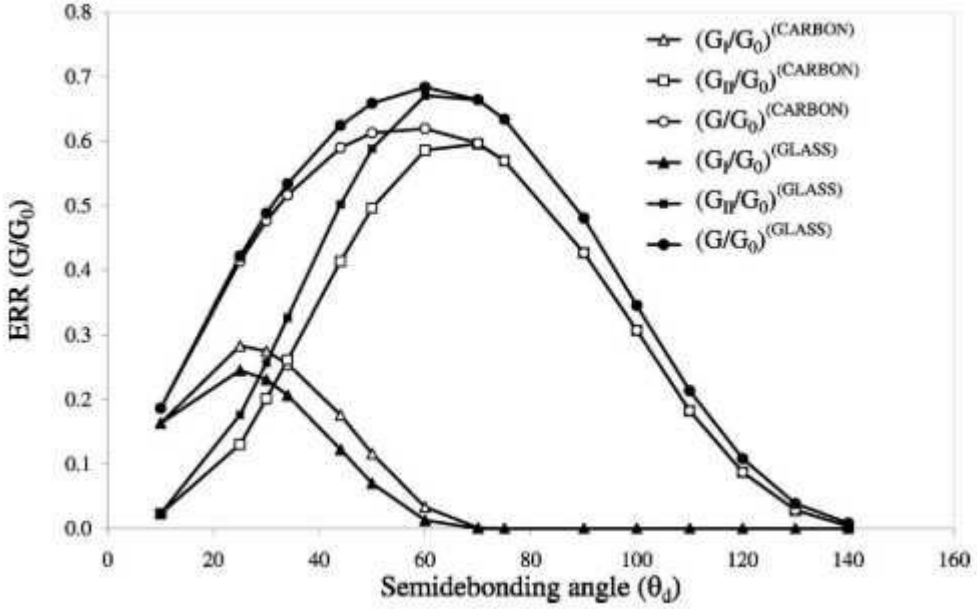

Fig.15 Illustration of the trend for ERR of the debond in a single fiber composite. Figure adopted from [101]

Although single fiber composites are very useful in helping researchers understand some basic mechanisms of fiber/matrix interface debong growth under transverse tension. There are some major limitations regarding to this type of model. One of the

most important limitations one might expect is whether single fiber composite could simulate the actual stress field in composite. Asp et al [93-95] studied the local stress field around fibers in the cross-section of a unidirectional (UD) composite loaded in transverse tension and based on energy considerations proposed that the debonding results from unstable growth of a cavity in the matrix near the fiber surface. These studies clarified the role of the triaxiality of the local stress field in initiation of debonding. Therefore, a proper understanding of debond initiation and growth is expected to come from multiple-fiber composite studies. Recently, a few studies have gone in this direction [109-111]. In [109, 111] the approach taken was to use a cohesive zone model, which has the interface strength and fracture toughness as two material properties. As noted above, Asp et al [93, 95] showed that failure at the fiber-matrix interface depends on the triaxial stress state, not on the tensile stress alone. This casts doubt on the use of a cohesive zone model for studying the debonding process. In [24], the concurrent and growth debonds have been investigated by linear elastic-brittle fracture based on a numerical model containing ten fibers embedded in a matrix cell. However, no detailed information about the influence of local fiber bundles on debond growth could be obtained from that paper. While these studies have been useful in generating understanding of the local interactions in the debonding process, two aspects need further clarity. First, the influence of inter-fiber distance on debond growth in a fiber cluster needs to be understood, and second, the debonding process should be analyzed in terms of the energy release rate (ERR) of the arc-shaped interface crack. These two aspects have been studied by Sandino et al [112], using a two-fiber model (Fig.16). As shown in Fig.16, an undamaged fiber at different locations near a central fiber with debond and it's found that the neighboring fiber has a protective effect on debond growth at all positions except when the fibers are aligned with the loading direction. As useful as their results are, however the two-fiber composite model is still not representative of a real composite where multiple neighboring fibers are distributed around the fiber with debond.

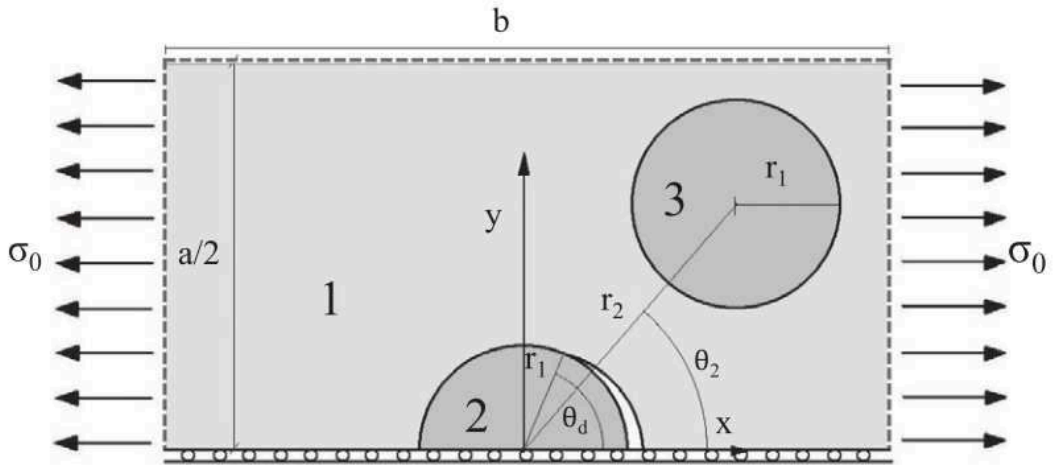

Fig.16 Illustration of two fibers numerical model. Figure adopted from [112]

2. Objectives of current thesis

Based on the previous discussions, it's clear that fiber/matrix interface debonding plays a key role in leading the initiation of the first damage event (i.e. transverse cracking) or final failure in a composite. Although single fiber composite model has been widely adopted by researchers conducting investigation on the fiber/matrix interface debonding mechanism, it's now commonly accepted that single fiber composite model has major limitations and thus could not be a good representative of real composite. Despite the efforts by various research groups, current state of understanding on the fiber/matrix debond process is still limited, especially when the local micro-structures are present. There are uncertainties regarding to the effects of local micro-structures on fiber/matrix interface debonding process. As a result, this thesis is aiming to clarify some of those mysteries by specifically investigating the effects of presence of neighboring fibers on debond growth under longitudinal tension or transverse tension. The objectives of current thesis could thus be summarized into following two parts:

1. As the first part of the research, we will try to clarify the effects of neighboring fibers and their closeness on fiber/matrix debond growth under longitudinal tension. In this part of investigation, the debond growth from single fiber break will be studied using both axisymmetric and 3-D finite element (FE) model.

ERR is considered as the driving force for debond growth. Both energy method and fracture mechanics method will be adopted in order to calculate ERR; the distance between neighboring fibers and debonded fiber is varied in order to investigate the effect of fiber closeness on debond growth. Finally, we will also compare the results obtained from both axisymmetric and 3-D models to make an assessment of the ability of different FE model on this issue.

2. As the second part of the research. We will investigate the influence of neighboring fibers on fiber/matrix debond growth under transverse tension. In this part of study, debond is assumed to grow along circumferential direction of the fiber. Two scenarios will be studied, in the first case, only one debond is assumed to initiated, and the distance between neighboring fibers and debonded fiber would vary in order to investigate the effect of fiber closeness on transverse debond growth; In second case, besides the original debonded fiber, we would assume another fiber/matrix debonding occur at a neighboring fiber and try to clarify the effect of this debond in the neighboring fiber on the growth of original debond.

The current thesis research results in 5 scientific papers and we'll describe some highlights of each paper in the following section.

3. Summary of appended papers

3.1. Paper A

Paper A is the beginning of current thesis research. In this paper, an axisymmetric FE model was developed in order to investigate the ERR of debond emanating from a fiber break along fiber axis. For this case, it was found that there are two distinct regions, one is when debond length are relatively long, and thus there is no interaction between debond tip and fiber break, debond growth in self-similar way; another situation is when debond length is short, and there is strong interaction between debond tip and fiber break.

For self-similar debond, the axisymmetric model is shown in Fig.17. The model consists of a fiber as a central phase (denoted as F), surrounded by a matrix phase (M), neighboring fiber phase (F), another matrix phase (M) and effective composite phase (C).

For self-similar debond growth the ERR can be calculated from the condition that at fixed applied load F the bonded region with length dl_d (Fig.17a) becomes a debonded region with the same length dl_d (Fig.17b). Hence, the ERR for self-similar debond growth can be found using the potential energy change ΔU as:

$$G_{II} = \frac{\Delta U}{2\pi r_f dl_d} \tag{2}$$

For short debond, the axisymmetric model generated is displayed in Fig.18. In principle it is very similar to the 5 cylinder model used for self-similar debond ERR calculation (see Fig.17) with the difference that the fiber break is included in the model, the fiber is partly debonded (with debond length denoted as l_d in Fig.18) and the length of the model L_f is significantly larger. The ERR is calculated using Virtual Crack Closure Technique (VCCT) and J integral methods.

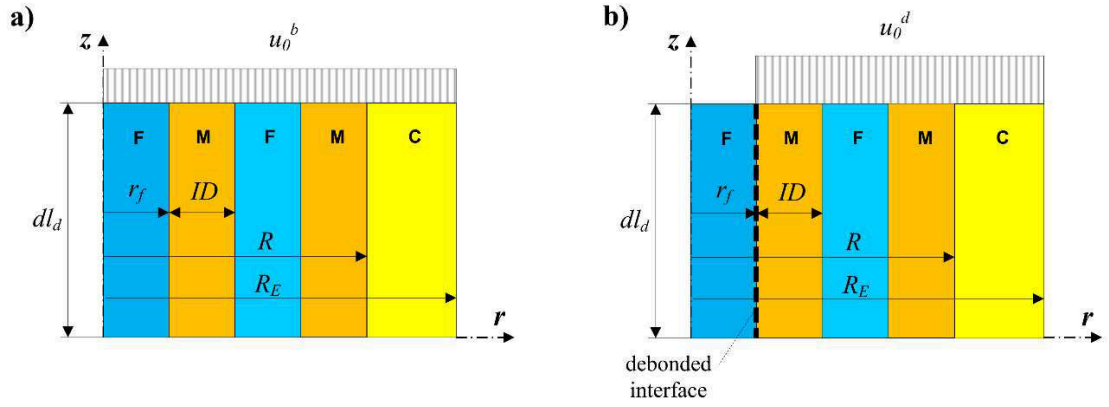

Fig.17 Schematic representation of a 5-phase FEM model: F – fiber, M – matrix, C – effective composite. a) bonded region; b) debonded region.

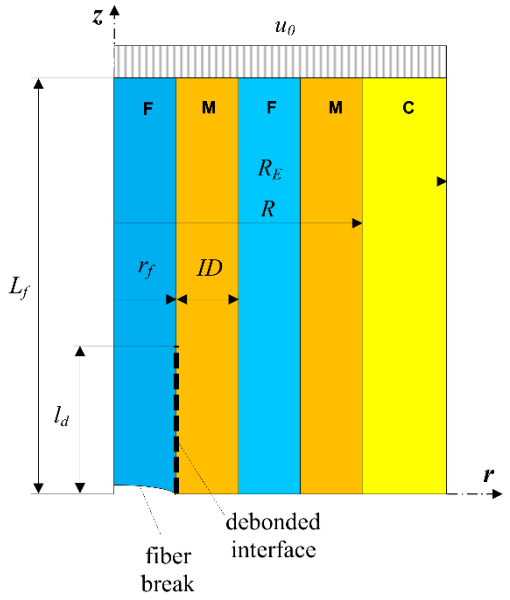

Fig.18 Schematic representation of a 5-phase concentric cylinder assembly FEM model for short debond energy release rate calculations: F –fiber, M – matrix, C – effective composite.

The major results of this paper are displayed in Figs.19 and 20. As shown in Fig. 19, for self-similar debond, for two fiber volume faction (Vf) studied, ERR is almost constant for differnet inter-fiber distance (IDn), which indicated that presence of fibers have little effect on ERR for self-similar debond. For short debond, as shown in Fig. 20, for each inter-fiber distance case, ERR decreases with increasing debond length and reaches a constant value when it approaches self-similar debond growth. The effect of neighboring fibers are more significant for shorter debond length.

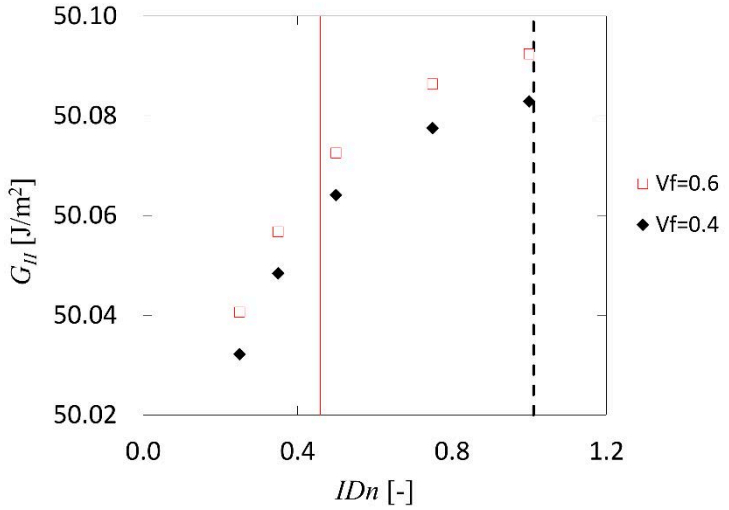

Fig. 19 Energy release rate as a function of inter-fiber distance for self-similar debond growth.

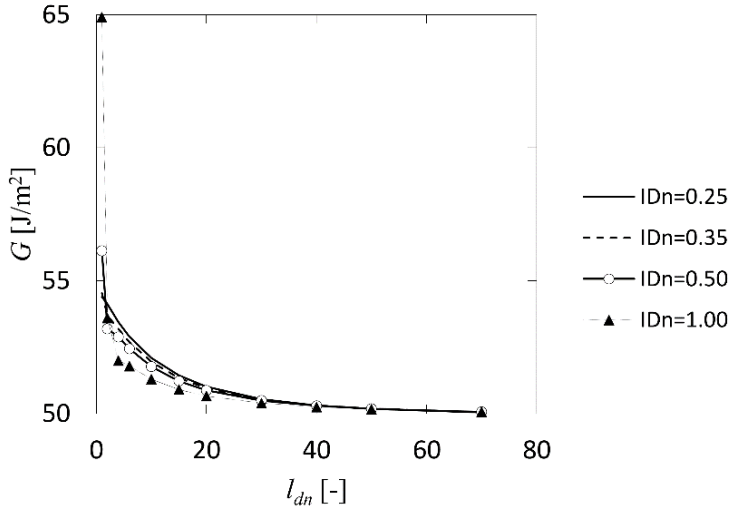

Fig. 20 Energy release rate as a function of normalized debond length.

3.2 Paper B

Paper B summarizes a countinous study following the work done in Paper A. In paper A, we investigated the longitudinal debond growth using an axisymmetric model. Although it's very convinient to use the axisymmtric model, we have to assume ERR is constant along debond front, which should not be the case as expected. As a result, In Paper B and Paper C, 3-D FE models (Fig.21) are created to investigate the possible angular variance of ERR and the difference between results obtained from 3-D model and axisymmetric model.

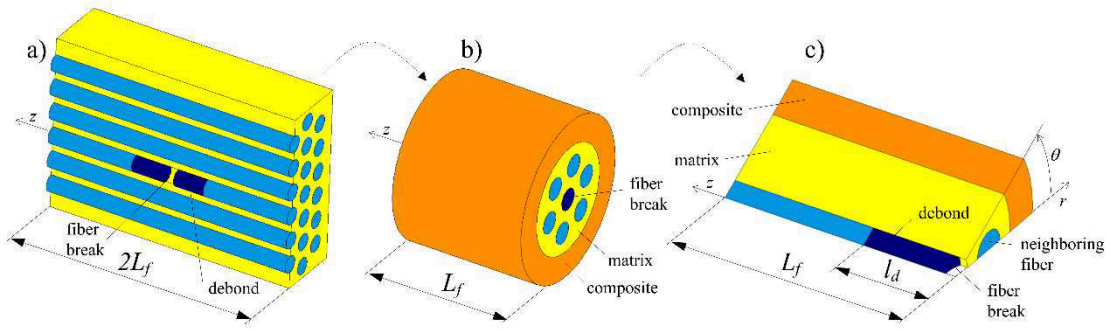

Fig. 21 a) UD composite with a broken and partially debonded fiber; b) Hexagonal distribution model; c) unit cell θ=30°

In Paper B, a 3-D FE model was first created to inverstigate the ERR of self-smiliar debond. Two different approaches are adopted to calculate the ERR. The first one is the enrgy method using the FE model shown in Fig. 22. It's based on the same procedures as decribed in Paper A, we calculated the ERR based on the difference of potential energy between two unit cells. The second approach was to using the short debond model (Fig.21), and calculate the ERR usnig VCCT and J integral for relatively long debond length when debond is in a self-similar growth. This approaches is based on the findings in Fig.20, as we found ERR reaches a plateau for long debond length.

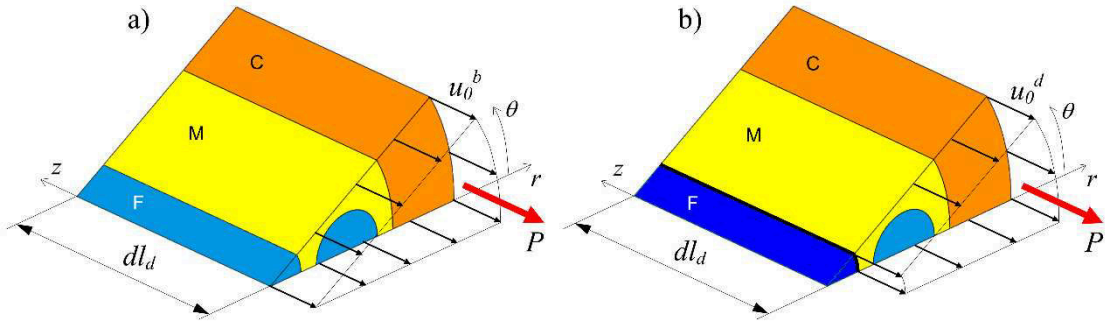

Fig.22. Representative volume element of bonded region (a) with length dl_d, which due to debond growth changes to debonded region (b) with length dl_d

We now discuss some major results obtained from this study. First let's look at the ERR result obtained using J integral based on short debond model. The angular variation of ERR along debond front is very clear for each inter-fiber distance case (represented by local volume fraction V_f^{loc}, as displayed in Fig.23. And ERR has the maximum at θ = 0º where distance between two fibers are the closest.

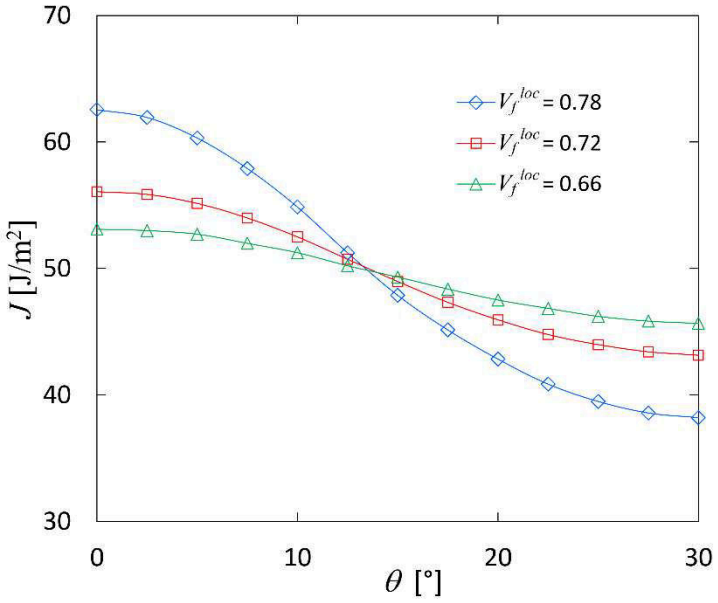

Fig.23 J-integral values for CF/EP $V_f = 0.6$ in purely mechanical loading $\varepsilon_z = 1\%$ obtained using the debond front model

Table 1. Energy release rate values for CF/EP $V_f = 0.6$ in purely mechanical loading $\varepsilon_z = 1\%$

	V_f^{loc}			
	0.66	0.72	0.78	0.60 (3-cyl)
G_{en} [J/m²]	50.22728	50.22197	50.21351	50.45131
J [J/m²]	49.38511	49.35217	49.27961	50.17184
G_I [J/m²]	-0.00238	-0.00241	-0.00210	0.01534
G_{II} [J/m²]	50.16155	50.21543	50.28309	49.08337
G_{III} [J/m²]	0.00460	0.00585	0.00500	0.000000

Table 2. Energy release rate values for CF/EP $V_f = 0.4$ in purely mechanical loading $\varepsilon_z = 1\%$

	V_f^{loc}		
	0.66	0.72	0.78
G_{en} [J/m^2]	50.22189	50.21631	50.20757
J [J/m^2]	49.54135	49.54620	49.47209
G_I [J/m^2]	-0.00245	-0.00246	-0.00219
G_{II} [J/m^2]	50.31723	50.39105	50.47968
G_{III} [J/m^2]	0.004496	0.00595	0.00453

Tables 1 and 2 show the comparison of averaged obtained ERR results for each debond length for each inter-fiber distance case with ERR calculated using energy method. Based on the results shown in Tables 1 and 2, ERR value is in good agreement for both models. Which give us an indication that for self-similar debond growth, although ERR is varied along debond front, the averaged ERR is almost constant and the presence of fibers has little effect on the averaged ERR.

The results discussed so far are for pure mechanical loading, the results for thermal loading could be found in Paper B attached in this thesis

3.3 Paper C

In Paper B, the ERR of self-similar debond emanating from a fiber break was calculated using 3-D models with the presence of neighboring fibers. In Paper C, we continued to look at the ERR of short debond using 3-D models displayed in Fig.21. Based on the discussion in Paper B, it's clearly that the ERR is varied along debond front. For short debond, under pure mechanical loading, the same feature is found, as

shown in Fig.24. As a result, it is suggested that debond front would not remain circular during growth in reality.

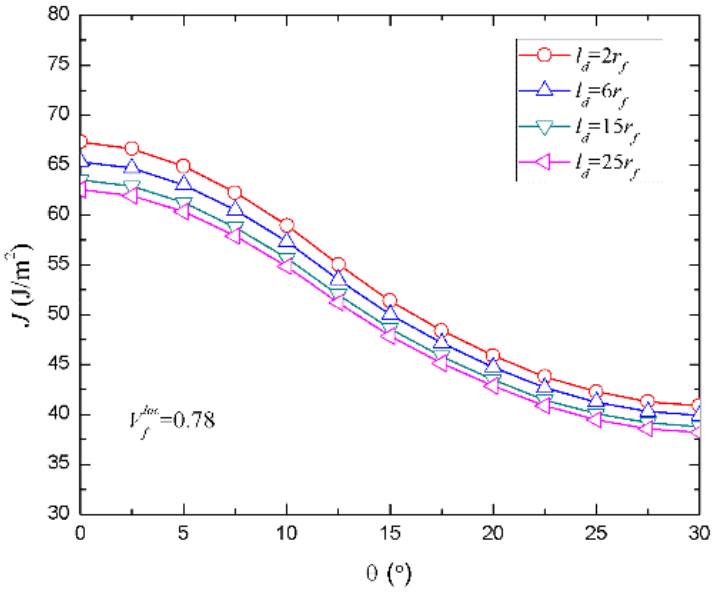

(a)

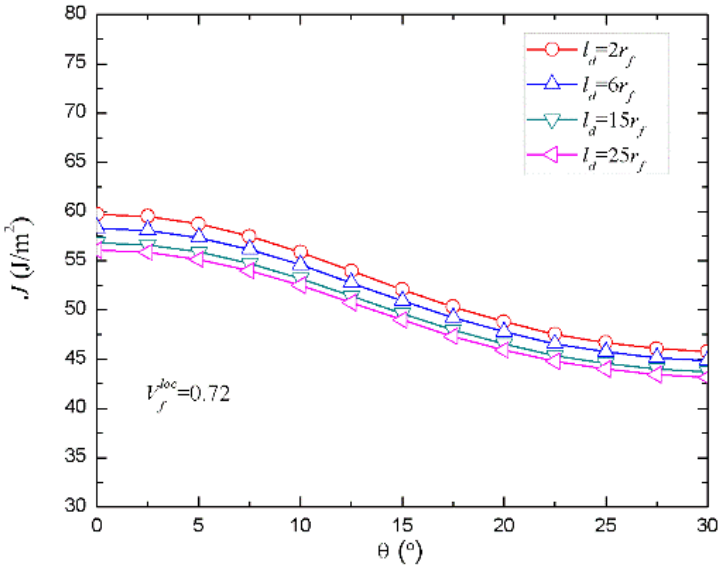

(b)

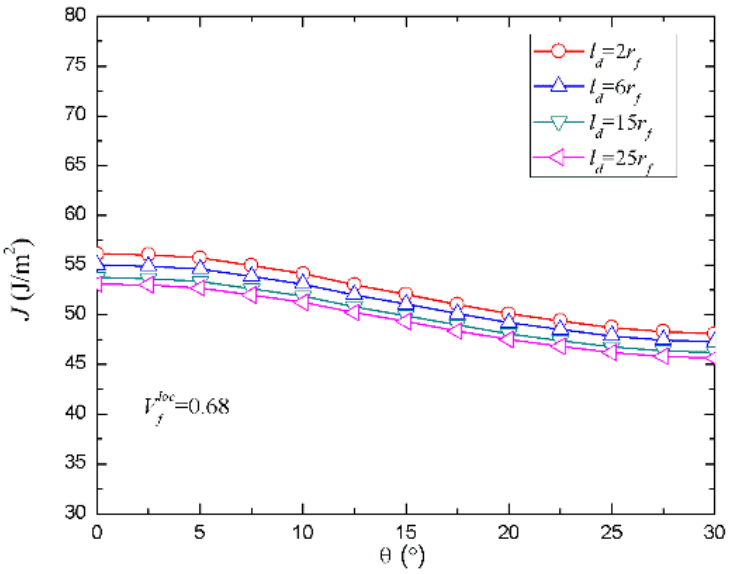

(c)

Fig.24 a). Angular dependence of J-integral values for CF/EP in mechanical loading. $\varepsilon_z = 1\%$, V_f^{loc}=0.78, b). Angular dependence of J-integral values for CF/EP in mechanical loading $\varepsilon_z = 1\%$, V_f^{loc}=0.72, c). Angular dependence of J-integral values for CF/EP in mechanical loading $\varepsilon_z = 1\%$, V_f^{loc}=0.68.

Another interesting finding is that when comparing the results between averaged ERR obtained through 3-D model and ERR calculated by axisymmetric model discussed in Paper A. As shown in Fig.25, the values obtained from axisymmetric model is slightly higher. This is due the fact the in axisymmetric model, the influence of neighboring fibers are highest and the same along debond front, as a result, the ERR calcuated by axisymmetric model could be viewed as the upper bond for this longitudinal debond growth case.

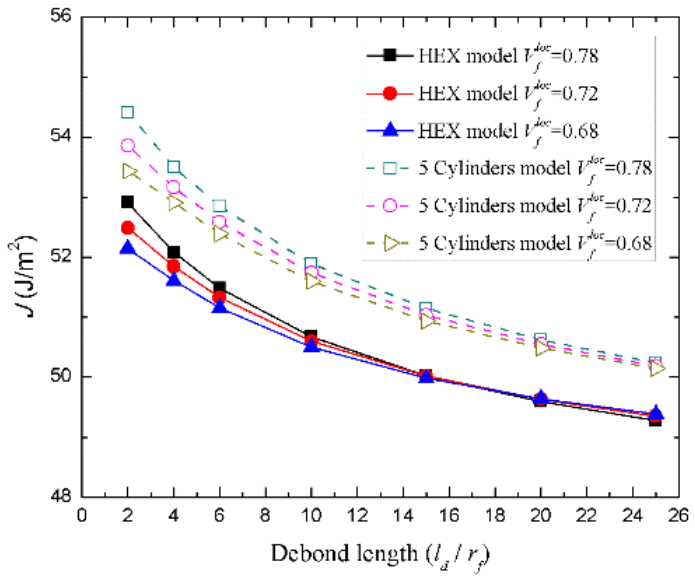

Fig. 25 Average ERR against normalized debond length obtained by the 3-D hexagonal model and axisymmetric model

3.4 Paper D

Previous 3 papers focus on investigating the growth of longitudinal debond with the presence of neighboring fibers. In Paper D, we switches out focus on the fiber/matrix interface debond growth under transverse tensile loading. In this case, the debond will grow along circumferential diretion along fiber/matrix interface. The FE model adopted in Paper D is shown in Fig.26, it follows the same concept as previous models developed for studying longitudinal debond growth: the debonded fiber is placed at the center of the model, surround by the nearest 6 fibers in a hexagonal array UD composite. The debond is assumed to initiated from the one side of fiber, as indicated in Fig.26. Due to symmetry, only one half of the composite is modelled.

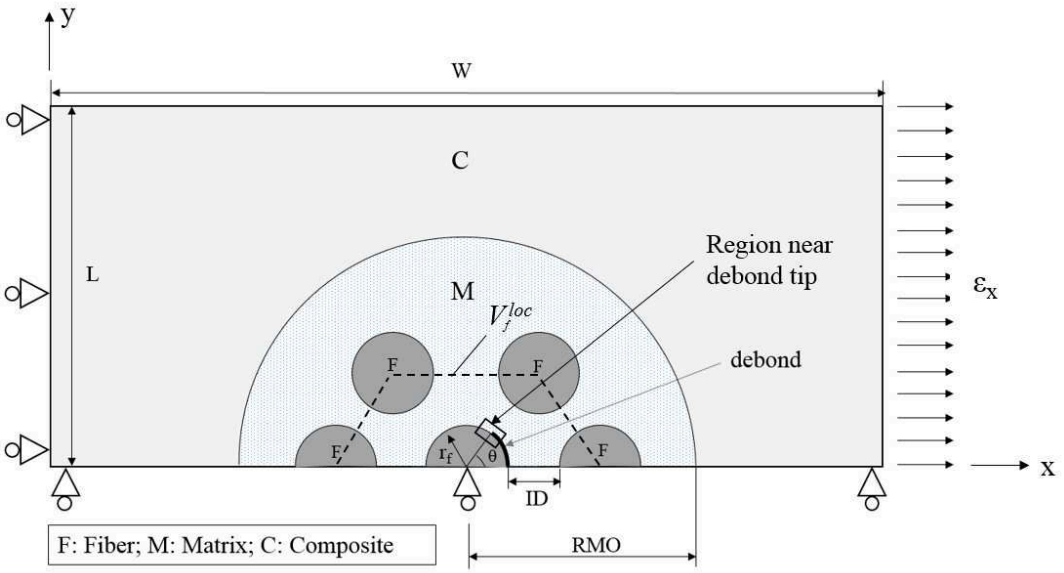

Fig.26 Model description

The general trend of ERR for transverse debond could be summarized in Figs. 27 – 29, which present the result for CF/Epoxy composite with volume fraction V_f=0.6. Fig.27 shows the ERR of debond under pure mechanical loading. It's shown that transverse debond growth is mixed-mode, for both mode I and mode II ERR components, they increases first with increasing debond angle and then decreases with further increasing of debond angle. For small debond angle, debond growth is mode I dominated and then switches to mode II dominated. At semi-debond angle at around 70º, crack surface come into contact significantly and debond grows in pure mode II. This angle where debond growth changes to pure mode II is called the transition angle, and that transition angle depends on the material system. For very small debond angle, the ERR increases with decreasing inter-fiber distance (or increasing V_f^{loc}).

For when theraml stress due to cooldown process is considered, the ERR is found to derease compared to the results obtained in pure mechanical loading (Fig.28). This is due to the compressive stress generated during thermal cooldown for UD composite. However, for a laminated composite, because of the constraint from neighboring plies, transverse plies developed tensile stress globally, which results in higher ERR for debond in a laminated composite , as shown in Fig.29.

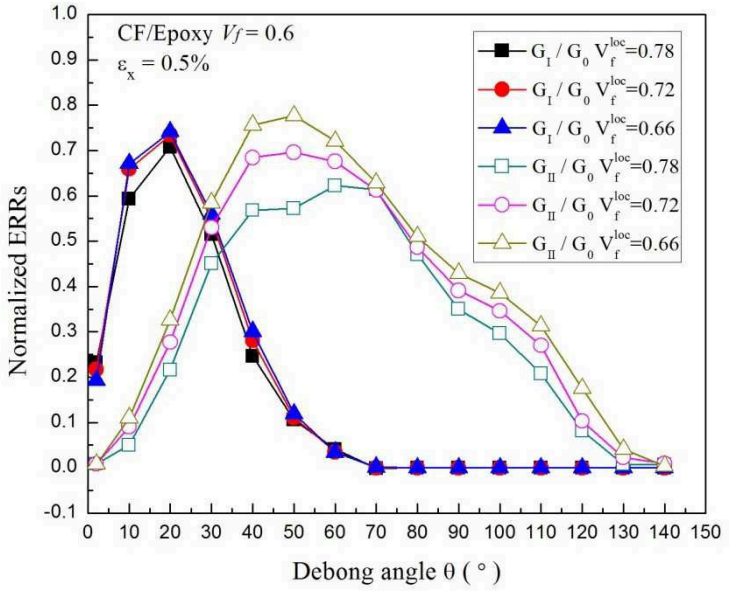

Fig.27 Normalized ERR with respect to debond angle for CF/EP UD composites under mechanical loading. $\varepsilon_x = 0.5\%$. $V_f = 0.6$

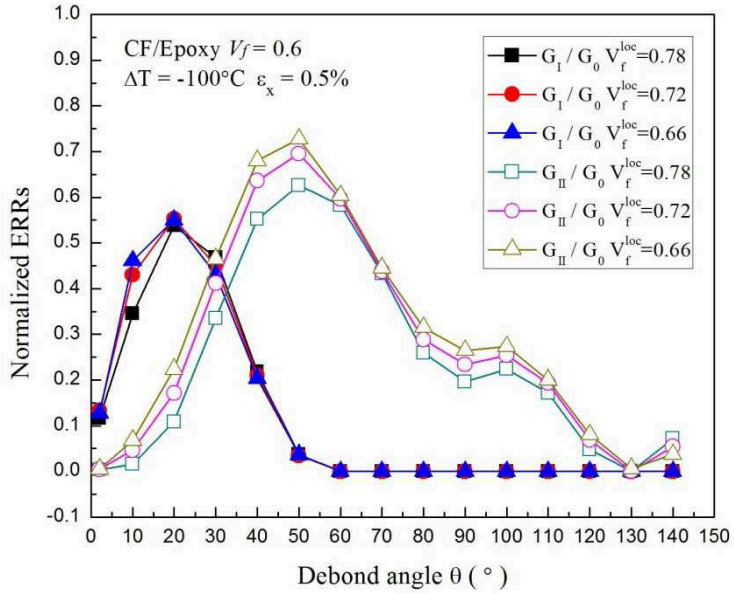

Fig.28 Normalized ERR with respect to debond angle for CF/EP UD composites under thermo-mechanical loading. $V_f = 0.6$, ΔT=-100°C, ε_x=0.5%

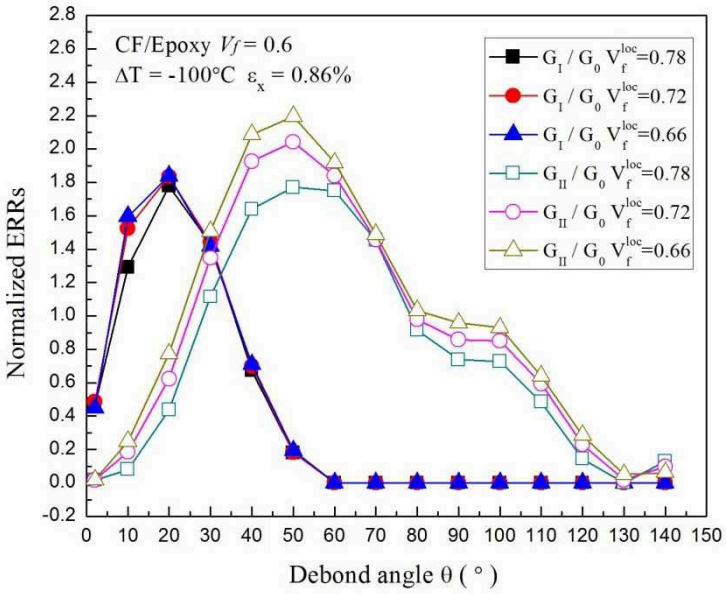

Fig. 29 Normalized ERR with respect to debond angle for CF/EP UD plies, equivalent to 90-layers of CF/EP cross-ply laminate under thermo-mechanical loading. V_f = 0.6, ΔT=-100°C, ε_x=0.86%

3.5 Paper E

In paper D we investigate the ERR of single transverse debond with the presence of neighboring fibers. Once the case for single transverse debond has been understood, we continue our inverstigation on the next relevant topic: what if there are two fiber/matrix interface debonds exist?.

In order to understand this problem, an FE model was created based on the previous mode discussed in Paper D. The difference is that in this model, another debond was assumed to be presence in neighboring fiber F1 or F2, as shown in Fig.30 (we only show debond in F1). Three cases of the composite with microdamage have been analyzed:

Case 1: The central fiber has a debond angle θ. Remaining fibers are perfectly bonded.

Case 2: The central fiber has a debond angle θ. Fiber F1 has Semi-angle of 60° debond on the left side.

Case 3: The central fiber has a debond angle θ. Fiber F2 has 60° debond on the right side.

The main results for Case 1 and Case 2 are shown in Fig. 31. Based on the results displayed in Fig.31, it is clear that the presence of neighboring debonds increase the

ERR of central debond significantly, and that effect is more prominent when inter-fiber distance (IDn) is smaller.

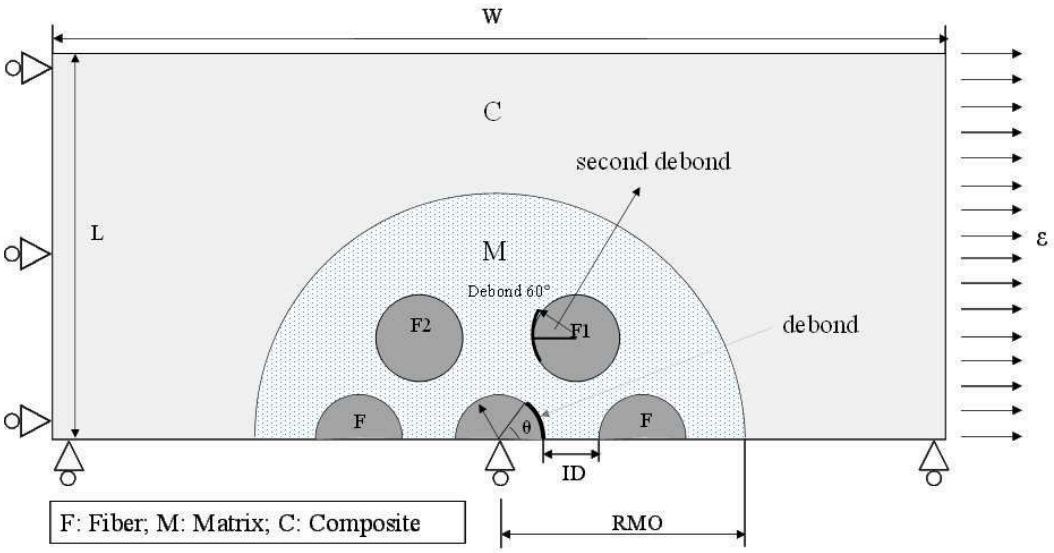

Fig.30 Schematics of the model used for debond growth analysis around the central fiber showing explicitly the central fiber and the 6 closest fibers. One of them may have a Semi-angle of 60° debond on one side. The fiber/matrix unit is embedded in a homogenized composite.

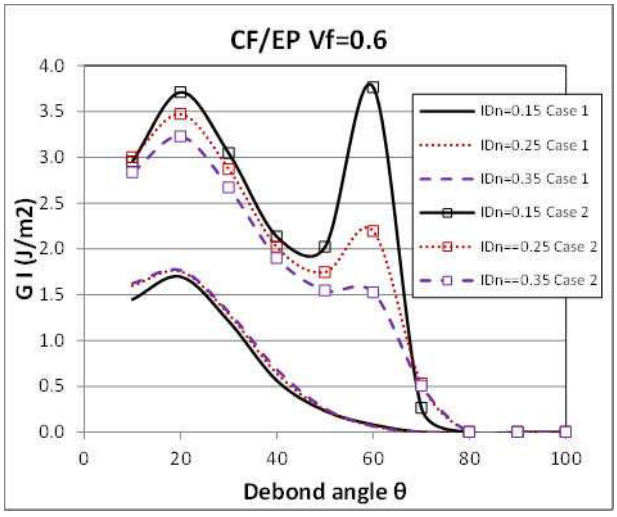

(a)

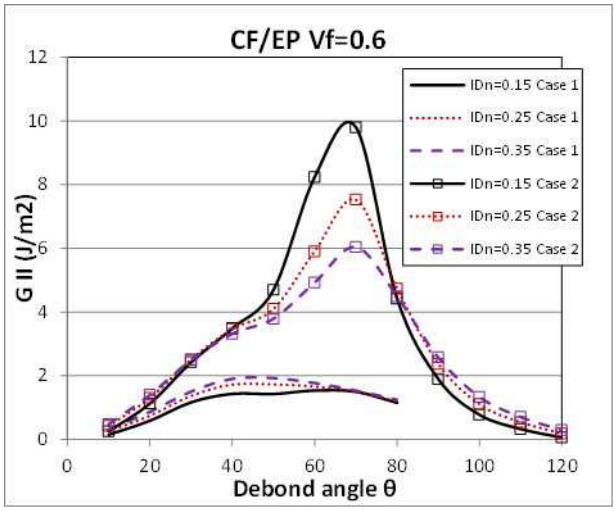

(b)

Fig.31 Energy release rate versus debond length and Case 1 and Case 2 for different values of interfiber distance: a) Mode I: b) Mode II.

References

1. Talreja, R., *Fatigue of composite materials: damage mechanisms and fatigue-life diagrams.* Proceedings of the Royal Society of London. A. Mathematical and Physical Sciences, 1981. **378**(1775): p. 461-475.
2. Gamstedt, E. and R. Talreja, *Fatigue damage mechanisms in unidirectional carbon-fibre-reinforced plastics.* Journal of Materials Science, 1999. **34**(11): p. 2535-2546.
3. Gamstedt, E.K., L.A. Berglund, and T. Peijs, *Fatigue mechanisms in unidirectional glass-fibre-reinforced polypropylene.* Composites Science and Technology, 1999. **59**(5): p. 759-768.
4. Pupurs, A., *Micro-crack Initiation and Propagation in Fiber Reinforced Composites*, in *Engineering Sciences and Mathematics*. 2012, Luleå University of Technology.
5. Hull, D. and T.W. Clyne, *An Introduction to Composite Materials:*. 1996, Cambridge: Cambridge University Press.
6. Hedgepeth, J.M., *Stress concentrations in filamentary structures.* NASA TND-882, 1961.
7. Hedgepeth, J.M. and P. Van Dyke, *Local stress concentrations in imperfect filamentary composite materials.* Journal of composite materials, 1967. **1**(3): p. 294-309.
8. Fukuda, H. and K. Kawata, *On the stress concentration factor in fibrous composites.* Fibre Science and Technology, 1976. **9**(3): p. 189-203.
9. Goree, J.G. and R.S. Gross, *Stresses in a three-dimensional unidirectional composite containing broken fibers.* Engineering Fracture Mechanics, 1980. **13**(2): p. 395-405.
10. Fukuda, H., *Stress concentration factors in unidirectional composites with random fiber spacing.* Composites Science and Technology, 1985. **22**(2): p. 153-163.
11. Ochiai, S., K. Schulte, and P.W. Peters, *Strain concentration factors for fibers and matrix in unidirectional composites.* Composites science and technology, 1991. **41**(3): p. 237-256.

12. Nedele, M. and M. Wisnom, *Stress concentration factors around a broken fibre in a unidirectional carbon fibre-reinforced epoxy.* Composites, 1994. **25**(7): p. 549-557.
13. Nedele, M.R. and M.R. Wisnom, *Three-dimensional finite element analysis of the stress concentration at a single fibre break.* Composites science and technology, 1994. **51**(4): p. 517-524.
14. Case, S., et al., *Fiber fracture in unidirectional composites.* Journal of composite materials, 1995. **29**(2): p. 208-228.
15. Grubb, D.T., Z.-F. Li, and S.L. Phoenix, *Measurement of stress concentration in a fiber adjacent to a fiber break in a model composite.* Composites science and technology, 1995. **54**(3): p. 237-249.
16. Beyerlein, I.J. and S.L. Phoenix, *Stress concentrations around multiple fiber breaks in an elastic matrix with local yielding or debonding using quadratic influence superposition.* Journal of the Mechanics and Physics of Solids, 1996. **44**(12): p. 1997-2039.
17. Heuvel, v.d.P., T. Peijs, and R. Young, *Analysis of stress concentrations in multi-fibre microcomposites by means of Raman spectroscopy.* Journal of materials science letters, 1996. **15**(21): p. 1908-1911.
18. Van den Heuvel, P., Y. Van der Bruggen, and T. Peijs, *Failure phenomena in multi-fibre model composites: Part 1. An experimental investigation into the influence of fibre spacing and fibre—matrix adhesion.* Composites Part A: Applied Science and Manufacturing, 1996. **27**(9): p. 855-859.
19. Chohan, V. and C. Galiotis, *Effects of interface, volume fraction and geometry on stress redistribution in polymer composites under tension.* Composites Science and Technology, 1997. **57**(8): p. 1089-1101.
20. van den Heuvel, P.W.J., T. Peijs, and R.J. Young, *Failure phenomena in two-dimensional multifibre microcomposites: 2. A Raman spectroscopic study of the influence of inter-fibre spacing on stress concentrations.* Composites Science and Technology, 1997. **57**(8): p. 899-911.
21. Van den Heuvel, P., T. Peijs, and R. Young, *Failure phenomena in two-dimensional multi-fibre microcomposites—3. A raman spectroscopy study of the influence of interfacial debonding on stress concentrations.* Composites science and technology, 1998. **58**(6): p. 933-944.

22. Van den Heuvel, P., et al., *Failure phenomena in two-dimensional multi-fibre model composites: 5. a finite element study.* Composites Part A: Applied Science and Manufacturing, 1998. **29**(9-10): p. 1121-1135.
23. Van den Heuvel, P., T. Peijs, and R. Young, *Failure phenomena in two-dimensional multi-fibre microcomposites. Part 4: a Raman spectroscopic study on the influence of the matrix yield stress on stress concentrations.* Composites Part A: Applied Science and Manufacturing, 2000. **31**(2): p. 165-171.
24. Van den Heuvel, P., et al., *Failure phenomena in fibre-reinforced composites. Part 6: a finite element study of stress concentrations in unidirectional carbon fibre-reinforced epoxy composites.* Composites science and technology, 2004. **64**(5): p. 645-656.
25. St-Pierre, L., N.J. Martorell, and S.T. Pinho, *Stress redistribution around clusters of broken fibres in a composite.* Composite Structures, 2017. **168**: p. 226-233.
26. Rosen, B.W., *Tensile failure of fibrous composites.* AIAA journal, 1964. **2**(11): p. 1985-1991.
27. Zweben, C., *Tensile failure of fiber composites.* AIAA journal, 1968. **6**(12): p. 2325-2331.
28. Zweben, C. and B.W. Rosen, *A statistical theory of material strength with application to composite materials.* Journal of the Mechanics and Physics of Solids, 1970. **18**(3): p. 189-206.
29. Harlow, D.G. and S.L. Phoenix, *The chain-of-bundles probability model for the strength of fibrous materials I: analysis and conjectures.* Journal of composite materials, 1978. **12**(2): p. 195-214.
30. Harlow, D.G. and S.L. Phoenix, *The chain-of-bundles probability model for the strength of fibrous materials II: a numerical study of convergence.* Journal of composite materials, 1978. **12**(3): p. 314-334.
31. Batdorf, S., *Tensile strength of unidirectionally reinforced composites—I.* Journal of reinforced plastics and composites, 1982. **1**(2): p. 153-164.
32. Batdorf, S. and R. Ghaffarian, *Tensile strength of unidirectionally reinforced composites—II.* Journal of reinforced plastics and composites, 1982. **1**(2): p. 165-176.

33. Wisnom, M.R. and D. Green, *Tensile failure due to interaction between fibre breaks.* Composites, 1995. **26**(7): p. 499-508.
34. Purslow, D., *Some fundamental aspects of composites fractography.* Composites, 1981. **12**(4): p. 241-247.
35. Blassiau, S., A. Thionnet, and A.R. Bunsell, *Micromechanisms of load transfer in a unidirectional carbon fibre–reinforced epoxy composite due to fibre failures. Part 1: Micromechanisms and 3D analysis of load transfer: The elastic case.* Composite structures, 2006. **74**(3): p. 303-318.
36. Blassiau, S., A. Thionnet, and A.R. Bunsell, *Micromechanisms of load transfer in a unidirectional carbon fibre–reinforced epoxy composite due to fibre failures. Part 2: Influence of viscoelastic and plastic matrices on the mechanisms of load transfer.* Composite Structures, 2006. **74**(3): p. 319-331.
37. Thionnet, A., H.Y. Chou, and A. Bunsell, *Fibre break processes in unidirectional composites.* Composites Part A: Applied Science and Manufacturing, 2014. **65**: p. 148-160.
38. Thionnet, A., H.-Y. Chou, and A. Bunsell, *Fibre Break Failure Processes in Unidirectional Composites. Part 1: Failure and Critical Damage State Induced by Increasing Tensile Loading.* Applied Composite Materials, 2014. **22**(2): p. 119-140.
39. Swolfs, Y., I. Verpoest, and L. Gorbatikh, *Issues in strength models for unidirectional fibre-reinforced composites related to Weibull distributions, fibre packings and boundary effects.* Composites Science and Technology, 2015. **114**: p. 42-49.
40. Swolfs, Y., I. Verpoest, and L. Gorbatikh, *A review of input data and modelling assumptions in longitudinal strength models for unidirectional fibre-reinforced composites.* Composite Structures, 2016. **150**: p. 153-172.
41. Aroush, D.R.-B., et al., *A study of fracture of unidirectional composites using in situ high-resolution synchrotron X-ray microtomography.* Composites science and technology, 2006. **66**(10): p. 1348-1353.
42. Garcea, S.C., I. Sinclair, and S.M. Spearing, *Fibre failure assessment in carbon fibre reinforced polymers under fatigue loading by synchrotron X-ray computed tomography.* Composites Science and Technology, 2016. **133**: p. 157-164.

43. Swolfs, Y., et al., *Matrix cracks around fibre breaks and their effect on stress redistribution and failure development in unidirectional composites.* Composites Science and Technology, 2015. **108**: p. 16-22.
44. Zhuang, L., R. Talreja, and J. Varna, *Tensile failure of unidirectional composites from a local fracture plane.* Composites Science and Technology, 2016. **133**: p. 119-127.
45. Kelly, A., *Interface effects and the work of fracture of a fibrous composite.* Proceedings of the Royal Society of London. A. Mathematical and Physical Sciences, 1970. **319**(1536): p. 95-116.
46. Nair, S.V., *Crack-Wake Debonding and Toughness in Fiber-or Whisker-Reinforced Brittle-Matrix Composites.* Journal of the American Ceramic Society, 1990. **73**(10): p. 2839-2847.
47. Hughes, J., *The carbon fibre/epoxy interface—a review.* Composites Science and Technology, 1991. **41**(1): p. 13-45.
48. Sjögren, B. and L.A. Berglund, *The effects of matrix and interface on damage in GRP cross-ply laminates.* Composites Science and Technology, 2000. **60**(1): p. 9-21.
49. Zafeiropoulos, N., et al., *Engineering and characterisation of the interface in flax fibre/polypropylene composite materials. Part I. Development and investigation of surface treatments.* Composites Part A: Applied Science and Manufacturing, 2002. **33**(8): p. 1083-1093.
50. Rich, M.J. and L. Drzal, *Interfacial properties of some high-strain carbon fibers in an epoxy matrix.* Journal of reinforced plastics and composites, 1988. **7**(2): p. 145-154.
51. Netravali, A., et al., *Interfacial shear strength studies using the single-filament-composite test. I: Experiments on graphite fibers in epoxy.* Polymer Composites, 1989. **10**(4): p. 226-241.
52. Tripathi, D. and F. Jones, *Single fibre fragmentation test for assessing adhesion in fibre reinforced composites.* Journal of materials science, 1998. **33**(1): p. 1-16.
53. Kim, B.W. and J.A. Nairn, *Observations of fiber fracture and interfacial debonding phenomena using the fragmentation test in single fiber composites.* Journal of Composite Materials, 2002. **36**(15): p. 1825-1858.

54. Okabe, T. and N. Takeda, *Elastoplastic shear-lag analysis of single-fiber composites and strength prediction of unidirectional multi-fiber composites.* Composites Part A: Applied Science and Manufacturing, 2002. **33**(10): p. 1327-1335.
55. Pupurs, A. and J. Varna, *Fracture mechanics analysis of debond growth in a single-fiber composite under cyclic loading.* Mechanics of Composite Materials, 2011. **47**(1): p. 109-124.
56. Wagner, H. and A. Eitan, *Interpretation of the fragmentation phenomenon in single-filament composite experiments.* Applied physics letters, 1990. **56**(20): p. 1965-1967.
57. Gulino, R. and S. Phoenix, *Weibull strength statistics for graphite fibres measured from the break progression in a model graphite/glass/epoxy microcomposite.* Journal of materials science, 1991. **26**(11): p. 3107-3118.
58. Zhao, F.M., T. Okabe, and N. Takeda, *The estimation of statistical fiber strength by fragmentation tests of single-fiber composites*

Composites science and technology, 2000. **60**(10): p. 1965-1974.
59. Yavin, B., et al., *Continuous monitoring of the fragmentation phenomenon in single fiber composite materials.* Polymer Composites, 1991. **12**(6): p. 436-446.
60. Kelly, A. and a.W. Tyson, *Tensile properties of fibre-reinforced metals: copper/tungsten and copper/molybdenum.* Journal of the Mechanics and Physics of Solids, 1965. **13**(6): p. 329in1339-338in2350.
61. Netravali, A., et al., *An acoustic emission technique for measuring fiber fragment length distributions in the single-fiber-composite test.* Composites science and technology, 1989. **35**(1): p. 13-29.
62. Liu, H.-Y., et al., *Stress transfer in the fibre fragmentation test: Part III Effect of matrix cracking and interface debonding.* Journal of materials science, 1997. **32**(3): p. 633-641.
63. Nishikawa, M., et al., *Micromechanics of the fragmentation process in single-fiber composites.* Modelling and Simulation in Materials Science and Engineering, 2008. **16**(5): p. 055009.

64. Selvadurai, A. and A. Ten Busschen, *Mechanics of the segmentation of an embedded fiber. II: Computational modeling and comparisons.* Journal of applied mechanics, 1995. **62**(1): p. 98-107.
65. Fraser, W., et al., *Evaluation of surface treatments for fibers in composite materials.* Polymer Composites, 1983. **4**(4): p. 238-248.
66. Curtin, W., *Exact theory of fibre fragmentation in a single-filament composite.* Journal of materials science, 1991. **26**(19): p. 5239-5253.
67. Nairn, J.A., *A variational mechanics analysis of the stresses around breaks in embedded fibers.* Mechanics of Materials, 1992. **13**(2): p. 131-154.
68. Graciani, E., et al. *Single fiber fragmentation test. A BEM analysis*. in *Collection of Technical Papers-AIAA/ASME/ASCE/AHS/ASC Structures, Structural Dynamics and Materials Conference*. 2003.
69. Sastry, A. and S. Phoenix, *Shielding and magnification of loads in elastic, unidirectional composites.* SAMPE journal, 1994. **30**: p. 61-61.
70. Li, Z.-F., D.T. Grubb, and S.L. Phoenix, *Fiber interactions in the multi-fiber composite fragmentation test.* Composites science and technology, 1995. **54**(3): p. 251-266.
71. Pupurs, A. and J. Varna, *Unidirectional composite in mechanical fatigue: modelling debond growth from fibre breaks.* Plastics, Rubber and Composites, 2010. **39**(3-5): p. 128-136.
72. Pupurs, A., A. Krasnikovs, and J. Varna, *Energy release rate based fiber/matrix debond growth in fatigue. Part II: Debond growth analysis using Paris law.* Mechanics of Advanced Materials and Structures, 2013. **20**(4): p. 288-296.
73. Pupurs, A. and J. Varna, *Energy release rate based fiber/matrix debond growth in fatigue. Part I: Self-similar crack growth.* Mechanics of Advanced Materials and Structures, 2013. **20**(4): p. 276-287.
74. Pupurs, A. and J. Varna, *FEM modeling of fiber/matrix debond growth in tension-tension cyclic loading of unidirectional composites.* International Journal of Damage Mechanics, 2013. **22**(8): p. 1144-1160.
75. Pupurs, A. and J. Varna, *Analytical solution for energy release rate due to steady-state fiber/matrix debond growth in UD composites.* International Journal of Damage Mechanics, 2016

76. Highsmith, A. and K. Reifsnider, *Stiffness reduction mechanisms in composite laminates.* Damage in composite materials, 1982. **775**: p. 103?17.
77. Laws, N., G.J. Dvorak, and M. Hejazi, *Stiffness changes in unidirectional composites caused by crack systems.* Mechanics of Materials, 1983. **2**(2): p. 123-37.
78. Manders, P.W., et al., *Statistical analysis of multiple fracture in 0/90/0 glass fibre/epoxy resin laminates.* Journal of Materials Science, 1983. **18**(10): p. 2876-2889.
79. Talreja, R., *Transverse cracking and stiffness reduction in composite laminates.* Journal of composite materials, 1985. **19**(4): p. 355.
80. Varna, J. and L. Berglund, *Multiple transverse cracking and stiffness reduction in cross-ply laminates.* Journal of Composites Technology and Research, 1991. **13**(2): p. 97-106.
81. Romanov, V.S., et al., *Modelling evidence of stress concentration mitigation at the micro-scale in polymer composites by the addition of carbon nanotubes.* Carbon, 2015. **82**: p. 184-194.
82. Garrett, K. and J. Bailey, *Multiple transverse fracture in 90 cross-ply laminates of a glass fibre-reinforced polyester.* Journal of Materials Science, 1977. **12**(1): p. 157-168.
83. Parvizi, A. and J. Bailey, *On multiple transverse cracking in glass fibre epoxy cross-ply laminates.* Journal of Materials Science, 1978. **13**(10): p. 2131-2136.
84. Parvizi, A., K. Garrett, and J. Bailey, *Constrained cracking in glass fibre-reinforced epoxy cross-ply laminates.* Journal of Materials Science, 1978. **13**(1): p. 195-201.
85. Reifsnider, K. *Some fundamental aspects of the fatigue and fracture response of composite materials*. in *Proceedings 14th Annual Meeting, Society of Engineering Science of Engineering Science*. 1977. Bethlehem, USA.
86. Stinchcomb, W.W. and K.L. Reifsnider, *FATIGUE DAMAGE MECHANISMS IN COMPOSITE MATERIALS: A REVIEW.* ASTM Special Technical Publication, 1979(675): p. 762-787.
87. Reifsnider, K. and A. Highsmith, *Characteristic damage states: a new approach to representing fatigue damage in composite laminates.* Materials Experimentation and Design in Fatigue, 1981: p. 246-260.

88. Aveston, J., G. Cooper, and A. Kelly. *The properties of fibre composites*. 1971.
89. Aveston, J. and A. Kelly, *Theory of multiple fracture of fibrous composites.* Journal of Materials Science, 1973. **8**(3): p. 352-362.
90. Hashin, Z., *Analysis of cracked laminates: a variational approach.* Mechanics of materials, 1985. **4**(2): p. 121-136.
91. Nairn, J.A., *The strain energy release rate of composite microcracking: a variational approach.* Journal of composite materials, 1989. **23**(11): p. 1106-1129.
92. Huang, Y., J. Varna, and R. Talreja, *Statistical methodology for assessing manufacturing quality related to transverse cracking in cross ply laminates.* Composites Science and Technology, 2014. **95**(0): p. 100-106.
93. Asp, L.E., L.A. Berglund, and P. Gudmundson, *Effects of a composite-like stress state on the fracture of epoxies.* Composites Science and Technology, 1995. **53**(1): p. 27-37.
94. Asp, L., L.A. Berglund, and R. Talreja, *Prediction of matrix-initiated transverse failure in polymer composites.* Composites Science and Technology, 1996. **56**(9): p. 1089-1097.
95. Asp, L., L.A. Berglund, and R. Talreja, *A criterion for crack initiation in glassy polymers subjected to a composite-like stress state.* Composites Science and Technology, 1996. **56**(11): p. 1291-1301.
96. Asp, L., L.A. Berglund, and R. Talreja, *Effects of fiber and interphase on matrix-initiated transverse failure in polymer composites.* Composites Science and Technology, 1996. **56**(6): p. 657-665.
97. Fiedler, B., et al., *Failure behavior of an epoxy matrix under different kinds of static loading.* Composites Science and Technology, 2001. **61**(11): p. 1615-1624.
98. Fiedler, B., et al., *Finite-element modeling of initial matrix failure in CFRP under static transverse tensile load.* Composites Science and Technology, 2001. **61**(1): p. 95-105.
99. Fiedler, B., M. Hojo, and S. Ochiai, *The influence of thermal residual stresses on the transverse strength of CFRP using FEM.* Composites Part A: applied science and manufacturing, 2002. **33**(10): p. 1323-1326.

100. Zhang, H., et al., *Transverse single-fibre test for interfacial debonding in composites: 1. Experimental observations.* Composites Part A: Applied Science and Manufacturing, 1997. **28**(4): p. 309-315.
101. París, F., E. Correa, and V. Mantič, *Kinking of transversal interface cracks between fiber and matrix.* Journal of Applied Mechanics, 2007. **74**(4): p. 703-716.
102. Toya, M., *A crack along the interface of a circular inclusion embedded in an infinite solid.* Journal of the Mechanics and Physics of Solids, 1974. **22**(5): p. 325-348.
103. París, F., J. Cano, and J. Varna, *The fiber-matrix interface crack—a numerical analysis using boundary elements.* International journal of fracture, 1990. **82**(1): p. 11-29.
104. Varna, J., F. Paris, and J.C. del Cano, *The effect of crack-face contact on fiber/matrix debonding in transverse tensile loading.* Composites Science and Technology, 1997. **57**(5): p. 523-532.
105. Correa, E., V. Mantič, and F. París, *Effect of thermal residual stresses on matrix failure under transverse tension at micromechanical level: A numerical and experimental analysis.* Composites Science and Technology, 2011. **71**(5): p. 622-629.
106. García, I.G., V. Mantič, and E. Graciani, *Debonding at the fibre–matrix interface under remote transverse tension. One debond or two symmetric debonds?* European Journal of Mechanics - A/Solids, 2015. **53**: p. 75-88.
107. Carraro, P.A. and M. Quaresimin, *Modelling fibre–matrix debonding under biaxial loading.* Composites Part A: Applied Science and Manufacturing, 2014. **61**(0): p. 33-42.
108. Mantič, V., et al., *A linear elastic-brittle interface model: application for the onset and propagation of a fibre-matrix interface crack under biaxial transverse loads.* International Journal of Fracture, 2015. **195**(1-2): p. 15-38.
109. Bouhala, L., et al., *Modelling of failure in long fibres reinforced composites by X-FEM and cohesive zone model.* Composites Part B: Engineering, 2013. **55**: p. 352-361.

110. Távara, L., et al., *Modelling interfacial debonds in unidirectional fibre-reinforced composites under biaxial transverse loads.* Composite Structures, 2016. **136**: p. 305-312.
111. Kushch, V.I., et al., *Numerical simulation of progressive debonding in fiber reinforced composite under transverse loading.* International Journal of Engineering Science, 2011. **49**(1): p. 17-29.
112. Sandino, C., E. Correa, and F. París, *Numerical analysis of the influence of a nearby fibre on the interface crack growth in composites under transverse tensile load.* Engineering Fracture Mechanics, 2016. **168, Part B**: p. 58-75.

Paper A

EFFECT OF NEIGHBORING FIBERS ON ENERGY RELEASE RATE DURING FIBER/MATRIX DEBOND GROWTH

EFFECT OF NEIGHBORING FIBERS ON ENERGY RELEASE RATE DURING FIBER/MATRIX DEBOND GROWTH

L. Zhuang[a,b], A. Pupurs[b,c*]

[a]*Department of Aerospace Engineering, Texas A&M University, College Station, TX-77843, USA*
[b]*Luleå University of Technology, SE 97187 Luleå, Sweden*
[c]*Swerea SICOMP, SE-94129, Piteå, Sweden*

**andrejs.pupurs@ltu.se*

Keywords: fiber breaks, debonding, energy release rate, FEM modeling

Abstract
In this paper fiber/matrix interface debond growth in unidirectional composites subjected to mechanical tensile loading is analyzed using fracture mechanics principles of energy release rate (ERR). The objective of the present study is to analyze the effect of neighboring fibers on the ERR. 5-cylinder axisymmetric FEM models with adjustable inter-fiber distance were used for ERR calculations. The results show that the ERR slightly increases with the inter-fiber distance in the case of long debonds. For short debonds, however, because the stress-state is more complex, it was found that the debond propagates in a mixed Mode I and Mode II and contribution of each mode to the ERR depends on the actual debond length. It was found that for very small debond lengths ERR significantly increases with the inter-fiber distance.

1. Introduction

When unidirectional (UD) composites are loaded in fiber direction in cyclic tension-tension and the tensile load is sufficiently high, multiple fiber breaks occur during the first cycle due to statistical distribution of fiber strength. Once the fiber breaks form, yielding of matrix or fiber/matrix debonding can be expected near the fiber breaks as a result of large shear stresses in the interface region. In the present paper we are focusing on fiber/matrix debonding (interface cracks) initiated at the fiber break and growing along the fiber, which may be the case for relatively weak fiber/matrix interfaces. Interface debond growth leads to progressive degradation of composite properties before the final catastrophic failure of the composite. Hence, quantification of debond crack growth rate in cyclic loading is important. The debond growth in UD polymer composites has been previously analyzed in [1-3] using fracture mechanics principles of energy release rate (ERR). In polymeric composites, due to larger Poisson's ratio and larger coefficient of thermal expansion of the matrix the debond growth was shown

to propagate purely in Mode II [1-4] when subjected to tensile loading and negative temperature changes. It was shown in [1-4] with analytical and numerical models that debond growth rate is higher for short debonds due to interaction with fiber break which results in magnification of the ERR. As the debond crack propagates and the debond crack tip advances far away from the fiber break the debond growth becomes self-similar [2,4]. For such case (long debonds) exact analytical models for ERR calculation were developed in [1,3]. In [1-3] a cylindrical unit cell was used consisting of a broken and partially debonded fiber which is surrounded by a matrix cylinder. The effect of the surrounding composite in [1-3] was represented by an effective composite cylinder surrounding the fiber/matrix concentric cylinder unit cell, see Fig.1.

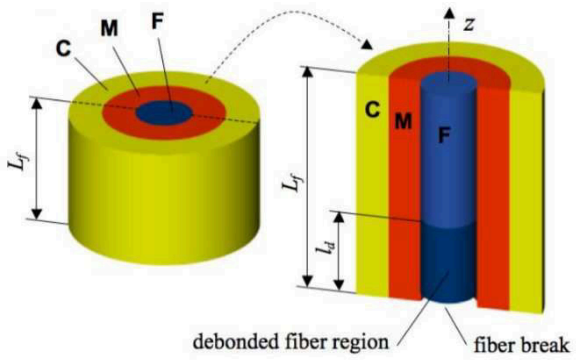

Figure 1. 3-phase concentric cylinder assembly model of a broken and partially debonded fiber in UD composite: F – fiber, M – matrix, C – effective composite.

Calculations in [3] showed that the presence of the effective composite phase in the model is important: ignoring it leads to significantly over-estimated ERR. Despite the accuracy of the analytical models, the previous studies [1-3] have analyzed an idealized geometry without taking into account the possible non-uniformity of the local fiber arrangement which is present in most of the real cases. Certainly, the local microstructure can affect the stress state around the broken fiber and hence it can affect the debond growth rate. The objective of the present paper is to study the effect of the neighboring fibers on debond growth in UD composites. A simple 5-phase concentric cylinder model with variable inter-fiber distance keeping the average volume fraction constant was used to calculate the ERR. FEM software ANSYS [5] was used to perform calculations. Only mechanical tensile loading was studied in the present paper.

2. Self-similar debond growth

2.1. Analytical solution for 3-phase composite

Prior to analyzing the influence of the neighboring fibers on the debond growth, previously obtained results and trends for a 3-phase composite will be briefly reviewed. As it will be shown they provide important information for establishing the geometry for a 5-phase concentric cylinder model used in the present study.

Energy release rate for self-similar debond growth in UD composites with uniform fiber distribution was previously calculated in [1-3] using a 3-phase concentric cylinder model. It was shown in [3] that the ERR for self-similar debond growth can be expressed as a square of a linear combination of applied mechanical strain ε_{mech} and temperature change ΔT as:

$$G_{II} = \frac{E_1^f r_f}{4}\left[k_m^{\infty}\varepsilon_{mech} + k_{th}^{\infty}\left(\alpha_1^c - \alpha_1^f\right)\Delta T\right]^2 \tag{1}$$

In (1) r_f is the fiber radius, E_1^f is the fiber longitudinal modulus, α_1^c and α_1^f are thermal expansion coefficients of composite and fiber respectively, k_m^{∞} and k_{th}^{∞} are parameters related to mechanical and thermal response respectively. In [3] it was found that their dependence on elastic properties of constituents and volume fraction V_f is weak and the values are very close to 1. On the other hand, parametric analysis performed in [3] showed significant dependency of the ERR on the size of the effective composite cylinder revealing that a smaller radius of the composite overestimates the ERR. It was found in [3] that the outer radius equal to 10 times the fiber/matrix cylinder assembly radius is sufficient to represent an infinite composite for ERR calculations with FEM. Based on this result the same proportion between the fiber/matrix assembly and the effective composite phase was used in 5 cylinder FEM model in the present study.

2.2. 5-phase composite FEM model for self-similar debonds

To study the effect of the neighboring fibers on the ERR related to debond growth a 5-phase composite model was used in the present study, see Fig.2. The model is 2-D

axisymmetric and it is similar to a 4 phase model used in [6] simplifying a hexagonal fiber alignment by a concentric cylinder assembly. The 5-phase axisymmetric model shown in Fig.2 consists of a fiber as a central phase (denoted as F), surrounded by a matrix phase (M), neighboring fiber phase (F), another matrix phase (M) and effective composite phase (C). For the models shown in Fig.2, z is the symmetry axis showing the axial direction and r is the radial direction. In Fig.2 r_f denotes the radius of the central fiber, ID is the arbitrary inter-fiber distance between the central and neighboring fiber cylinder, R is the radius of fiber/matrix unit, R_E is the external radius of the concentric cylinder model including the effective composite phase, dl_d is the length of the model. In all calculations fiber radius was fixed to r_f =4μm, the model length was dl_d =2μm, ID was arbitrarily chosen, the radius of the neighboring fiber phase was determined from the condition that it represents the area of 6 fibers surrounding the central fiber in a hexagonal fiber arrangement, radius R of the fiber/matrix unit was determined from the given volume fraction V_f and the previously defined geometry entities. The outer radius of the concentric cylinder model was $R_E = 10 \cdot R$ based on the analysis performed in [3].

As it was shown in [3], for self-similar debond growth the ERR can be calculated from the condition that at fixed applied load F the bonded region with length dl_d (Fig.2a) becomes a debonded region with the same length dl_d (Fig.2b). Hence, the ERR for self-similar debond growth can be found using the potential energy change ΔU as:

$$G_{II} = \frac{\Delta U}{2\pi r_f dl_d} \tag{2}$$

The potential energy difference ΔU due to debond growth by a unit length dl_d is equal to the difference between the additional work (ΔW) performed due to the crack length increase and the change in the strain energy (ΔU_s), i.e.,:

$$\Delta U = \Delta W - \Delta U_s \tag{3}$$

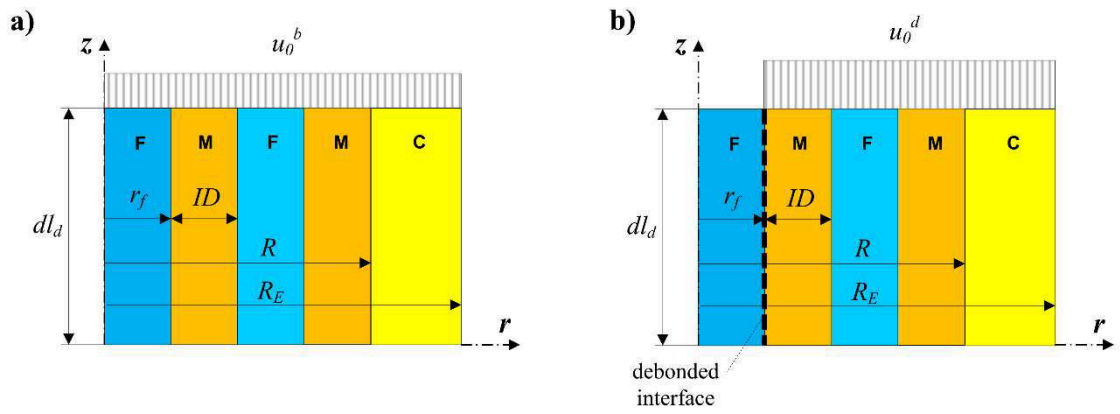

Figure 2. Schematic representation of a 5-phase FEM model: F – fiber, M – matrix, C – effective composite. a) bonded region; b) debonded region.

Additional work due to debond growth by dl_d is equal to:

$$\Delta W = F\Delta u \tag{4}$$

where Δu is the difference between displacements u_0^d and u_0^b in the debonded and bonded regions respectively (see Fig.2a and 2b). To find the displacement difference Δu and the strain energy change ΔU_s necessary for ERR calculation FEM software ANSYS version 13.0 [5] was used. A 2-D model with axisymmetric element behavior was generated. The bonded model (Fig.2a) was generated so that the neighboring areas share the interface line. In the debonded model (Fig.2b) exactly the same geometry as in the bonded model was used, however two coinciding lines were generated on the fiber/matrix interface one belonging to fiber and the other to matrix area. Contact elements were generated on the fiber/matrix interface in the debonded model (Fig.2b). The contact elements were set to comply with pure Lagrange multiplier method which enforces zero penetration when nodes are in contact [5]. Uniform axial displacement was applied on the bonded model as shown in Fig.2a. Reaction force F for the bonded model was calculated and then applied to the 4 phases in the debonded model as shown in Fig.2b. Strain energy for each case was calculated using element table command (ETABLE) in ANSYS [5]. Displacement difference Δu between bonded and debonded models was calculated using simple post-processing. According to the objective of the present study the ERR was calculated for various inter-fiber distances ID.

3. Short debond growth

For short debonds the debond crack tip is close to the fiber break. It was clearly shown in [2] using a 3-phase composite model and in [4] for the single fiber fragmentation test analysis that due to interaction between debond and the fiber break, the ERR for short debond growth is magnified. In the present study the objective is to find the effect of the neighboring fibers on the ERR therefore a 5-phase cylinder assembly model was used. Axisymmetric FEM model schematically shown in Fig.3 was generated in ANSYS [5] to calculate ERR for short debonds. In principle it is very similar to the 5 cylinder model used for self-similar debond ERR calculation (see Fig.2) with the difference that the fiber break is included in the model, the fiber is partly debonded (with debond length denoted as l_d in Fig.3) and the length of the model L_f is significantly larger. A uniform axial displacement u_0 was applied in the FEM model as shown in Fig.3. The ERR was calculated using the virtual crack closure technique (VCCT) routine in ANSYS [5]. VCCT is based on the principle that the energy released due to crack propagation is equal to the work required to close the same crack surface and that the stress-state near the crack tip is not changing when the increase of the crack length is small. Using VCCT routine in ANSYS allows to obtain the total ERR as well as components of Mode I and Mode II.

The geometrical entities r_f, ID, R and R_E were the same as in the case of self-similar debonds described in Section 2. The length of the FEM model was in all cases $L_f = 200 \cdot r_f$. The ERR was calculated for various debond lengths l_d and inter-fiber distances ID.

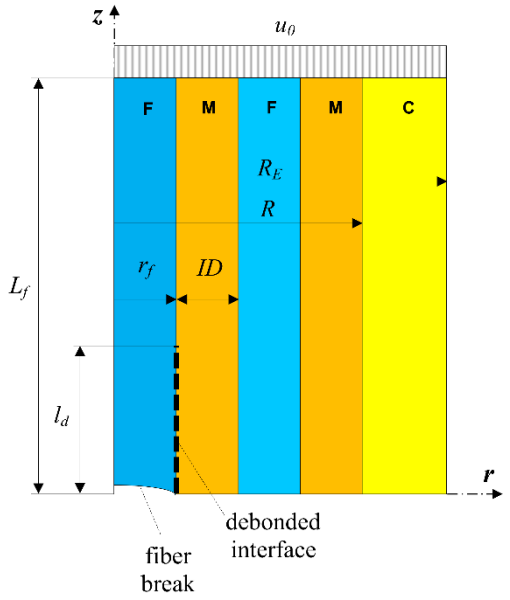

Figure 3. Schematic representation of a 5-phase concentric cylinder assembly FEM model for short debond energy release rate calculations: F –fiber, M – matrix, C – effective composite.

4. Results and discussion

4.1. Material properties

In the present paper a carbon fiber/epoxy composite (denoted as CF/EP) was studied. The elastic properties of the constituents are presented in Table 1. Elastic properties of the effective composite phase were calculated using Hashin's concentric cylinder assembly model [7] and Christensen's self-consistent model [8] for out-of-plane shear modulus. Calculated properties for CF/EP with volume fractions V_f=0.6 and V_f=0.4 are presented in Table 2.

Material	**E_1 [GPa]**	**E_2 [GPa]**	**ν_{12} [-]**	**G_{12} [GPa]**	**ν_{23} [-]**	**α_1 [1/°C]**	**α_2 [1/°C]**
CF	500	30	0.20	20	0.45	$-1\cdot10^{-6}$	$7.8\cdot10^{-6}$
EP	3.5	3.5	0.40	1.25	0.40	$60\cdot10^{-6}$	$60\cdot10^{-6}$

Table 1. Elastic properties of constituents. CF – carbon fiber, EP – epoxy matrix.

V_f [-]	**E_1 [GPa]**	**E_2 [GPa]**	**ν_{12} [-]**	**G_{12} [GPa]**	**ν_{23} [-]**	**G_{23} [GPa]**	**α_1 [1/°C]**	**α_2 [1/°C]**
0.6	301.4422	11.0389	0.2734	4.0625	0.5432	3.5767	$-0.6631\cdot10^{-6}$	$35.8513\cdot10^{-6}$
0.4	202.1433	7.5694	0.3133	2.6136	0.5899	2.3803	$-0.2842\cdot10^{-6}$	$50.9694\cdot10^{-6}$

Table 2. Elastic properties of carbon fiber/epoxy composite with volume fractions V_f=0.6 and V_f=0.4.

For the elastic properties listed in tables index 1 corresponds to fiber direction, 2 corresponds to transverse to fiber direction and 3 corresponds to out-of-plane direction. The isotropic epoxy matrix (EP) properties are presented in the same coordinate system in Table 1.

4.2. Effect of the inter-fiber distance on self-similar debond growth

Calculation results showing the effect of the inter-fiber distance on self-similar debond growth ERR are shown in Fig.4. The results correspond to mechanical loading with the strain level of $\varepsilon_{mech} = 0.01$. It was found that in mechanical loading the self-similar debonds grow in pure Mode II, hence notation G_{II} in Fig.4. The horizontal axis in Fig.4 shows the inter-fiber distance normalized with respect to the fiber radius, i.e., $IDn = ID / r_f$, see Fig.2. In Fig.4 results for volume fractions V_f =0.6 and V_f =0.4 are shown. The solid vertical line in Fig.4 indicates the inter-fiber distance that corresponds to uniform hexagonal packing for V_f =0.6. The dashed vertical line in Fig.4 indicates the same for V_f =0.4.

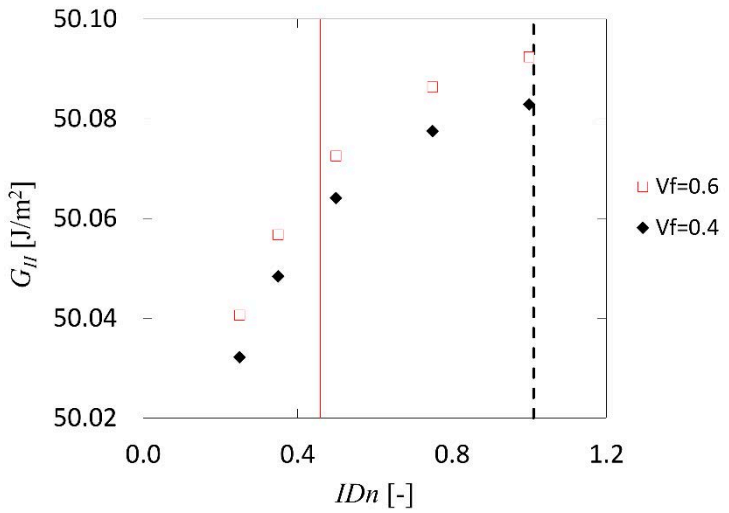

Figure 4. Energy release rate as a function of inter-fiber distance for self-similar debond growth.

In general, results in Fig.4 show that for both studied volume fractions the ERR slightly increases with the inter-fiber distance IDn. The corresponding analytical result for a 3-

phase composite obtained using Equation (1) for V_f =0.6 and V_f =0.4 is equal to 50.45 J/m^2 which is higher than the results obtained with a 5-phase composite model in Fig.4.

4.3. Effect of the inter-fiber distance on short debond growth

Calculation results showing the effect of the inter-fiber distance on short debond growth ERR are shown in Fig.5. The results only for volume fraction V_f =0.6 are presented. The results correspond to mechanical loading with the strain level of $\varepsilon_{mech} = 0.01$. The solid vertical line in Fig.5 indicates the inter-fiber distance that corresponds to uniform hexagonal packing for V_f =0.6. Unlike for self-similar debonds which propagate in pure Mode II, for short debonds it was found that in some cases Mode I contribution is significant. The results in Fig.5 show the total ERR, denoted as G, containing both Mode I and Mode II components. ERR is plotted against the normalized inter-fiber distance $IDn = ID / r_f$. Curves corresponding to different normalized debond lengths $l_{dn} = l_d / r_f$ are presented. The results in Fig.5 show that when the debond length is very small, for example, $l_{dn} = 1$, the ERR significantly increases with the inter-fiber distance IDn. It was also found that for very small debond lengths the contribution of Mode I is larger than for longer debond lengths.

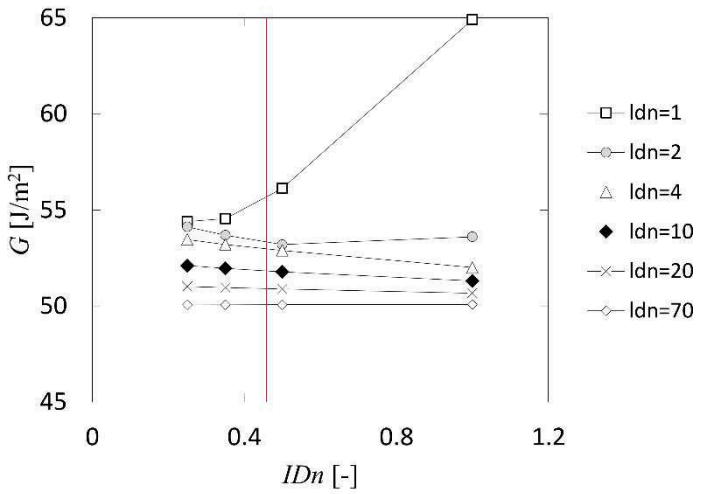

Figure 5. Energy release rate as a function of inter-fiber distance for short debonds.

It was found that for debond lengths $4 \le l_{dn} \le 50$ the ERR decreases slightly with the increase of the inter-fiber distance IDn (see Fig.5). However, when debond length

$l_{dn} > 50$, the ERR was found to increase slightly with the inter-fiber distance IDn, which is well consistent with the trends found for self-similar debond growth (see Fig.4)

Another way to analyze results for short debonds is to plot the magnification of ERR as a function of debond length l_{dn} at fixed inter-fiber distance IDn. Such plots are presented in Fig.6. The results plotted in Fig.6 consistently show larger magnification of ERR when the inter-fiber distance IDn is larger.

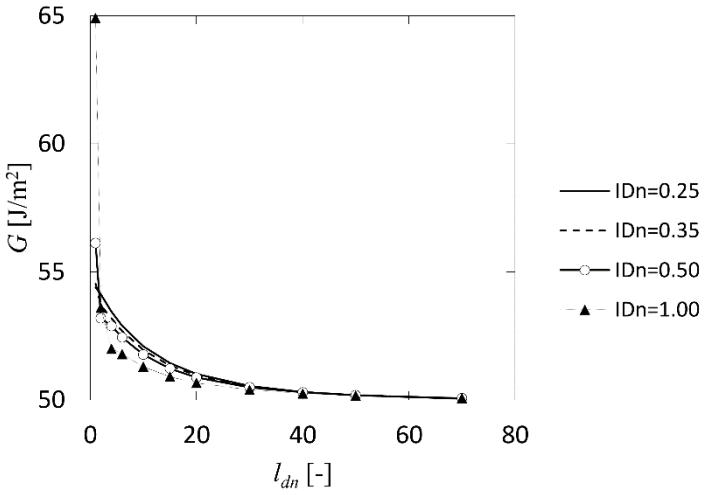

Figure 6. Energy release rate as a function of normalized debond length.

5. Conclusions

The effect of neighboring fibers on the energy release rate (ERR) for debond growth in unidirectional carbon fiber/epoxy composites was analyzed. 5-phase concentric cylinder FEM model was used for calculations. The model consists of a broken fiber embedded in matrix and surrounded by a cylinder of fiber material representing the neighboring fibers with variable distance to the broken fiber. It is followed by a matrix cylinder with outer radius ensuring that the fiber content in the unit is the same as for composite in average. This unit is embedded in the effective composite cylinder. Only mechanical tensile loading was considered. Different FEM models were used for self-similar and for short debond growth analysis. It was found for self-similar debond growth that the ERR slightly increases with the inter-fiber distance and propagation is purely in Mode II. For short debonds, on the other hand, it was found that Mode I

contribution to ERR can be significant, especially when debonds are very small. It was found that the ERR can either increase or decrease with the inter-fiber distance depending on the debond length. For shorter debonds it was found that ERR significantly increases with the inter-fiber distance. When the normalized debond length l_{dn} is in the range of $4 \le l_{dn} \le 50$ the ERR slightly decreases with the inter-fiber distance. Finally, it was found that when the debond length $l_{dn} > 50$ the ERR slightly increases with the inter-fiber distance resembling the trend found for self-similar debond growth.

References

[1] A. Pupurs and J. Varna. Energy release rate based fiber/matrix debond growth in fatigue. Part I: Self-similar crack growth. *Mechanics of Advanced Materials and Structures*, 20(4):276-287, 2013.

[2] A. Pupurs, A. Krasnikovs and J. Varna. Energy release rate based fiber/matrix debond growth in fatigue. Part II: Debond growth analysis using Paris law. *Mechanics of Advanced Materials and Structures*, 20(4):288-296, 2013.

[3] J. Varna and A. Pupurs. Analytical solution for energy release rate due to steady-state fiber/matrix debond growth in UD composites. *Composites Science and Technology*, submitted, 2014.

[4] E. Graciani, V. Mantic, F. Paris, J. Varna. Numerical analysis of debond propagation in the single fiber fragmentation test. *Composites Science and Technology*, 69(15-16):2514-2520, 2009.

[5] ANSYS Academic Research, Release 13.0, Canonsburg, Pennsylvania, 2011.

[6] S. W. Case, G. P. Carman, J. J. Lesko. A. B. Fajardo, K. L. Reifsnider. Fiber fracture in unidirectional composites. *Journal of Composite Materials*, 29(2):208-228, 1995.

[7] Z. Hashin. Analysis of composite materials – a survey. *Journal of Applied Mechanics*, 50(3):481-505, 1983.

[8] R. M. Christensen and K. H. Lo. Solutions for effective shear properties in three phase sphere and cylinder models. *Journal of the Mechanics and Physics of Solids*, 27(4):315-330, 1979.

Paper B

Effect of fiber clustering on debond growth energy release rate in UD composites with hexagonal packing

Effect of fiber clustering on debond growth energy release rate in UD composites with hexagonal packing

Linqi Zhuang[1,2,4], Andrejs Pupurs[2,3*], Janis Varna[2], Zoubir Ayadi[4]

[1]Texas A&M University, TX-77843, College Station, USA

[2] Luleå University of Technology, SE-97187 Luleå, Sweden

[3] Swerea SICOMP, SE-94129, Piteå, Sweden

[4] University of Lorraine, F-54010, Nancy, France

[*] Corresponding author, e-mail: andrejs.pupurs@ltu.se, phone: +46 920 49 1783

Abstract

Steady-state energy release rate (ERR) for fiber/matrix interface debond growth originated from fiber break in unidirectional composite is calculated using 3-D FEM models with hexagonal fiber arrangement. In the model the debonded fiber is central in the hexagonal unit which is surrounded by effective composite. The effect of neighboring fibers focusing on local fiber clustering on the ERR is analyzed by varying the distance between fibers in the unit. The steady-state ERR is calculated from potential energy difference between a unit in the bonded region far away from the debond front and a unit in the debonded region far behind the debond front. The ERR for different modes of crack propagation is obtained from a FEM model containing a long debond by analyzing the stress at the debond front.

Results show that in mechanical axial tensile loading fracture Mode II is dominating, it has strong angular dependence (effect of closest fibers) but the average ERR is not sensitive to the local fiber clustering. In thermal loading the Mode III is dominating and the average ERR is highly dependent on the distance to neighboring fibers. However, for realistic loads the thermal ERR is much smaller than the mechanical.

Keywords: A. UD composite, B. Debonding, C. Energy release rate, C. Finite element analysis

1. Introduction

When unidirectional (UD) composites are loaded with high tensile load in fiber direction, multiple fiber breaks occur due to statistical distribution of fiber strength. Once the fiber breaks form, yielding of matrix or fiber/matrix debonding can be expected near the fiber breaks as a result of large shear stresses in the interface region. In the present paper we are focusing on fiber/matrix debonding (interface cracks) initiated at the fiber break and growing along the fiber in the subsequent quasi-static or cyclic loading (see Fig.1a), which may be the case for relatively weak fiber/matrix interfaces. Growth of multiple interface debonds cause progressive degradation of the composite properties eventually leading to the final catastrophic failure of the composite. Hence, investigation of parameters affecting the debond growth is important and in the present paper it is performed using fracture mechanics: considering the debond as an interface crack. Whereas numerous papers deal with debonds in single fiber composites [1-4], the debond growth in UD polymeric composites has been previously analyzed in few papers [5-7] using fracture mechanics concept of potential energy release rate (ERR). In polymeric composites, due to larger Poisson's ratio and larger coefficient of thermal expansion of the matrix, the debond growth was shown to propagate purely in Mode II [4-7] when subjected to tensile loading and negative temperature changes. It was shown in [4-7] with analytical and numerical models that for short debonds, due to interaction with the fiber break stress-state, the ERR is magnified. As the debond crack propagates and the debond crack front advances far away from the fiber break, the debond growth becomes self-similar (steady-state growth) [4,6]. For such case (long debonds) exact analytical models for ERR calculation were developed in [5,7].

However, all the studies mentioned above used fiber distribution models with axial symmetry. For example, in [5-7] a cylindrical unit cell was used consisting of a broken and partially debonded fiber which is surrounded by a matrix cylinder. The effect of the surrounding heterogeneous composite in [5-7] was represented by an effective composite cylinder surrounding the concentric cylinder fiber/matrix unit cell.

Calculation results in [7] showed that the presence of the effective composite phase in the model is important: ignoring it leads to significantly over-estimated ERR [8]. Despite the fact that analytical solution for steady-state debond growth in axisymmetric

case is exact, these studies [5-7] have analyzed an idealized geometry with a “smeared out” effect of neighboring fibers. These models: a) cannot describe the effect of closest fibers on the ERR; b) cannot be used to analyze the effect of local fiber clustering (locally higher fiber volume fraction).

Authors are aware only about four papers [9-12] addressing the problem of the “heterogeneous neighborhood”. In [9] the adjacent fibers in the hexagonal array were replaced by a ring consisting of fiber material and the obtained axisymmetric problem was solved analytically to find stress concentrations in the neighboring fibers. In [12] a similar model with fiber ring representing the closest fibers and broken central fiber was solved numerically with an aim to analyze stress concentrations in closest fibers. A model with local hexagonal fiber with central broken fiber (zero debonding) embedded in an effective homogenized composites was used in [11]. The local fiber content was varied to find the effect of local clustering on axial stress concentration in the closest fiber.

The effect of local fiber clustering (explicit effect of the closest fibers) was first investigated in [10] using axisymmetric model with five concentric cylinders: the partially debonded fiber was surrounded by matrix, which was surrounded by a fiber cylinder (representing the neighboring fibers) and matrix cylinder. This entire unit was embedded in the effective composite. The local fiber content was varied changing the distance between the debonded fiber and the fiber cylinder, showing very small effect on ERR in mechanical loading (the ERR decreased for the lowest inter-fiber distance by 0.1% comparing to the uniform fiber distribution case and the global fiber volume fraction change from 0.4 to 0.6 resulted in an increase of the ERR by 0.02%). Using the same 5-cylinder model it was also shown that the local fiber clustering has significantly larger effect for short debonds. Unfortunately, conclusions from these studies are based on cylindrical model and it is not clear at all if they hold when the local microstructure (explicit consideration of the neighboring fibers and the varying local volume fraction) is analyzed. The microstructure affects the stress state around the broken fiber (the axial symmetry is lost) and hence it can affect the ERR during the debond growth. The objective of the present paper is to study the effect of the neighboring fibers on the debond growth ERR in UD composites. In the model a unit with hexagonal arrangement of fibers with variable inter-fiber distance keeping the average volume fraction constant is embedded in the effective composite, see Fig.1b. This model is used to calculate the

ERR due to debond growth along the broken central fiber. The steady-state debond growth ERR is calculated using two FEM models. In the first model the potential energy change of the system is calculated comparing two units of the composite, both far away from the debond crack front (one in the bonded and one in the debonded zone). In the second model the ERR at the front of a very long debond representing the steady-state is calculated using J-integral and VCCT with the aim to gain more detailed understanding regarding the fracture modes: in some cases there is a gap in radial and hoop displacements in the debonded zone and angle dependent tensile radial and tearing shear stresses in the bonded part. FEM software ANSYS [13] with contact elements was used to perform the required 3-D calculations. Mechanical tensile loading and negative temperature loading were studied in the present paper. The calculation results are compared with results obtained from axisymmetric 3 cylinder assembly model [7], where the local fiber distribution and its variation (clustering) were not considered.

The presented analysis of identifying parameters significantly affecting ERR in the steady-state is of direct practical importance for understanding microdamage mechanisms in composites with weak fiber/matrix interface. If the interface is strong, the steady-state conditions are never reached and clustering of fiber breaks with short debonds lead to final failure. Nevertheless, even in this case the much simpler steady-state solution gives a useful insight on the importance of different parameters of non-uniform fiber distribution and on expected trends. The steady-state solution is basically 2-D and therefore computationally much easier. The obtained results will allow minimizing the number of parameters and the range of their variation in a complex 3-D analysis of single or multiple short debonds originating from fiber breaks.

2. Modeling ERR due to debond growth

2.1 Model for UD composite with hexagonal local fiber array

We consider a UD composite with a broken and partially debonded fiber in the bulk of the composite far away from specimen surface, as shown schematically in Fig.1. The length of the composite is $2L_f$, z axis denotes the axial (fiber) direction of the composite. In the present study we represent the composite shown in Fig.1a with a simplified cylindrical shape model with length L_f (assuming symmetry with respect to the fiber break plane) and with hexagonal fiber arrangement as shown in Fig.1b. The

broken and partially debonded fiber is located at the center of the model, the neighboring fibers are situated in a hexagonal pattern surrounding the broken central fiber. The geometrical parameters are shown in detail in a cross-section of the model in Fig.2. In Fig.2, r and θ are the radial and angular coordinates respectively. The central and neighboring fibers are embedded in a matrix phase with the outer radius r_m. The fiber volume fraction V_f in this region is equal to the fiber content in the effective composite which is surrounding the unit with seven fibers. The effective (homogenized) composite phase with volume fraction V_f has the outer radius r_c.

The objective of the present paper is to study the effect of the clustering of the neighboring fibers on steady-state debond growth ERR, hence cases with different inter-fiber distance values, a_f, are studied without changing the radius of the fiber/matrix unit r_m. For each inter-fiber distance a_f we can define a local fiber volume fraction V_f^{loc}, which represents the volume fraction of fibers inside the hexagon joining the centers of the surrounding fibers, see Fig.2. In the present paper we will use local volume fraction V_f^{loc} as a measure of the local fiber distribution, meaning that a lower local volume fraction represents larger inter-fiber distance a_f and vice versa:

$$V_f^{loc} = \frac{2\pi}{\left(2+\frac{a_f}{r_f}\right)^2\sqrt{3}} \qquad (1)$$

Due to periodicity of the model shown in Fig.1b and Fig.2, a unit cell corresponding to $\theta = 30°$ can be divided. A 3-D schematic representation of the $\theta = 30°$ unit cell is shown in Fig.1c. In Fig.1c and further in the text l_d denotes the debond length measured from the fiber break plane.

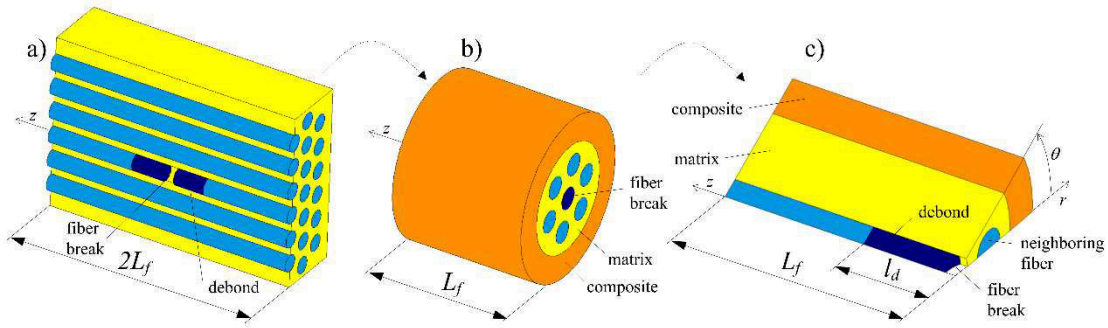

Fig. 1. a) UD composite with a broken and partially debonded fiber; b) Hexagonal distribution model; c) unit cell θ=30°

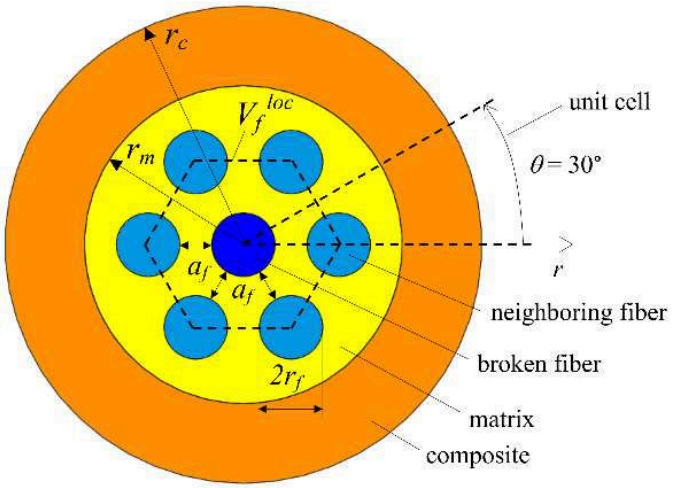

Fig.2. Cross-section of the hexagonal model and division of unit cell θ=30°

Consideration of a $\theta = 30°$ unit cell is particularly useful for Finite Element (FEM) modeling employed in the present study by significantly reducing the volume of the model and thus saving calculation time.

2.2 ERR during steady-state debond growth

We will analyze a case, when the front of the fiber/matrix debond crack is far away from the fiber break, where it was initiated, and when it is also far from another debond, which may be approaching from the other end of the fiber. In such case the debond crack propagation can be considered as steady-state. It means that the crack front moves along the fiber without changing its shape. However, it does not mean that the crack

front's shape is circular. More probable for hexagonal array is that the debond length depends on the angular coordinate, $l_d = l_d(\theta)$. In models with axial symmetry the debond length does not depend on the angular coordinate and the crack front is circular. Generally speaking, the shape of the crack front is not known *a priori*, it can be obtained only in result of complex calculations.

In terms of Fig.1c the geometrical condition for steady-state growth can be written mathematically as $l_{d(\min)} >> r_f$ and $L_f >> l_{d(\max)}$. Here $l_{d(\min)}$, $l_{d(\max)}$ are the smallest and the largest debond length values respectively measured from the fiber break plane. When the debond propagates by dl_d

a) The debond crack front (and the corresponding singular stress state in its vicinity) shifts in the z-direction by dl_d without changing its unknown shape;
b) The complex stress state in the region close to the fiber break does not change;
c) The perfectly bonded region volume far ahead from the debond front reduces by $\pi r_c^2 dl_d$;
d) The debonded region volume far behind the crack front increases by the same amount.

The bonded and debonded regions of length dl_d are shown in Fig.3a and 3b respectively.

The advantage of the calculation method for steady-state debond growth ERR presented below is that we do not need to know the shape of the crack front and the stress state there. The disadvatage of the method is that we can calculate only the total ERR without any possibility for deeper analysis of the different modes of crack propagation.

The ERR, denoted as G_{en}, is calculated according to:

$$G_{en} = \frac{\Delta U}{2\pi r_f dl_d} = \frac{\Delta U_f + \Delta U_m + \Delta U_c}{2\pi r_f dl_d} \qquad (2)$$

Indexes f , m and c are used for fiber, matrix and the effective composite respectively, ΔU is the potential energy change due to debond growth by dl_d .

In the steady-state growth case the potential energy of the whole model consists of fiber break region, debond front region, bonded part far away from the debond front, debonded part far away from the fiber break and far behind the debond front. From the above discussion follows that the only change due to debond growth is that a region of length dl_d which had perfectly bonded fiber is replaced be the region of the same size where the fiber is debonded.

According to definition the change of the potential energy in the system is equal to the difference between the additional work performed during the crack length increase and the change in strain energy

$$\Delta U = \Delta W - \Delta U_S \qquad (3)$$

In our case the change is that at fixed applied force P the bonded region with length dl_d in Fig.3a becomes debonded as shown in Fig.3b. The strain energy is changed and an additional work is performed as the result of the additional displacement due to compliance reduction of the region. The ΔU_S is found as the strain energy difference in these two states, the additional work $\Delta W = P\Delta u$, where P is the applied force and $\Delta u = u_0^d - u_0^b$ is the length change of the considered region in Fig. 3.

In purely thermal loading the work $\Delta W = 0$ therefore the potential energy change becomes equal to the change in strain energy $\Delta U = -\Delta U_S$.

More details regarding the significance of different modes of crack propagation can be obtained performing accurate stress state analysis at the debond front and using J-integral or virtual crack closure technique (VCCT). However, this type of analysis requires knowledge or assumptions regarding the shape of the debond crack front in the steady-state. In the present study a simplified approach was used by assuming a circular shape of the debond front and studying the ERR as a function of the angular coordinate θ.

Another alternative not considered in the present study is the use of cohesive elements with critical ERR as a criterion for crack surface separation which would allow determination of the crack front shape.

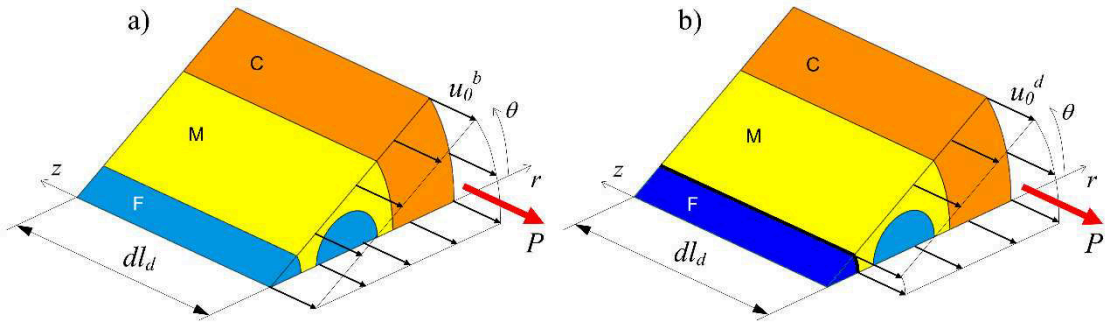

Fig.3. Representative volume element of bonded region (a) with length dl_d , which due to debond growth changes to debonded region (b) with length dl_d

3. FEM models

Two different FEM models were used in the present study for steady-state ERR calculation: 1) FEM model to calculate the potential energy difference and 2) FEM model with debond front, which in addition to ERR calculation also allows analyzing modes of crack propagation. FEM software ANSYS version 14.5 [13] was used in all cases. The boundary conditions and the calculation procedure is described in the following subsections.

3.1. FEM model for potential energy difference calculation

As described in Section 2.2 the steady-state ERR can be calculated without knowing the exact shape of the debond front by considering representative volumes from bonded and debonded regions far from the crack front. The ERR is calculated from potential energy change due to debond growth by dl_d , Eqs (2), (3). 3-D FEM models of representative bonded and debonded regions are schematically shown in Fig.3a and 3b, respectively. The representative regions are circular sectors corresponding to $\theta = 30°$ following the division of a unit cell in Fig.2. In Fig.3 *F, M* and *C* denote the central fiber, matrix and effective composite phases respectively. In all calculations the fiber radius was equal to $r_f = 4$ μm, the length of the FEM models was $dl_d = 2$ μm, the outer

radius of the effective composite phase (see Fig.2) was $r_c = 5r_m$. The size of the r_c was found from a parametric study, which showed that $r_c = 5r_m$ is the minimum size that satisfactory represents an infinite effective composite and hence does not magnify the ERR values.

In FEM model of the bonded region (Fig.3a) the interface areas between any two neighboring phases are shared. In FEM model of the debonded region (Fig.3b) a completely debonded interface was modeled between the central fiber and the matrix phase by generating two coinciding areas one belonging to the fiber and the other to the matrix volume. Contact elements with pure Lagrange multiplier on contact normal and tangent were generated on the debonded fiber/matrix interface. Such contact element type was chosen for the purpose of minimizing the inter-penetration due to radial compression on the contact surface. The friction on the interface was neglected. All geometrical parameters of the debonded model were exactly the same as for the bonded model.

Purely mechanical and purely thermal loading cases were studied.

In mechanical loading symmetry conditions were applied on nodes at $z = dl_d$ and on nodes corresponding to angular coordinates $\theta = 0°$ and $\theta = 30°$ for both bonded and debonded models. A uniform displacement u_0^b leading to strain $\varepsilon_z = 1\%$ in z axis direction was applied on the surface of the bonded model corresponding to $z = 0$ as shown in Figure 3a. The resulting force P corresponding to the applied displacement u_0^b was found in the post-processing. Coupling for displacement in z axis direction was applied on the surface $z = 0$ of all phases in the debonded model except the central fiber. Force P was applied on these coupled surfaces leading to uniform displacment u_0^d as shown in Fig.3b. Since the load is not applied on the debonded central fiber (Fig.3b) it will have a different axial displacement than the rest of the phases. To ensure independency of the solution on the z coordinate and hence the validity of the steady-state model, the nodes of the central fiber at $z = 0$ were coupled for displacement in z axis direction. The strain energy difference ΔU_S between the bonded and the debonded models was calculated using element table command (ETABLE) in ANSYS [13].

Displacement difference between bonded and debonded models $\Delta u = u_0^d - u_0^b$ was found with simple post-processing.

In purely thermal loading the symmetry conditions were applied on nodes at $z = dl_d$ and on nodes corresponding to angular coordinates $\theta = 0°$ and $\theta = 30°$. All nodes of the bonded model (Fig.3a) at $z = 0$ were coupled for displacement in z axis direction. In the debonded model (Fig.3b) the nodes of the central fiber and the nodes of the remaining phases at $z = 0$ were seperately coupled for displacement in z axis direction. Thermal load was applied as a uniform temperature applied on all nodes of the model.

3.2. FEM model for ERR analysis at debond front

For a more detailed analysis of the steady-state debond propagation modes a 3-D FEM model with broken, partially debonded fiber and debond front far away from the fiber break was generated according to Fig.1c. The model is a circular sector corresponding to $\theta = 30°$ following the division of a unit cell in Fig.2. Although it was discussed previously that due to the considered hexagonal arrangement of neighboring fibers the shape of the debond front in the steady-state region is most probably a function of the angular coordinate θ, for simplicity the shape was assumed circular in the present study.

To conform with conditions of steady-state debond growth (see description in Section 2.2), the length of the model $L_f = 80r_f$ and the debond length equal to $l_d = 25r_f$ was used in calculations. These values of L_f and l_d were found from a parametric study as the ones where the ERR becomes independent of them. The geometric parameters of the cross-section of the model with debond front were identical to those of the steady-state models described before in Section 3.1.

The debonded fiber/matrix interface was modeled by generating coinciding areas with contact elements of the same type as described in Section 3.1.

Symmetry conditions were applied on nodes corresponding to angular coordinates $\theta = 0°$ and $\theta = 30°$. Symmetry conditions were also applied on nodes of the matrix,

neighboring fiber and the effective composite at $z = 0$. The area of the central fiber at $z = 0$ was free of constraints representing the fiber break.

Purely mechanical and purely thermal loading cases were studied. In addition to the boundary conditions described above, the following conditions were applied:

In purely mechanical loading a uniform displacement leading to strain $\varepsilon_z = 1\%$ in z axis direction was applied on all nodes at $z = L_f$;

In purely thermal loading, the nodes at $z = L_f$ were coupled for displacement in z axis direction and the thermal load was applied as uniform temperature applied on all nodes of the model.

The ERR was calculated using built-in calculation routines in ANSYS 14.5 [13], namely, the J-integral and the VCCT. The J-integral routine gives the total ERR while the VCCT calculation routine allows calculating the ERR components of Mode I, II and III.

Appropriate mesh refinement was used in the vicinity of the debond front region to ensure the accuracy of J-integral and VCCT calculations.

4. Results and discussion

In the present study the ERR in carbon fiber/epoxy and glass fiber/epoxy UD composites was analyzed. Thermo-elastic properties of constituents are presented in Table 1. Carbon fibers, glass fibers and epoxy matrix are denoted as CF, GF and EP respectively.

Table 1. Thermo-elastic properties of constituents

Material	E_L	E_T	G_{LT}	ν_{LT}	ν_{23}	α_L	α_T
	[GPa]	[GPa]	[GPa]	[-]	[-]	[1/°C]	[1/°C]
CF	500	30	20.0	0.20	0.45	$-1\cdot10^{-6}$	$7.8\cdot10^{-6}$
GF	70	70	29.2	0.20	0.20	$4.7\cdot10^{-6}$	$4.7\cdot10^{-6}$
EP	3.5	3.5	1.3	0.40	0.40	$60\cdot10^{-6}$	$60\cdot10^{-6}$

Table 2. Thermo-elastic properties of UD composites

Material	V_f	E_L	E_T	G_{LT}	G_{23}	ν_{LT}	ν_{23}	α_L	α_T
	[-]	[GPa]	[GPa]	[GPa]	[GPa]	[-]	[-]	[1/°C]	[1/°C]
CF/EP	0.6	301.44	11.04	4.06	3.58	0.27	0.54	$-0.66\cdot10^{-6}$	$35.85\cdot10^{-6}$
CF/EP	0.4	202.14	7.57	2.61	2.38	0.31	0.59	$-0.28\cdot10^{-6}$	$50.97\cdot10^{-6}$
GF/EP	0.6	43.44	13.71	4.31	4.68	0.27	0.47	$6.86\cdot10^{-6}$	$32.21\cdot10^{-6}$

The high value of the transverse isotropic CF axial modulus was selected to have a case with high anisotropy in contrast to GF, which is isotropic. The elastic properties of the UD composties with a given volume fraction V_f were calculated using Hashin's concentric cylinder assembly model [14] and Christensen's self-consistent scheme for out-of-plane shear modulus [15]. In the present paper CF/EP composites with volume fractions V_f =0.6 and V_f =0.4 and GF/EP composite with volume fraction V_f =0.6 were analyzed. The calculated thermo-elastic properties of the studied UD composites are presented in Table 2.

4.1. ERR in mechanical loading

The ERR values obtained from FEM model calculating potential energy difference (Section 3.1) in a purely mechanical loading equal to ε_z =1% are presented in Tables 3

to 5 (data in the first row denoted as G_{en}). The local volume fraction V_f^{loc} of fibers was varied by changing the inter-fiber distance a_f. Composites with 3 different local volume fractions were studied V_f^{loc}=0.66, 0.72 and 0.78 corresponding to $a_f = 0.35r_f$, $0.25r_f$ and $0.15r_f$ respectively (see Fig.2).

Results in Tables 3 to 5 show that increasing the local fiber content leads to the decrease of the ERR but the effect is negligible. The ERR change is of the same magnitude and even smaller than the one calculated in [10] using the 5-cylinder model, by this supporting the conclusions of the 5-cylinder model in the mechanical loading case. The ERR values for uniform fiber distribution obtained using 3-cylinder assembly model [7], also presented in Tables 3, 5 (4^{th} column), are slightly higher which is consistent with the above discussed ERR decrease due to clustering. It can be noted that for the 3 cylinder model the size of the outer effective composite cylinder was 10 times the radius of the fiber matrix unit. For CF/EP composite the ERR values at $V_f = 0.6$ (Table 3) are in average 0.01 % higher than for $V_f = 0.4$ (Table 4) which is a similar trend as found in [10]. However, the main conclusion is that the total ERR due to steady-state debond growth is very insensitive to the local variation (increase) of the fiber content.

Analysis of stress distributions in the bonded and debonded steady-state models revealed some features that could indicate that several modes of the debond crack propagation are active. For example the presence of θ - dependent hoop displacement gap Δu_θ at the debonded interface and relevant shear stresses $\sigma_{r\theta}$ in the bonded model. The radial stresses at the interface in the bonded model, Fig. 4a, are tensile for $V_f^{loc} = 0.78$ (potential for Mode I) but the radial stresses in the debonded model, Fig. 4b, are compressive for the same V_f^{loc}, which kind of forbids Mode I. It has to be emphasized that these stress distributions are for regions far away from the debond front and, hence, they cannot be used to characterize fracture mode mixity at the debond front.

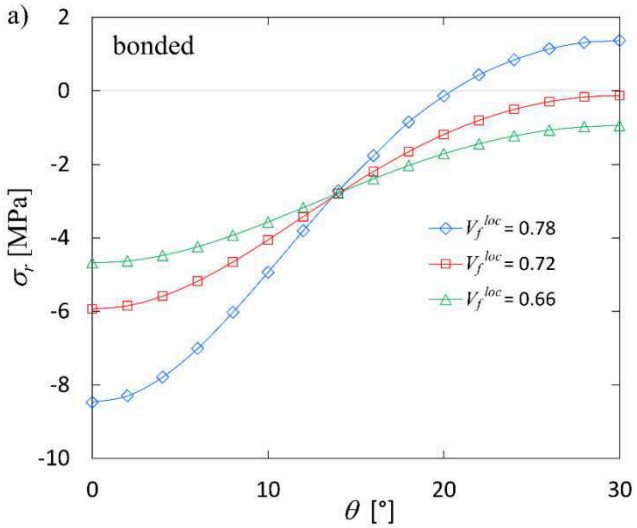

(a)

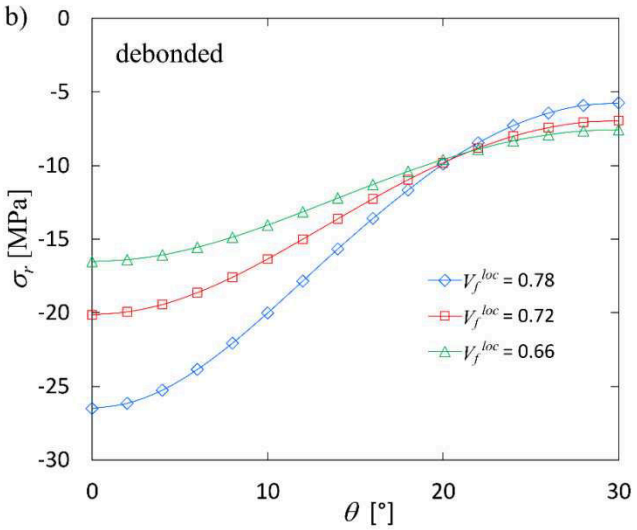

(b)

Fig.4. Radial stress σ_r distribution at the interface for CF/EP $V_f = 0.6$ in mechanical loading case $\varepsilon_z = 1\%$: a) bonded interface; b) debonded interface

Table 3. Energy release rate values for CF/EP $V_f = 0.6$ in purely mechanical loading $\varepsilon_z = 1\%$

	V_f^{loc}			
	0.66	0.72	0.78	0.60 (3-cyl)
G_{en} [J/m^2]	50.22728	50.22197	50.21351	50.45131
J [J/m^2]	49.38511	49.35217	49.27961	50.17184
G_I [J/m^2]	-0.00238	-0.00241	-0.00210	0.01534
G_{II} [J/m^2]	50.16155	50.21543	50.28309	49.08337
G_{III} [J/m^2]	0.00460	0.00585	0.00500	0.000000

Table 4. Energy release rate values for CF/EP $V_f = 0.4$ in purely mechanical loading $\varepsilon_z = 1\%$

	V_f^{loc}		
	0.66	0.72	0.78
G_{en} [J/m^2]	50.22189	50.21631	50.20757
J [J/m^2]	49.54135	49.54620	49.47209
G_I [J/m^2]	-0.00245	-0.00246	-0.00219
G_{II} [J/m^2]	50.31723	50.39105	50.47968
G_{III} [J/m^2]	0.004496	0.00595	0.00453

To obtain more clarity regarding the possible crack propagation modes in steady-state debond growth, calculations at the front of a long debond were performed as described in Section 3.2. It is noteworthy that the applied 1% strain to the model correspond to

slightly lower load than in the steady-state modeling where the load was selected to give 1% in the bonded zone and not in average as it is in the model with debond front. Therefore the ERR values are slightly lower using the debond front model. Assuming that the debond front is circular ($l_d \neq f(\theta)$) the J -integral was calculated and the VCCT was used to determine G_I (Mode I), G_{II} (Mode II) and G_{III} (Mode III). The calculated values strongly depend on the angular coordinate θ as shown in Fig.5 for CF/EP with $V_f = 0.6$. The variation is large and the amplitude increases with increasing local fiber content V_f^{loc}. If one would use the critical values of the J -integral as a propagation criterion the consequences are obvious: the debond propagation at $\theta = 0$ would start before the propagation starts at other angles. This leads to conclusion that the debond front in steady-state growth will not be circular. Therefore, all conclusions below obtained solving the case with circular debond front should be considered as indicative only.

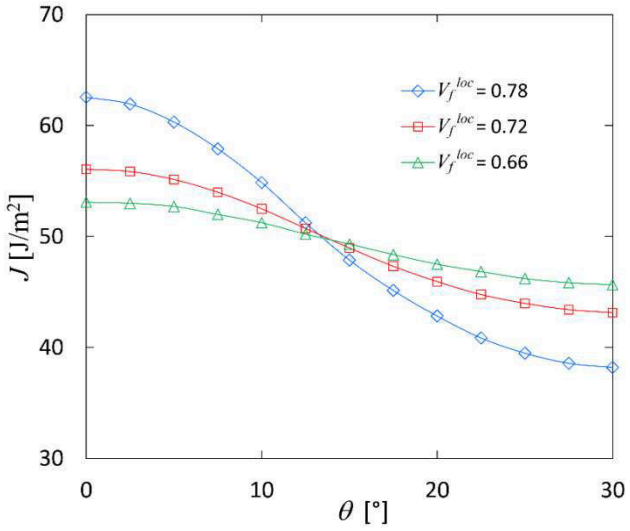

Fig.5. J-integral values for CF/EP $V_f = 0.6$ in purely mechanical loading $\varepsilon_z = 1\%$ obtained using the debond front model

The average of the J -integral over θ was calculated and the average values are presented in Tables 3 to 5 (data in row 2). The J -integral was calculated also for the

3-cylinder model where it is independent on the angle. The J -integral values are slightly lower than the G_{en} but the difference is small. Since the value of the J -integral has to depend on the selected profile of the crack front and since the used circular shape is not the right one for the steady-state case, we can conclude that the shape of the crack front has a relatively small effect on the total ERR. The values of the J -integral in Tables 3 to 5 have exactly the same trends with respect to the local fiber content change as the G_{en} but the magnitude of the change is slightly larger.

Table 5. Energy release rate values for GF/EP $V_f = 0.6$ in purely mechanical loading $\varepsilon_z = 1\%$

	V_f^{loc}			
	0.66	0.72	0.78	0.60 (3-cyl)
G_{en} [J/m^2]	6.96651	6.95730	6.94100	7.00873
J [J/m^2]	6.86011	6.84045	6.80875	6.96138
G_I [J/m^2]	-0.00065	-0.00066	-0.00065	0.00096
G_{II} [J/m^2]	6.94240	6.93421	6.91895	6.80645
G_{III} [J/m^2]	0.00009	0.00006	0.00001	0.00000

The magnitude of the angular variation of the J -integral is shown in Fig. 6 where the ratio between values at $\theta = 0°$ (J_0) and at $\theta = 30°$ (J_{30}) is presented as a function of V_f^{loc} for different materials and global fiber contents. The result is remarkable: the global fiber content and/or the fiber material has no effect on this ratio. One possible consequence of this result may be that the shape of the debond front in steady-state is insensitive to these parameters. On the other hand the local increase of the fiber content increases the considered ratio of J -integral values and the debond front is expected to deviate more from the circular shape.

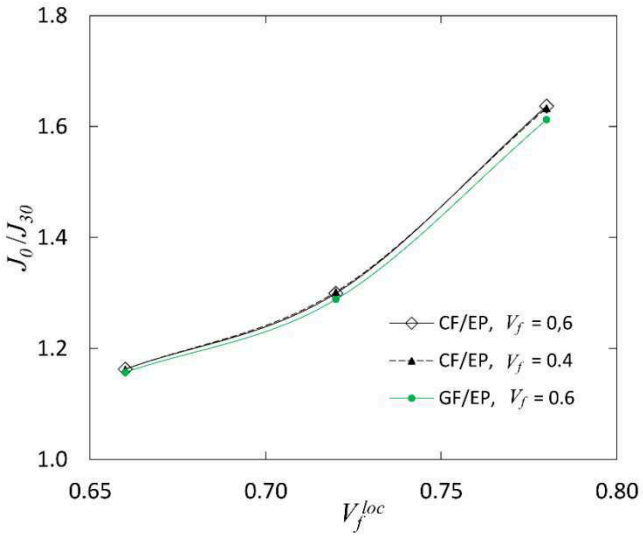

Fig.6. Ratio between maximal and minimal J-integral values in purely mechanical loading $\varepsilon_z = 1\%$ obtained using the debond front model

Similar averaging as with the J - integral was performed also with G_I , G_{II} and G_{III} (obtained with VCCT). The results are presented in Tables 3 to 5 (data in rows 3 to 5). One may notice two anomalies important for the estimation of the accuracy of these results:

a) the axisymmetric 3-cylinder model gives nonzero G_I even if it is absolutely clear that due to compressive radial stresses in the debonded zone the Mode II is the only mode in this model. Nevertheless, combination of negative radial displacement gap due to small interpenetration with compressive radial stress lead to values 0.01534 J/m^2 (Table 3 for CF/EP) and 0.00096 J/m^2 (Table 5 for GF/EP) for a simple axisymmetric case using contact elements. These values indicate the error we have to expect in using the same elements in the more complex hexagonal model The G_I in the hexagonal model is even negative (values around 0.002) which, of course, is impossible and is an artifact of using contact elements. We conclude that Mode I ERR is zero in the considered mechanical loading cases

b) Calculations show that there is Mode III ERR. The value is very small, in the order of magnitude of 0.005 J/m^2 for CF/EP. This value is several times lower than the accuracy of Mode I ERR determination discussed above. Therefore, it could be considered as a calculation error or just as being negligible comparing with G_{II}.

However, the angular displacement gaps and the shear stresses found in the steady-state model force us to accept that the Mode III, even being small, is real.

A simple estimate of the three fracture modes can be obtained using stresses and displacement gaps calculated using the steady-state models (Fig.3). The work to close the gaps for different displacement components is calculated to bring the debonded element to its bonded state. Hence, the displacement gaps are from the debonded model and the interface stresses and the axial stress in the fiber from the bonded model. Dividing the work by the new crack area $A_d = \frac{\pi}{6} r_f dl_d$ we obtain expressions (indexes b and d denote the bonded and debonded model respectively and Δu is used for displacement gap)

$$G_I = \frac{3}{\pi} \int_0^{\pi/6} \sigma_r^b \Delta u_r^d d\theta \qquad (4)$$

$$G_{II} = \frac{3}{\pi} \int_0^{\pi/6} \sigma_{zf}^b \Delta u_z^d d\theta \qquad (5)$$

$$G_{III} = \frac{3}{\pi} \int_0^{\pi/6} \sigma_{r\theta}^b \Delta u_\theta^d d\theta \qquad (6)$$

Using equations (4), (6) we calculate $G_I \equiv 0$ and $G_{III} = 0.0013$ J/m^2 for CF/EP with $V_f = 0.6$ and $V_f^{loc} = 0.78$, which is of the same order of magnitude as the value from the debond front solution (Table 3). Nevertheless in any crack growth criterion only G_{II} because of its magnitude will be important.

4.2. ERR in thermal loading.

For the ERR results corresponding to the purely thermal loading case with $\Delta T = -100°C$ presented in Table 6, the same notation as in mechanical loading case (Table 3 to 5) is used.

Table 6. Energy release rate for thermal loading case $\Delta T = -100°C$, CF/EP with $V_f = 0.6$

	V_f^{loc}				
	0.66	0.72	0.78	0.60 (3-cyl)	0.60 (3-cyl), $\Delta T = +100°C$
G_{en} [J/m^2]	0.00409	0.00702	0.01358	0.00077	0.02052
J [J/m^2]	0.00387	0.00678	0.01342	0.00081	0.02052
G_I [J/m^2]	0.00005	0.00006	0.00106	0.00002	0.01786
G_{II} [J/m^2]	0.00097	0.00106	0.00110	0.00077	0.00260
G_{III} [J/m^2]	0.00304	0.00586	0.01137	0.00000	0.00000

In addition to results for hexagonal fiber packing (G_{en} obtained from the potential energy difference in the steady-state models and J, G_I, G_{II}, G_{III} from the debond front stress state models) the results from axisymmetric 3 cylinder assembly model [7] for composites with the same V_f are also presented in Table 6 (4th and 5th column). The results in the last column are for the nonrealistic case of $\Delta T = +100°C$, when the debond is fully open and the G_I is dominating and responsible for the much larger ERR than in the negative temperature change case. For negative temperature change G_I does not exist and G_{III} is zero in models with axial symmetry. The nonzero value for G_I in

Table 6 for $\Delta T = -100°C$ can be used to estimate the accuracy obtained using contact elements.

Generally speaking, the values of the ERR in the thermal case are much smaller than in the mechanical loading at $\varepsilon_z = 1\%$ strain, see Tables 3 to 5, and, hence, the thermal part in the ERR in many practical cases could be neglected. Nevertheless, an in-depth analysis of purely thermal case was performed to understand the underlying mechanics.

The ERR values obtained from the potential energy change and from the J -integral are in a very good agreement. The J -integral values in Table 6 are the average of the θ −distribution shown in Fig. 7. The shape of the dependence is very different than in the mechanical loading case, but the increase of the local fiber content has a similar magnifying effect on the ERR. The most favorable debond propagation direction in thermal case is at approximately $\theta = 14°$.

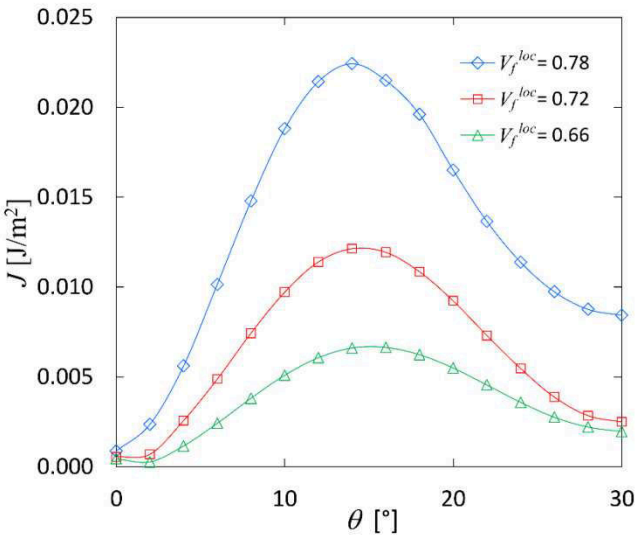

Fig.7. J-integral values for CF/EP $V_f = 0.6$ in thermal loading $\Delta T = -100°C$ obtained using debond front stress state model

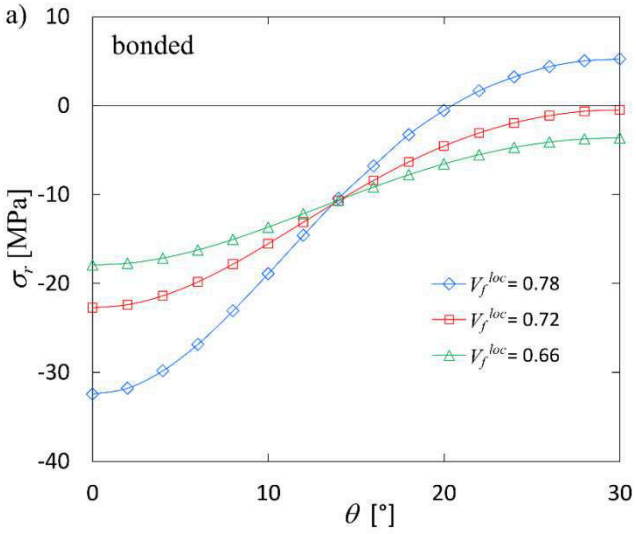

(a)

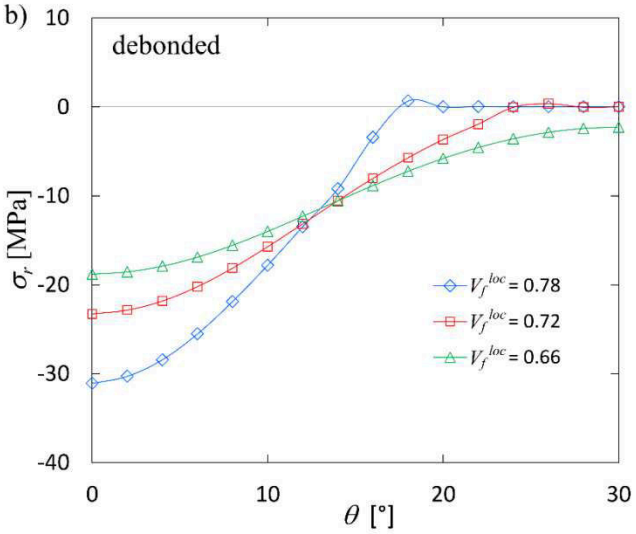

(b)

Fig.8. Radial stress distribution at the interface for CF/EP $V_f = 0.6$ in thermal loading $\Delta T = -100°C$: a) bonded interface; b) debonded interface

Models with hexagonal symmetry show all three modes of debond propagation. In the case with the highest local fiber content $V_f^{loc} = 0.78$, see Fig. 8a, the radial stresses in part of the interface in the bonded model (Fig.3a) are tensile and in approximately the same region of the debonded model (Fig.3b) the debond is partially open, (zero radial

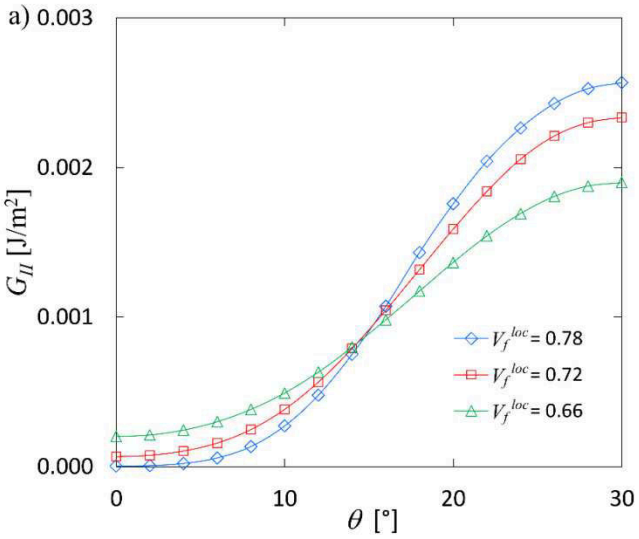

(a)

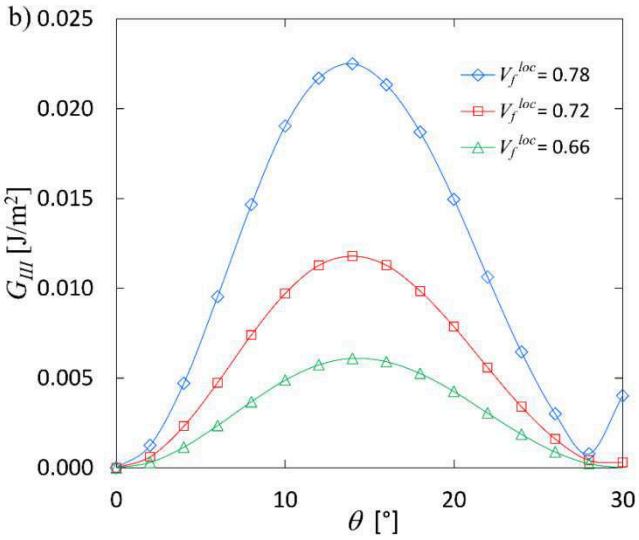

(b)

Fig.9. Energy release rate values for CF/EP $V_f = 0.6$ in purely thermal loading $\Delta T = -100°C$ obtained using debond front stress-state model: a) Mode II, b) Mode III

stress on interface) see Fig.8b. The size of the contact zone depends on the local fiber volume fraction and, for example, for $V_f^{loc} = 0.66$ the debond is closed. Still, the values of G_I obtained from the debond front calculations are much lower than from other modes. Using expression (4) for $V_f^{loc} = 0.78$ we obtain G_I=0.00090 J/m^2 which is of

the same order of magnitude and confirms the result from the debond front solution (Table 6).

The Mode II and Mode III ERR dependence on angle are shown in Fig. 9. According to the debond front analysis G_{III} is the largest and it dominates the J - integral (total ERR) behavior in Fig. 7.

The shear stress $\sigma_{r\theta}^{b}$ distribution at the fiber surface in the bonded model (Fig.3a) and the gap in hoop displacements Δu_{θ}^{d} in the debonded model (Fig.3b) are shown in Fig. 10. For $V_f^{loc} = 0.78$ calculations using expressions (5) and (6) give $G_{II} = 0.00091$ J/m^2, $G_{III} = 0.012$ J/m^2 which are rather close to the corresponding values from the debond front analysis given in Table 6.

In a real situation the loading contains both, the thermal and the mechanical component. The analysis performed in this paper proves that superposition of thermal and mechanical stresses obtained from two corresponding solutions cannot be used to calculate the thermo-mechanical ERR in an arbitrary combination of applied stress and temperature. The main reason is that the thermal and the mechanical solutions are obtained from two different boundary-value problems: in the mechanical case the debonded interface is closed or opened in a small region only whereas in the thermal loading case the opening zone is different. Obviously, in a general thermo-mechanical loading case the existence of opened zone depends on the ratio of these two loading components.

5. Conclusions

Energy release rate (ERR) due to steady-state propagation of a debond along the fiber/matrix interface in a unidirectional composite is analyzed assuming hexagonal fiber packing. The broken and partially debonded fiber is a central fiber in a hexagonal unit with locally larger fiber content than in average. This hexagonal unit is surrounded by large volume of effective composite and the model is subjected to mechanical and thermal loadings.

The importance of the explicit inclusion of the neighboring fibers in the model and the effect of the local fiber clustering on the ERR is investigated using 3-D FEM models

with contact elements. Two types of solutions are obtained: a) steady-state solution, in which the ERR is calculated from the potential energy difference between a bonded and debonded unit far from the debond front; b) local stress state at the front of a long debond with circular front is used to find the total ERR as well as its three components.

The results show that at high local fiber content the debond crack may be a) partially opened; b) local hoop displacement gap exists and that the contact/opening zones as well as the ERR has an angular distribution, which is very different in mechanical and in thermal loading. However, in mechanical loading the average value of the ERR rate is very similar as in models assuming axial symmetry.

This means that the boundary conditions at interfaces are different in thermal and mechanical loading and, therefore, linear superposition of thermal and mechanical stress states to calculate the ERR in combined loading is not possible.

However, for realistic loadings the thermal ERR according to the hexagonal model is much smaller than the mechanical and may be neglected when solving practical problems.

Acknowledgements

Funding from the strategic innovation programme LIGHTer provided by Vinnova (Sweden) is acknowledged.

References

[1] Nairn J.A., Liu Y.C. On the use of energy methods for interpretation of results of single-fiber fragmentation experiments. Compos Interfac 1996;4:241-267.

[2] Nairn J.A., Exact and variational theorems for fracture mechanics of composites with residual stresses, traction loaded cracks, and imperfect interfaces. Int J Fract 2000;105: 243-271.

[3] Wu W., Verpoest I., Varna J. Prediction of energy release rate due to the growth of interface crack by variational analysis. Compos Sci Tech 2000;60:351-360.

[4] Graciani E., Mantič V., París F., Varna J. Numerical analysis of debond propagation in the Single Fibre Fragmentation Test. Compos Sci Tech 2009;69(15-16):2514-2520.

[5] Pupurs A., Varna J. Energy release rate based fiber/matrix debond growth in fatigue. Part I: Self-similar crack growth. Mech Adv Mater Struct 2013;20(4):276-287.

[6] Pupurs A., Krasnikovs A., Varna J. Energy release rate based fiber/matrix debond growth in fatigue. Part II: Debond growth analysis using Paris law. Mech Adv Mater Struct 2013;20(4):288-296.

[7] Varna J., Pupurs A. Analytical solution for energy release rate due to steady-state fiber/matrix debond growth in UD composites. Int J Damage Mech 2015, submitted.

[8] McCartney LN. Analytical model for debonded interfaces associated with fibre fractures or matrix cracks, In: Proceedings of the 12th International Conference on Composite Materials ICCM-12 (eds Massard T, Vautrin A) Paris, France, 1999, paper no. 322.

[9] Case S.W., Carman G.P., Lesko J.J., Fajardo A.B., Reifsnider K.L. Fiber fracture in unidirectional composites. J Compos Mater 1995;29(2):208-228.

[10] Zhuang L., Pupurs A. Effect of neighboring fibers on energy release rate during fiber/matrix debond growth (Conference Paper), 16th European Conference on Composite Materials, ECCM 2014; Seville; Spain; June 22-26, 2014; Code 109290.

[11] Nedele M.R., Wisnom M.R. Three-dimensional finite element analysis of the stress concentration at a single fibre break, Compos Sci Tech 1994;51:517-524.

[12] Nedele M.R., Wisnom M.R. Stress concentration factors around a broken fibre in a unidirectional carbon fibre epoxy, Proceedings of Interfacial Phenomena in Composite Materials, Cambridge, UK, 1993.

[13] ANSYS Academic Research, Release 14.5, Canonsburg, Pennsylvania, 2012.

[14] Hashin Z. Analysis of composite materials – a survey. J Appl Mech, 1983;50(3):481-505.

[15] Christensen R. M., Lo K.H. Solutions for effective shear properties in three phase sphere and cylinder models. J Mech Phys Solid 1979;27(4):315-330.

Paper C

Fiber/matrix debond growth from fiber break in unidirectional composite with local hexagonal fiber clustering

Fiber/matrix debond growth from fiber break in unidirectional composite with local hexagonal fiber clustering

Linqi Zhuang[1,2,4], Andrejs Pupurs[2,3*], Janis Varna[2], Zoubir Ayadi[4]

[1]Texas A&M University, TX-77843, College Station, USA

[2] Luleå University of Technology, SE-97187 Luleå, Sweden

[3] Swerea SICOMP, SE-94129, Piteå, Sweden

[4] University of Lorraine, F-54010, Nancy, France

[*] Corresponding author, e-mail: andrejs.pupurs@ltu.se, phone: +46 920 49 1783

Abstract

Energy release rate (ERR) for fiber/matrix debonding in composite with local fiber clustering, subjected to axial tension, has been investigated numerically by a 3-D finite element (FE) model. In the model, broken fiber is central in a hexagonal unit which is embedded in an effective composite. Fiber/matrix debond with circular front is assumed to be originated from the fiber break. The effect of the local fiber clustering on ERR is studied by varying distance between the broken fiber and the neighboring fibers. For very short debonds as well as for long debonds (almost steady-state growth) the ERR was calculated by both the J integral and the Virtual crack closure technique (VCCT). Results show that the debond growth is Mode II dominated and that the ERR strongly depends on the angular coordinate. The local fiber clustering has larger effect on the angular variation for shorter debonds and the effect increases with larger local fiber volume fraction. The results obtained from the 3-D hexagonal model are compared with those obtained previously using 5-cylinder axisymmetric model developed by the same authors. The ERR values from 5-cylinder axisymmetric model could be considered as upper bound for the 3-D hexagonal model.

Keywords: A. Polymer-matrix composites (PMCs), B. Debonding, C. Finite element analysis (FEA)

1. Introduction

Tensile failure of unidirectional (UD) composites has been widely investigated [1-8] due to their broad applications in load bearing composite structures. When UD composites are loaded in fiber direction in quasi-static or cyclic tension-tension loading and the tensile load is sufficiently high, multiple fiber breaks occur first due to statistical distribution of fiber strength. Once the fiber breaks form, yielding of matrix [9] or fiber/matrix debonding [10] can be expected near the fiber breaks as a result of large stress concentrations. For the case of a relatively weak fiber/matrix interface, which is the case studied in the present paper, fiber/matrix debonding (interface cracks) would initiate at the fiber break and grow along the fiber, which leads to progressive degradation of composite properties [3, 10, 11]. Matrix cracking leads to coalescence of isolated fiber breaks with debonds to form a critical fracture plane which propagates unstably as a crack to cause the final catastrophic failure of the composite. Hence, it is of importance to quantify debond crack growth rate in quasi-static or in cyclic loading.

Typically for polymeric composites with relatively weak interface loaded in fiber direction, the excess energy during the fiber break formation produces a short interface debond crack in vicinity of the fiber break. Thereafter under increased loading the debond crack grows along the fiber/matrix interface without deviation unless there is, for example, some interaction with fiber breaks or debonds in the neighboring fibers. Thus for an isolated debond studied in the present paper the fracture mechanics concept of energy release rate (ERR) is suitable for crack growth analysis in quasi-static or cyclic loading.

Single fiber composite due to its relative simplicity of conducting experiment and modeling [12-18] has been proven useful in understanding the fiber/matrix interface debonding mechanism and for interface characterization. However, when composites

are analyzed the negligence of surrounding constituents might affect the accuracy of the calculated potential ERR. Generalizing the single fiber composite model to UD composite case, a three cylindrical phase composite model was suggested in [6, 7, 19] where the fiber/matrix unit with the broken and partially debonded fiber was embedded in effective composite phase. Results in [19] showed that the presence of the effective composite phase in the model is important: ignoring it by using models with a unit cell consisting of fiber and matrix only leads to significantly over-estimated ERR.

Despite the efficiency of axisymmetric numerical calculations for short debonds and the availability of analytical steady state solution [19], the three phase composite models analyze an idealized geometry without explicitly taking into account the neighboring fiber especially the possible non-uniformity of the local fiber arrangement which is present in most of the real cases. It can be expected that the local microstructure affects the stress state around the broken and partially debonded fiber and hence it can affect the ERR during debond growth. Several research efforts [20-26] have been made in order to account for the fiber non-uniformity on fiber breakage process (stress magnification in the neighboring fiber), however, the effect of local fiber non-uniformity on debond growth is yet to be well understood. One of the first studies on the effect of local fiber clustering (explicit effect of the closest fibers) on debonding [27] was conducted using axisymmetric model with five concentric cylinders: the partially debonded fiber was surrounded by matrix, which was surrounded by a fiber cylinder (representing the six neighboring fibers) followed by a matrix cylinder. This entire unit was embedded in the effective composite cylinder. The local fiber content was varied changing the distance between the debonded fiber and the fiber cylinder. For relatively long debond (nearly steady-state growth), it shows a very small effect of

the clustering on the ERR in mechanical loading (the ERR decreased for the lowest inter-fiber distance by 0.1% comparing to the uniform fiber distribution case whereas the global fiber volume fraction change from 0.4 to 0.6 resulted in an increase of the ERR by 0.02%). Using the same 5-cylinder model it was also shown in [27] that the local fiber clustering has significantly larger effect on ERR for short debonds. Unfortunately, conclusions from these studies are based on cylindrical model and it is not clear at all if they hold when the local microstructure (explicit consideration of the neighboring fibers and the varying local volume fraction) is analyzed. Recently a 3-D model [28] with hexagonal arrangement of fibers has been developed in order to investigate the fiber clustering effect on ERR of steady-state debond growth. Similar hexagonal arrangement models have been successfully used by several researchers [21, 25] in order to investigate the stress magnifications in neighboring fibers caused by fiber breakage with or without fiber/matrix interfacial debonding.

In the current study, the ERR is calculated using 3-D FEM model with a hexagonal array of fiber cluster embedded in the homogenized effective composite. The ERR is calculated using J-integral and the Virtual Crack Closure Technique (VCCT) originally proposed by Rice[29] and Rybicki [30], respectively. The results from [28] for steady-state debond growth in the same model show that fiber clustering has significant effects on angular variation of ERR, however, the average ERR is not sensitive to fiber clustering, which is similar to conclusions obtained in [20] from axisymmetric model. For steady state conditions, the debond length is very long and the interaction between debond tip and fiber break is negligible. The present paper is a continuation of the studies in [28] focusing on cases when the debond length is relatively short and the interaction with fiber crack cannot be ignored. For short debonds, the interaction

between fiber break and debond front is not negligible and an analytical solution is impossible to obtain. Therefore FE software ANSYS [31] was used to perform the FE calculations in the present paper.

2. Debond in UD composite: Material model

A UD composite with an isolated fiber break and an interface debond with a circular debond front (the debond length does not depend on the angular coordinate) close to the fiber break is investigated in the current study. Fibers within the UD composite are assumed to have hexagonal packing, as shown schematically in Fig.1. The length of the composite model is $2L_f$, and L_f could also be viewed as the half-distance to next fiber break which is assumed to be large enough for stress perturbations not to overlap. As a result, the interaction between two fiber breaks is not significant and therefore it is not analyzed in this paper. z axis denotes the axial (fiber) direction of the composite. In the present study the UD composite shown in Fig.1a is represented by a cylindrical shape model with length L_f (assuming symmetry) as shown in Fig.1b. The broken and partially debonded fiber is located at the center of the model, the neighboring fibers are situated in a hexagonal pattern surrounding the broken central fiber. The geometrical parameters are shown in detail in a cross-section of the model in Fig.2. In Fig.2, r and θ are the radial and angular coordinates, respectively. The central and neighboring fibers are surrounded by matrix with the outer radius of the matrix phase r_m defining the global volume fraction of the fibers V_f. The fiber and the matrix unit is surrounded by the effective (homogenized) composite phase with volume fraction V_f. The outer radius of the effective composite is denoted as r_c. In order to study the effect of the neighboring fibers on debond growth ERR, the inter-fiber distance value a_f is considered as variable while the radius of the fiber/matrix unit r_m is fixed. For each

inter-fiber distance we can define a local fiber volume fraction V_f^{loc} which represents the fraction of fibers inside the hexagon joining the centers of the surrounding fibers, see Fig.2. In the present paper we will use the local volume fraction V_f^{loc} as a measure of the local fiber distribution as displayed in Eqn (1). A lower local volume fraction represents larger inter fiber distance a_f and vice versa. Due to periodicity, only one twelfth of the composite is modeled, as shown in Fig.1c. In Fig.1c and further in the text l_d denotes the debond length measured from the fiber break and $l_d \neq l_d(\theta)$.

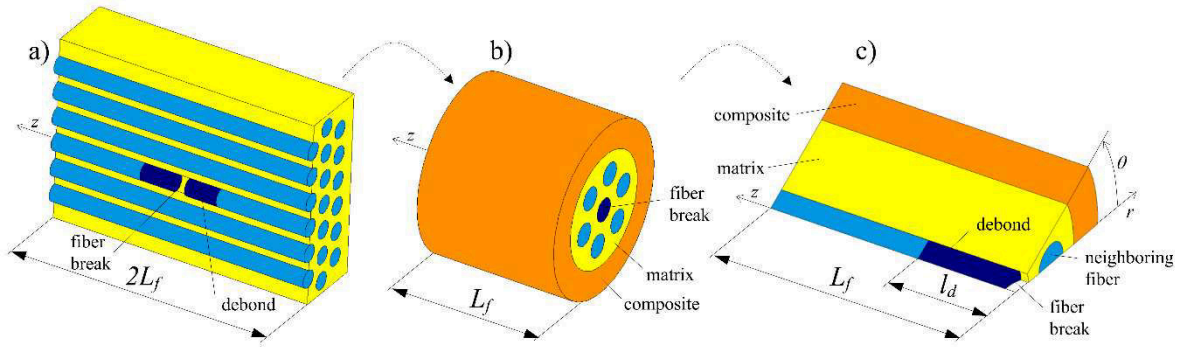

Fig.1. a) UD composite with a broken and partially debonded fiber; b) Hexagonal arrangement model; c) One twelfth of model, θ=0°-30°

3. FE model and boundary conditions

In order to study the debond growth from fiber break a 3-D FE model with hexagonal fiber arrangement representing the material geometry described in Fig.1(c) was created. In the FE model, the fiber radius r_f =4μm, the inter-fiber distance a_f and the debond length l_d are variables in order to study the effect on ERR of the debond growth. r_m is chosen to ensure fiber volume fraction is 0.6 within fiber/matrix unit, the local fiber volume fraction V_f^{loc} is varying with changing a_f. The length of the composite model L_f =80 r_f and the radius r_c=5 r_m were chosen based on a previous parametric study

conducted as a part of investigation in [28] as a region where the ERR becomes independent of these parameters.

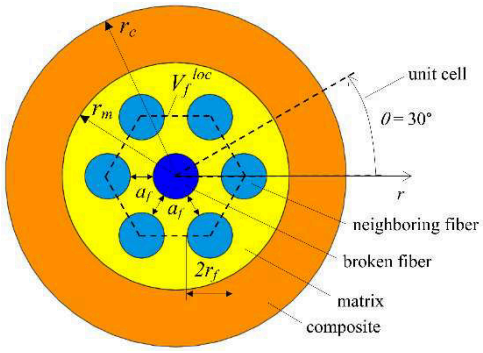

Fig.2 Cross-section of the hexagonal model and extraction of the unit cell.

$$V_f^{loc} = \frac{2\pi}{\left(2 + \frac{a_f}{r_f}\right)^2 \sqrt{3}} \tag{1}$$

In the present study, ERR is investigated as driving force for debond growth and it is calculated by both, the J integral and the VCCT methods through ANSYS built-in routines [31] . The ANSYS J-integral and VCCT calculation routines [31] implemented in the present study were previously validated against analytical solution for a 3 cylinder axisymmetric model used, for example, in [6]. Both routines showed an excellent agreement with analytical results at converged mesh size.

8 node 3-D solid elements were adopted here and appropriate mesh refinement was used in the vicinity of the debond front region to ensure the accuracy of J-integral and VCCT calculations.

The detail of the used finite element mesh is shown in Fig.3. As shown in the figure, there are 12 elements along the debond front, which results in 2.5 degrees of angular resolution. In front of and behind the debond front along fiber axis a mesh refinement region with length t = 2 μm was created with 10 elements along t. Further refinement of mesh yielded similar results, indicating the convergence of the used finite element mesh configuration. In VCCT the adopted value of the crack extension corresponds to the length of the element behind the crack tip, in this case 0.2 μm, which is much smaller than the considered debond crack lengths.

The mesh in the debond front region t was not varied with changing the debond length l_d.

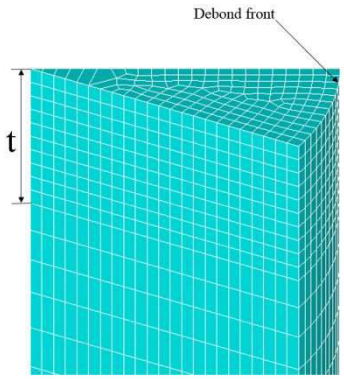

Fig.3 Detail of the finite element mesh in vicinity of the crack front. Volume representing the fiber shown.

Previous study has shown that thermal loading effect on ERR in composite (in contrast to the situation in a single fiber specimen) is negligible compared to that of mechanical loading [28]. As a result, only mechanical loading is considered in the present paper. In the FE model (see Fig.1c), nodes at r=0 and θ =0° are fixed. Nodes on θ=0 °and θ=30° planes are fixed in θ direction. At z=0 plane, symmetric boundary condition is applied except for fiber break surface which is traction free. At far end z=L_f plane, uniform

displacement which equals to 1% of average tensile strain ε_z along z direction is applied to all nodes belonging to that plane.

The outer cylindrical surface of the model ($r = r_c$) is traction free.

3-D 8-node contact elements with pure Lagrange multiplier on normal and tangential contact were generated on the debonded fiber/matrix interface in order to minimize the inter-penetration due to radial compression on the contact surface, which was proved to be efficient in the previous study [28].

4. Results and discussion

In the present study carbon fiber/epoxy (CF/EP) composite with global fiber volume fraction V_f =0.6 was analyzed. Limited investigation of Glass fiber/epoxy (GF/EP) composite with fiber volume fraction V_f =0.6 was also performed in order to demonstrate that the trends are similar as in CF/EP composite. Elastic properties of phases in the model in Fig. 1 and Fig. 2 are presented in Table 1. The effective elastic constants of the homogenized composite were calculated using the Hashin's Concentric Cylinder Assembly model [32] and the self-consistent scheme suggested by Christensen [33] (for the out-of-plane shear modulus). All the following discussions are based on the pure mechanical loading which equals to ε_z =1%.

Table 1. Elastic properties of constituents

Material	E_1(GPa)	E_2(GPa)	υ_{12}	G_{12}(GPa)	υ_{23}
CF	500	30	0.2	20	0.45
GF	70	70	0.2	29.2	0.20
EP	3.5	3.5	0.4	1.25	0.4
CF/EP	301.44	11.039	0.273	4.063	0.543
GF/EP	43.443	13.715	0.273	4.314	0.465

Note: CF-Carbon fiber , GF-Glass fiber, EP-epoxy resin, V_f =0.6 for both composites.

4.1 Carbon fiber/epoxy composites

We start with the case of carbon fiber/epoxy composites. Table 2 gives an example of the obtained ERR values using both, the J-intergral and the VCCT methods for two extreme local clustering cases with debond length l_d=25r_f. It was found that the debond remains closed for all the cases studied, which means Mode I ERR G_I=0 all the time. The obtained very small negative G_I value is an artificial effect of the numerical procedure related to approximate nature of the achieved contact: small oscillations of the relative radial displacement. For long debonds, see [28], the formally calculated small G_I value can be even positive. It should be noted that such findings in the contact analysis have been well documented in literature, for example, in [34]. Therefore the G_I value in Table 2 can be considered as an indicator of the accuracy achievable with the used mesh. The same reasoning goes for the obtained G_{III} value at θ=0° and θ=30° in Table 2 which should be zero due to symmetry. Meanwhile, for other angles, mode III ERR G_{III} is found to be less than 0.01% of the mode II ERR G_{II}. From Table 2 it is also seen that the ERR obtained from J-integral method is slightly lower than G_{II} obtained by VCCT. In contrary, in work on debond growth based on 3-cylinder FE model [6], Pupurs el al found that using the 3-cylinder axisymmetric model the J-integral values are slightly higher than G_{II} . Since there are no systematic trends we cannot conclude which method is better. We choose to use J-integral value in the following discussion as it is less sensitive to mesh refinement compared to those obtained through VCCT method.

The ERR calculated by J-integral along the front of debonds of different length in three local fiber volume fraction cases under pure mechanical loading are displayed in Fig.4 (a)-(c). Fig 10 in [18] shows that the fiber break (crack) in reality is not a geometrical plane, there is a small damage zone which is about the size of fiber radius. Meanwhile, matrix plasticity is also expected around the damage zone due to large stress concentration. As a result, in order to ensure numerical accuracy and the adequacy of the model, the ERR should be calculated for the debond length larger than the damage zone. In the present study, the shortest debond length investigated is l_d=2r_f.

Table 2. The highest and the lowest ERR values at the circular debond front for l_d=25r_f, CF/EP

	V_f^{loc}=0.68				V_f^{loc}=0.78			
θ (°)	J (J/m^2)	G_I (J/m^2)	G_{II} (J/m^2)	G_{III} (J/m^2)	J (J/m^2)	G_I (J/m^2)	G_{II} (J/m^2)	G_{III} (J/m^2)
0	53.0957	-0.0033	54.1728	0.0000	62.5439	-0.0026	64.2726	0.0000
30	45.6617	-0.0028	46.3251	0.0000	38.2090	-0.0027	38.7811	0.0002

Fig.4 (a)-(c) show that ERR is not constant along the debond front, which indicates that the debond front might not be circular during propagation as it was assumed: the debond would grow sooner in the directions with the highest ERR. For each debond length, maximum ERR occurs at θ=0° where the distance between the debond front and the neighboring fiber surface is the smallest. ERR decreases with increasing angle until θ=30°. However, with decreasing local fiber volume fraction, the variation of the ERR along the debond front (θ direction) becomes less significant, as the perturbation from the neighboring fiber becomes smaller with neighboring fibers moving away from the broken fiber. It would be expected that the ERR would be constant along the debond

front when neighboring fibers are sufficiently far away where the effect of the neighboring fibers could not be felt. Meanwhile, for each local fiber volume fraction case, it is also found that the ERR decreases with increasing debond length at each angular location along the debond front. For each debond length, the maximum ERR is higher in larger local volume fraction case suggesting debonds tend to grow first in the fiber clustering regions.

To better interpret the angular variation of results in Fig.4 (a)-(c), the ratio and the difference between ERR at θ=0° and θ=30° is also calculated for each local volume fraction case and it is displayed in Fig. 5(a) and Fig. 5(b), respectively. The larger ratio or difference means more variation of ERR along debond front, which also indicates more significant effect of the neighboring fibers. As shown in Fig.5 (a) and (b), both the ratio and the difference show the same trend: it is the highest in V_f^{loc}=0.78 case, and decreases with decreasing local fiber volume fraction. Meanwhile, for each local volume fraction case, both the ratio and the difference decrease slightly with increasing debond length and then they tend to become constant when steady state growth region is approached. The observed insensitivity to debond length indicates that the debond, even if its shape is not circular, would not change the shape during propagation.

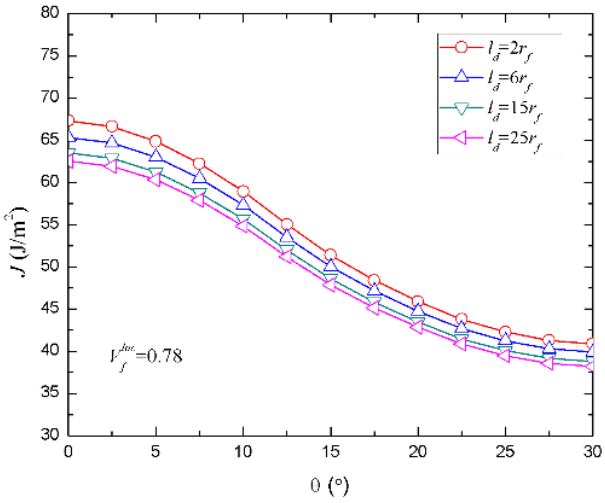
80
75
70
65
60
55
50
45
40
35
30
0
5
10
15
20
25
30
J (J/m²)
θ (°)
$l_d=2r_f$
$l_d=6r_f$
$l_d=15r_f$
$l_d=25r_f$
$V_f^{loc}=0.78$

Fig. 4 (a)

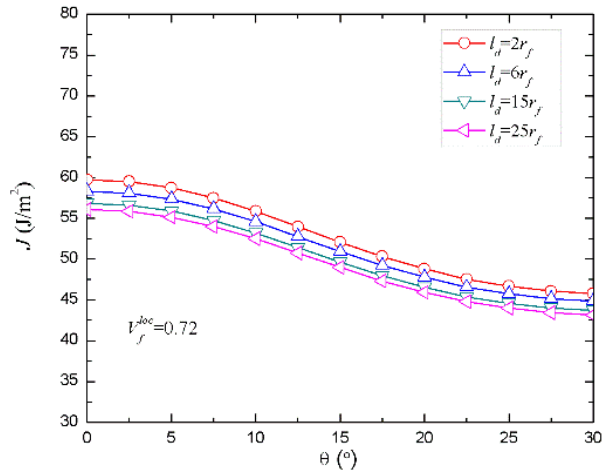
80
75
70
65
60
55
50
45
40
35
30
0
5
10
15
20
25
30
J (J/m²)
θ (°)
$l_d=2r_f$
$l_d=6r_f$
$l_d=15r_f$
$l_d=25r_f$
$V_f^{loc}=0.72$

Fig. 4 (b)

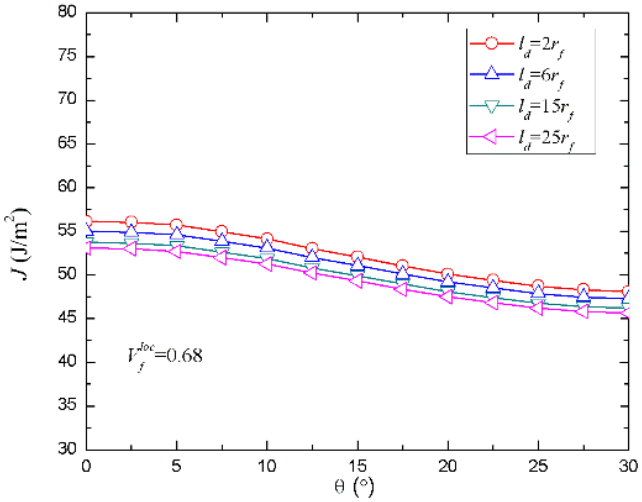

Fig. 4 (c)

Fig.4 a). Angular dependence of J-integral values for CF/EP in mechanical loading. $\varepsilon_z = 1\%$, V_f^{loc} =0.78,

b). Angular dependence of J-integral values for CF/EP in mechanical loading $\varepsilon_z = 1\%$, V_f^{loc} =0.72,

c). Angular dependence of J-integral values for CF/EP in mechanical loading $\varepsilon_z = 1\%$, V_f^{loc} =0.68.

From Fig.4 it is clear that the ERR depends on the local fiber volume fraction and for each debond length, the maximum ERR occurs at θ=0 °, where the circular debond is most likely to grow first. In order to demonstrate the effects of the local fiber clustering on the ERR, the ERR at θ=0° was calculated against debond length for three local fiber volume fraction cases and the results are displayed in Fig. 6.

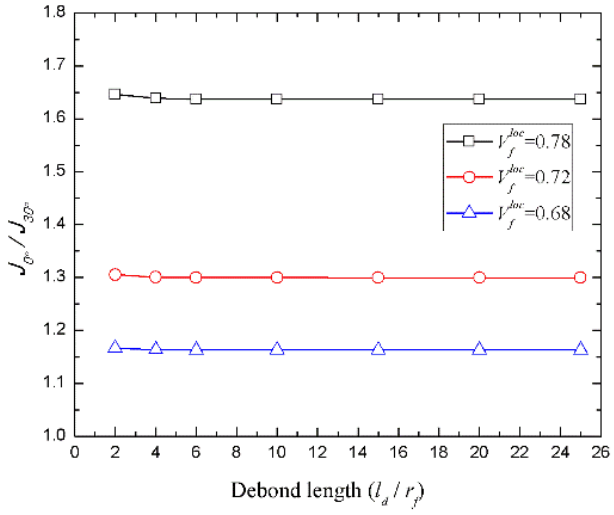

Fig. 5 (a)

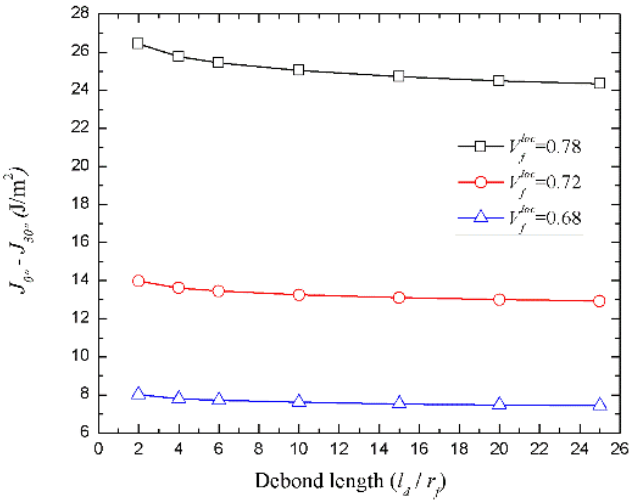

Fig. 5 (b)

Fig.5. a) The ratio of J-integral values obtained at θ=0 ° and at θ=30 °; b) The difference between J-integral value at θ=0 ° and that at θ=30 ° against normalized debond length for three local fiber volume fractions

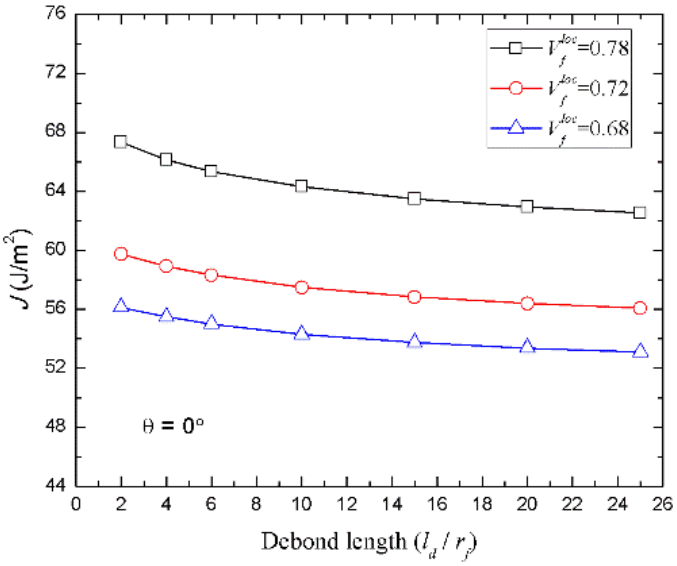

Fig. 6 The ERR at θ=0° against normalized debond length

Locally higher fiber volume fraction facilitates the debond growth: the ERR is significantly higher at V_f^{loc} =0.78 than at V_f^{loc} =0.68 and the effect is nonlinearly increasing. In all cases the ERR is decreasing with increasing debond length, monotonously approaching the corresponding steady state value. Direct comparison with the steady state solution presented for hexagonal model in [28] is not possible because that solution is based on potential energy change when a perfectly bonded element is replaced by element with debonded fiber and, therefore, the steady state model gives the average value and not the angular dependence of the ERR.

It should be noted that the same trend for the ERR holds for all angles along the debond front.

The ratio of the J-integral value at θ=0° obtained in V_f^{loc} =0.78 case and the one obtained for the same angle in V_f^{loc} =0.68 case is also calculated and plotted against the normalized debond length in Fig.7. The higher the ratio is, the more significant the fiber

clustering effect on the ERR is. From Fig.7 it can be seen that the ratio decreases gradually with the increase of the debond length and becomes constant for long debonds, when the steady stress state is approached.

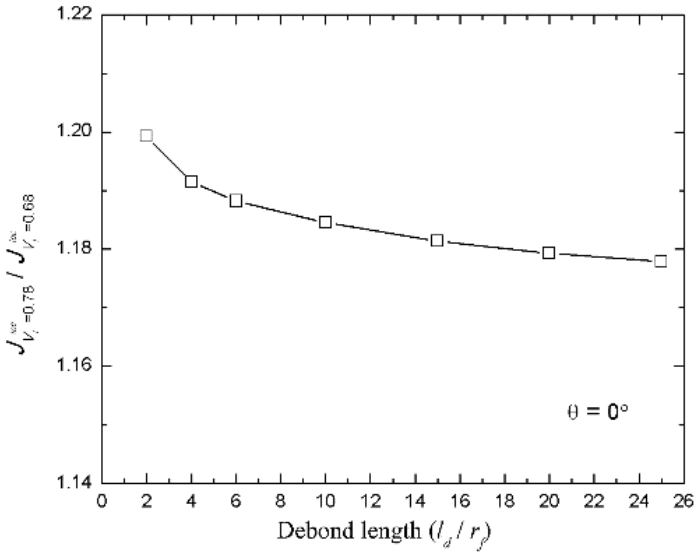

Fig. 7 Ratio of the J-integral values at θ=0° obtained in V_f^{loc} =0.78 case and those obtained in V_f^{loc} =0.68 case against normalized debond length.

So far we have discussed results based on angle dependent ERR values and it is obvious that the debond front would not be circular during loading. However, since in reality, the exact shape of debond front is difficult to define as it depends on many factors. Therefore, it is also of merit to calculate the average of the angle dependent ERR along the crack front.

Fig.8 shows the average ERR obtained by the 3-D hexagonal model and the ERR calculated by the 5 cylinder axisymmetric model developed in [27] for three local fiber volume fractions. The ERR obtained from both models has similar trend against the

debond length, although the ERR obtained in the axisymmetric case, with introduced fiber cylinder surrounding the investigated debonded fiber, is higher than the average ERR obtained in 3-D model. It is expected, as using a ring of fiber material in an axisymmetric model to represent the fiber clustering could be considered as an extreme case for fiber clustering where neighboring fibers are touched by each other in the 3-D model. In both models the effect of the local clustering diminishes with increasing debond length.

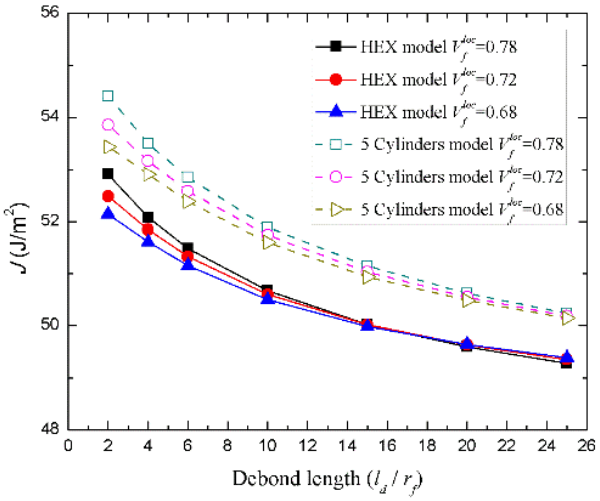

Fig. 8 Average ERR against normalized debond length obtained by the 3-D hexagonal model and axisymmetric model

Fig.9 shows the ratio of the average J-integral values obtained in V_f^{loc}=0.78 case and those obtained in the V_f^{loc}=0.68 case. Similar trend is found as that in Fig.7 for the same ratio at θ=0, however, the effect of neighboring fiber is much less significant and for long debonds the ratio is almost equal to one.

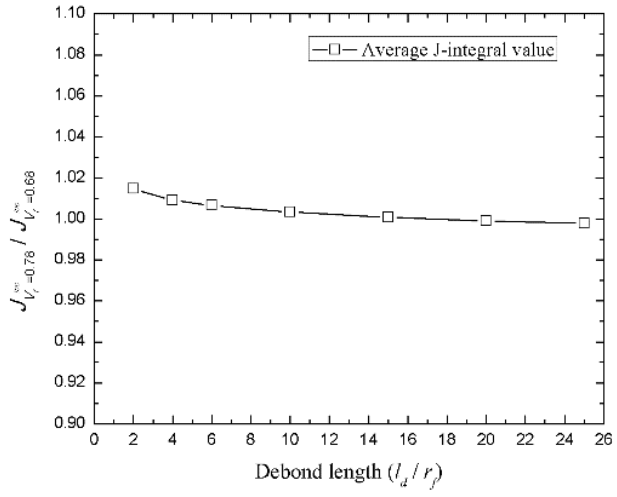

Fig. 9 Ratio of the average J-integral values for V_f^{loc}=0.78 and those for V_f^{loc}=0.68 against normalized debond length.

4.2 Glass fiber/epoxy composites

In order to account for the effect of the fiber properties on the debond growth, the local fiber clustering in glass fiber/epoxy (GF/EP) composite with local fiber volume fraction V_f^{loc}=0.78 under the same tensile strain as in the CF/EP case was studied. V_f^{loc}=0.78 represents the most severe fiber clustering case among investigated in the CF/EP material system. It was found that for GF/EP composite, similarly as to CF/EP composite, the debond growth under tensile mechanical loading is in Mode II. In the following only results obtained through J-integral method are presented.

Fig.10 shows the ERR for GF/EP obtained by the J-integral along debond front of debonds with different length. Due to the lower elastic modulus of the glass fiber, the ERR is much lower than that in the CF/EP case. However, similar trend as that in Fig.4 for CF/EP is found: for each debond length, the ERR has a maximum at θ=0° and decreases with increasing angle until θ=30°. The shape of the ERR variance along the debond front is very similar with the CF/EP case. The average ERR versus debond

length is plotted in Fig.11. As shown in Fig.11, the average ERR is decreasing with increasing debond length and tend to become constant as debond reaches the steady state growth region, observation that is similar to what was found in the CF/EP case.

Finally, the ratio of the ERR at θ=0° and θ=30° is calculated for each debond length and compared with that in CF/EP case, see Fig.12. It is found that although the ratio (angle dependence) is slightly higher in the CF/EP cases, the same trend could be found for both cases: the ratio decreases slightly for debond length l_d up to 4 r_f and then the ratio tends to become constant with increasing debond length. Based on the discussion above, it could be concluded that the ERR obtained for the initial stage of debond growth in GF/EP composites has a similar trend as that in CF/EP composites, which also indicates that a similar debond growth behavior could be found for both material systems.

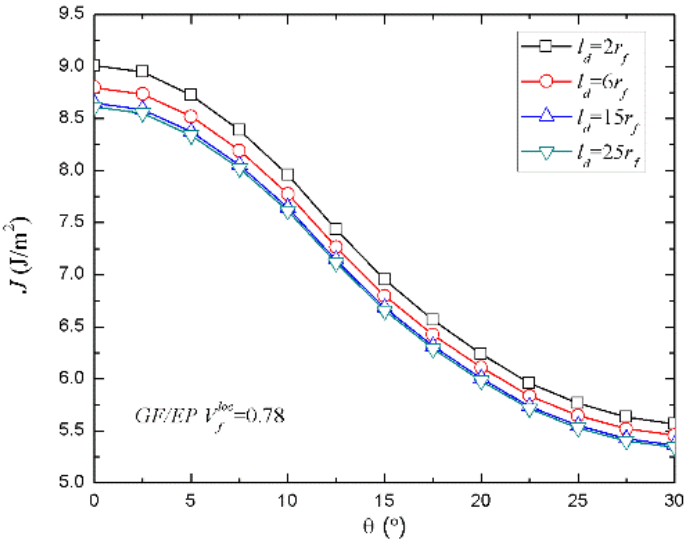

Fig. 10 J-integral dependence on θ for GF/EP composite in mechanical loading $\varepsilon_z = 1\%$, V_f^{loc}=0.78

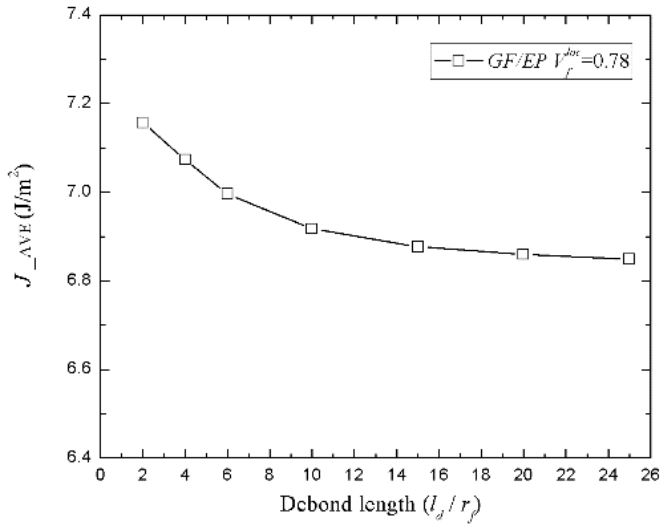

Fig. 11 Average value of the J-integral for GF/EP composite versus normalized debond length.

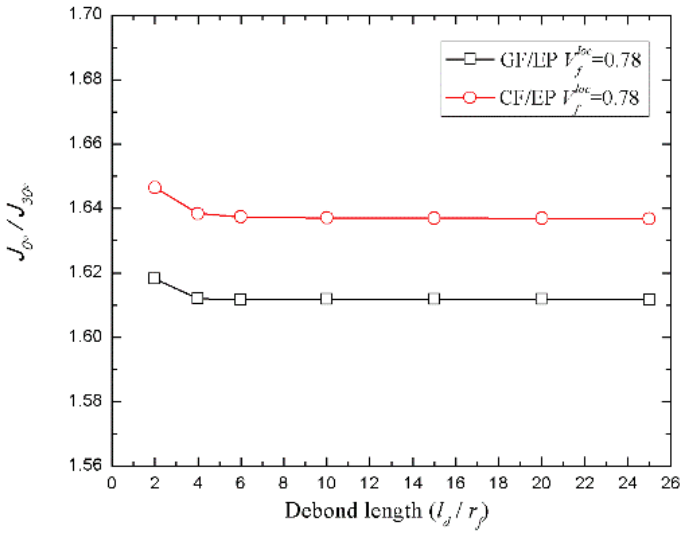

Fig. 12 Ratio of the J-integral value obtained at θ=0 ° and that at θ=30 ° for both CF/EP and GF/EP composites.

5. Conclusions

The effect of local fiber clustering on potential energy release rate (ERR) during the initial stage of debond growth along a broken fiber in UD composite under tensile axial loading has been investigated using a model with local hexagonal fiber array with central broken fiber, this unit being surrounded by homogenized effective composite. A 3-D hexagonal FE model with contact elements on the debond surfaces was used. The J-integral and the VCCT method were adopted in order to calculate the ERR assuming thet the debond front is circular. The ERR results collected from the 3-D model were then compared with those obtained using a 5-cylinder axisymmetric model developed earlier by the same authors. Carbon fiber/epoxy UD composite and glass fiber/epoxy composites with global fiber volume fraction V_f=0.6 were studied. Based on these investigations, following conclusions are drawn:

1. For CF/EP composites, in the presence of local fiber clustering, the ERR of initial short debond shows significant dependence on angle θ along the debond front, with the maximum ERR always found at θ=0° , where the distance between the broken fiber and the neighboring fiber is the shortest. That angular dependence is magnified for more dense fiber clustering or for shorter debond length cases.
2. For CF/EP composites, for each local fiber clustering case, ERR decreases with increasing debond length. Although the ERR varies along the debond front, the shape of the ERR variance is similar for each debond length, which suggests that the shape of debond front, which in fact is not circular, would remain similar and independent on the debond length.
3. For CF/EP composites, the avarage ERR is not senstitive to fiber clustering..
4. The ERR of GF/EP composite shows similar trends as found in the CF/EP composite.

5. The average ERR obtained from the 3-D hexagonal model is slightly lower than the ERR from 5-cylinder axisymmetric model, which indicates that the axisymmetric model could be used as an upper bound to the hexagonal 3-D model.

Acknowledgements

Funding from the strategic innovation programme LIGHTer provided by Vinnova (Sweden) is acknowledged. Linqi Zhung would like to thank European DocMASE program for the financial support.

References

[1] Rosen BW. Tensile failure of fibrous composites. AIAA journal. 1964;2(11):1985-91.

[2] Zweben C. Tensile failure of fiber composites. AIAA journal. 1968;6(12):2325-31.

[3] Talreja R. Fatigue of composite materials: damage mechanisms and fatigue-life diagrams. Proceedings of the Royal Society of London A Mathematical and Physical Sciences. 1981;378(1775):461-75.

[4] Lorenzo L, Hahn HT. Fatigue failure mechanisms in unidirectional composites. Composite Materials: Fatigue and Fracture. 1986:210-32.

[5] Curtin W. Stochastic damage evolution and failure in fiber-reinforced composites. Advances in applied mechanics. 1998;36:163-253.

[6] Pupurs A, Krasnikovs A, Varna J. Energy release rate based fiber/matrix debond growth in fatigue. Part II: Debond growth analysis using Paris law. Mechanics of Advanced Materials and Structures. 2013;20(4):288-96.

[7] Pupurs A, Varna J. Energy release rate based fiber/matrix debond growth in fatigue. Part I: Self-similar crack growth. Mechanics of Advanced Materials and Structures. 2013;20(4):276-87.

[8] Pupurs A, Varna J. FEM modeling of fiber/matrix debond growth in tension-tension cyclic loading of unidirectional composites. Int J Damage Mech. 2013;22(8):1144-60.

[9] Behzadi S, Curtis PT, Jones FR. Improving the prediction of tensile failure in unidirectional fibre composites by introducing matrix shear yielding. Composites Science and Technology. 2009;69(14):2421-7.

[10] Gamstedt E, Talreja R. Fatigue damage mechanisms in unidirectional carbon-fibre-reinforced plastics. Journal of Materials Science. 1999;34(11):2535-46.

[11] Gamstedt EK, Berglund LA, Peijs T. Fatigue mechanisms in unidirectional glass-fibre-reinforced polypropylene. Composites Science and Technology. 1999;59(5):759-68.

[12] Curtin W. Exact theory of fibre fragmentation in a single-filament composite. Journal of materials science. 1991;26(19):5239-53.

[13] Kim BW, Nairn JA. Observations of fiber fracture and interfacial debonding phenomena using the fragmentation test in single fiber composites. Journal of composite materials. 2002;36(15):1825-58.

[14] Pupurs A, Varna J. Fracture mechanics analysis of debond growth in a single-fiber composite under cyclic loading. Mechanics of Composite Materials. 2011;47(1):109-24.

[15] Graciani E, Mantič V, París F, Varna J. Single fiber fragmentation test. A BEM analysis. Collection of Technical Papers-AIAA/ASME/ASCE/AHS/ASC Structures, Structural Dynamics and Materials Conference2003. p. 988-97.

[16] Wagner H, Nairn J, Detassis M. Toughness of interfaces from initial fiber-matrix debonding in a single fiber composite fragmentation test. Appl Compos Mater. 1995;2(2):107-17.

[17] Nairn JA. A variational mechanics analysis of the stresses around breaks in embedded fibers. Mechanics of Materials. 1992;13(2):131-54.

[18] Pupurs A, Goutianos S, Brondsted P, Varna J. Interface debond crack growth in tension–tension cyclic loading of single fiber polymer composites. Composites Part A: Applied Science and Manufacturing. 2013;44:86-94.

[19] Pupurs A, Varna J. Analytical solution for energy release rate due to steady-state fiber/matrix debond growth in UD composites. Int J Damage Mech. 2016

[20] Li H, Jia Y, Luan S, Xiang Q, Han CC, Mamtimin G, et al. Influence of inter-fiber spacing and interfacial adhesion on failure of multi-fiber model composites: Experiment and numerical analysis. Polymer Composites. 2008;29(9):964-71.

[21] Van den Heuvel P, Goutianos S, Young R, Peijs T. Failure phenomena in fibre-reinforced composites. Part 6: a finite element study of stress concentrations in unidirectional carbon fibre-reinforced epoxy composites. Composites science and technology. 2004;64(5):645-56.

[22] Van den Heuvel P, Peijs T, Young R. Failure phenomena in two-dimensional multi-fibre microcomposites—3. A raman spectroscopy study of the influence of interfacial debonding on stress concentrations. Composites science and technology. 1998;58(6):933-44.

[23] van den Heuvel PWJ, Peijs T, Young RJ. Failure phenomena in two-dimensional multifibre microcomposites: 2. A Raman spectroscopic study of the influence of inter-fibre spacing on stress concentrations. Composites Science and Technology. 1997;57(8):899-911.

[24] Case S, Carman G, Lesko J, Fajardo A, Reifsnider K. Fiber fracture in unidirectional composites. Journal of composite materials. 1995;29(2):208-28.

[25] Nedele MR, Wisnom MR. Three-dimensional finite element analysis of the stress concentration at a single fibre break. Composites science and technology. 1994;51(4):517-24.

[26] Nedele M, Wisnom M. Stress concentration factors around a broken fibre in a unidirectional carbon fibre-reinforced epoxy. Composites. 1994;25(7):549-57.

[27] Zhuang L, Pupurs A. Effect of neighboring fibers on energy release rate during fiber/matrix debond growth. 16th European Conference on Composite Materials, ECCM 20142014.

[28] Zhuang L, Pupurs A, Varna J, Ayadi Z. Effect of fiber clustering on debond growth energy release rate in UD composites with hexagonal packing. Engineering Fracture Mechanics. 2015:Submittted

[29] Rice JR. Mathematical analysis in the mechanics of fracture. Fracture: an advanced treatise. 1968;2:191-311.

[30] Rybicki EF, Kanninen M. A finite element calculation of stress intensity factors by a modified crack closure integral. Engineering Fracture Mechanics. 1977;9(4):931-8.

[31] ANSYS Academic Research, Release 14.0. Canonsburg, Pennsylvania2011

[32] Hashin Z. Analysis of composite materials—a survey. Journal of Applied Mechanics. 1983;50(3):481-505.

[33] Christensen R, Lo K. Solutions for effective shear properties in three phase sphere and cylinder models. Journal of the Mechanics and Physics of Solids. 1979;27(4):315-30.

[34] Whitcomb JD. Analysis of a laminate with a postbuckled embedded delamination, including contact effects. Journal of composite materials. 1992;26(10):1523.

Paper D

Effects of Inter-Fiber Spacing on Fiber-matrix debond Crack Growth in Unidirectional Composites Under Transverse Loading

Effects of Inter-Fiber Spacing on Fiber-matrix Debond Crack Growth in Unidirectional Composites under Transverse Loading

Linqi Zhuang[a,b,c], Andrejs Pupurs[b,c*], Janis Varna[b], Ramesh Talreja[a,b], Zoubir Ayadi[c]

[a] Texas A&M, College Station, USA

[b] Lulea University of Technology, Sweden

[c] University of Lorraine, France

[d] SICOMP Swerea, Sweden

[*]Corresponding author, e-mail: andrejs.pupurs@ltu.se, phone: +46 920 49 1783

Abstract

The energy release rate (ERR) of a fiber-matrix debond crack in a unidirectional composite subjected to transverse tension is studied numerically. The focus of the study is the effect of the proximity of the neighboring fibers on the ERR. For this, a hexagonal pattern of fibers in the composite cross-section is considered. Assuming one fiber to be debonded at different initial debond arc-lengths, the effect of the closeness of the surrounding six fibers on the ERR of the crack is studied with the inter-fiber distance as a parameter. Using an embedded cell consisting of discrete fibers in a matrix surrounded by the homogenized composite, a finite element model and the virtual crack closure technique are used to calculate the ERR. Results show that the presence of the local fiber cluster accelerates the crack growth up to a certain initial crack angle, beyond which the opposite effect occurs. It is also found that the residual stress due to thermal cooldown reduces the ERR. However, the thermal cooldown is found to enhance the debond growth in plies within a cross-ply laminate.

Keywords: A. Polymer-matrix composites (PMCs), B. Debonding, C. Finite element analysis (FEA)

1. Introduction

In many applications of composite materials, design is based on the threshold for first crack formation. In multidirectional composite laminates loaded in tension along 0^0 plies, transverse cracking in 90° plies has been found to be the first failure mechanism and has been studied extensively by numerous researchers. While some of the studies (e.g. [1-8]) have focused on multiple transverse cracking and its effect on laminate deformational response, others (e.g. [9, 10]) have studied the mechanisms underlying formation of a transverse crack. It is commonly accepted that a macroscale transverse crack forms by the coalescence of fiber/matrix debonds. Asp et al [11-13] studied the local stress field around fibers in the cross-section of a unidirectional (UD) composite loaded in transverse tension and based on energy considerations proposed that the

debonding results from unstable growth of a cavity in the matrix near the fiber surface. These studies clarified the role of the triaxiality of the local stress field in initiation of debonding. Therefore, while many studies of debonding have focused on single-fiber composites [14-22], a proper understanding of debond initiation and growth is expected to come from multiple-fiber composite studies. Recently, a few studies have gone in this direction [23-25]. In [23, 25] the approach taken was to use a cohesive zone model, which has the interface strength and fracture toughness as two material properties. As noted above, Asp et al [11, 13] showed that failure at the fiber-matrix interface depends on the triaxial stress state, not on the tensile stress alone. This casts doubt on the use of a cohesive zone model for studying the debonding process. In [24], the concurrent and growth debonds have been investigated by linear elastic-brittle fracture based on a numerical model containing ten fibers embedded in a matrix cell. However, no detailed information about the influence of local fiber bundles on debond growth could be obtained from that paper. While these studies have been useful in generating understanding of the local interactions in the debonding process, two aspects need further clarity. First, the influence of inter-fiber distance on debond growth in a fiber cluster needs to be understood, and second, the debonding process should be analyzed in terms of the energy release rate (ERR) of the arc-shaped interface crack. These two aspects have been studied by Sandino et al [26], but only for a two-fiber case. These authors placed an undamaged fiber at different locations near a central fiber with debond and investigated how that affected the ERR of the debond crack. In their work, they found that the neighboring fiber has a protective effect on debond growth at all positions except when the fibers are aligned with the loading direction. As useful as their results are, the two-fiber composite model is still not representative of a real composite where multiple neighboring fibers are distributed around the fiber with debond.

The present paper specifically investigates the influence of neighboring fibers on the growth of a debond crack in a UD composite subjected to uniaxial transverse loading. Previous works by some of the current authors [27-29] for longitudinal debond growth along the fiber length of a fragmented fiber under axial loading indicated that the neighboring intact fibers influence this debonding at short debond lengths before the debond reaches the state-steady growth stage. Following [28, 29], we place an initially

debonded fiber at the center of a hexagonal fiber arrangement. Recognizing that the nearest fibers have the most significant effects on the stress field near the debond crack tip, six nearest surrounding fibers are modelled explicitly. The inter-fiber distance between the central fiber and the neighboring fibers is varied in order to capture the local fiber clustering effects. The rest of the hexagonally packed composite is represented by a homogenized effective composite material with its thermo-elastic properties calculated by micromechanics. The whole UD composite is subjected to transverse loading.

Experimental observations in [17] indicated that a fiber in transverse tension debonds from the matrix over a much larger length in the axial direction than in the circumferential direction. Therefore, the analysis here is carried out under plane strain conditions. Assuming linear elastic matrix and fibers, the ERR, which is the driving force for debond growth, was calculated by the Virtual Crack Closure Technique (VCCT) using Finite Element (FE) software ANSYS [30].

2. Finite element model and boundary conditions

Details of the model are shown in Fig. 1. Due to the symmetry, only half of the composite is modelled. For the finite element (FE) computations, the initially debonded fiber is placed at the center of the model. The debond crack is placed on one side of the fiber surface with its mid-point normal aligned with the transverse loading direction. The debond have two tips and is assumed to propagate symmetrically with respect to the symmetric line, as shown in Fig.1. The debond crack size is quantified by the angle θ, as indicated in Fig. 1. The debonded fiber is surrounded by six intact fibers in hexagonal pattern and the seven-fiber assembly within a circular matrix region is embedded in the homogenized composite. The fiber radius r_f = 4 μm and the radius of circular matrix region *RMO* is chosen such that the fiber volume fraction (denoted V_f) within this region equals the global fiber volume fraction of the composite. The half-height and width of the model are chosen as L=20*RMO* and

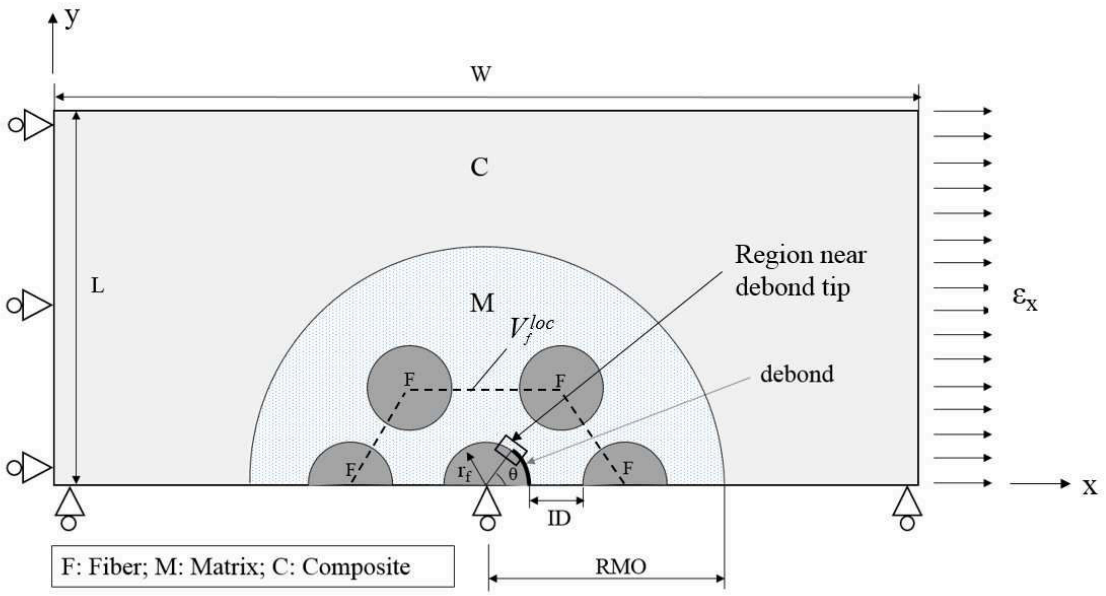

Fig.1 Model description

W=40*RMO*, respectively, beyond which the calculated ERR of the debond crack is not affected by the size of the model. As a measure of the local fiber distribution, we will use here the local volume fraction V_f^{loc} as defined in Eqn (1).

$$V_f^{loc} = \frac{2\pi}{\left(2+\frac{ID}{r_f}\right)^2\sqrt{3}} \tag{1}$$

As indicated in Fig. 1, V_f^{loc} represents the fraction of the cross-sectional area of the fibers inside the hexagon joining the centers of the fibers surrounding the debonded fiber, as shown in Fig.1. Thus, a lower local volume fraction represents larger inter fiber distance *ID* and vice versa.

As shown in Fig.1, the x-displacement is applied uniformly to the right edge (x = W) of the model, while it is constrained on the left edge, to induce the strain ε= 0.5%. For relatively small debond angles, 2-D quadratic plane strain elements with pure Lagrange multipliers on normal and tangential contact were generated on the debond surface to

model contact behavior with minimal interpenetration. When the debond grows to a much larger angles ($\theta > 90°$), penalty-based contact elements were generated to ensure quicker convergence. It is noted that a separate study (not presented here) of the effects of different contact algorithms on the calculated ERR was also conducted, finding that the difference between the two algorithms adopted here is small when debond surfaces are in contact.

In the present paper, dimensionless ERR will be presented by normalizing the obtained ERR by G_0 (Eqn. 2), as in previous studies [14, 26]. It is noted that although G_0 in [14] was proposed for isotropic materials, we shall use it here with the justification that the UD composites considered here are transversely isotropic. For each fiber volume fraction of the composite, G_0 will be calculated using the composite properties in the transverse plane (see Table 1). G_0 is given by

$$G_0 = ((1+k) / 8\mu)\, \sigma_0^2\, r_f \pi \tag{2}$$

where $k = 3 - 4\nu$, and ν is the Poisson's ratio and μ is the shear modulus. These elastic properties here are for the isotropic transverse plane of the composite. The applied tensile stress σ_0 is calculated using the imposed strain ε_x and the transverse composite modulus.

3. Results and discussions

The material in the present study is carbon fiber/epoxy (CF/EP) composite with global fiber volume fraction V_f =0.6 and V_f =0.4. To confirm the observed trends a limited investigation of Glass fiber/epoxy (GF/EP) composite with fiber volume fraction V_f =0.6 was also conducted. Material thermo-elastic properties in the model are presented in Table 1. The effective elastic constants of the homogenized composite were calculated using Hashin's Concentric Cylinder Assembly model [31] and the self-consistent scheme suggested by Christensen [32] (for the out-of-plane shear modulus).

Table 1. Thermal-elastic properties of constituents

Material	E_1 (GPa)	E_2 (GPa)	υ_{12}	G_{12} (GPa)	υ_{23}	α_1 (1/°c)	α_2 (1/°c)	G_0 (J/m^2)
CF	500	30	0.2	20	0.45	$-1\cdot10^{-6}$	$7.8\cdot10^{-6}$	N/A
GF	70	70	0.2	29.2	0.2	$4.7\cdot10^{-6}$	$4.7\cdot10^{-6}$	N/A
Epoxy	3.5	3.5	0.4	1.25	0.4	$60\cdot10^{-6}$	$60\cdot10^{-6}$	N/A
CF/EP (V_f = 0.6)	301.4	11.04	0.27	4.06	0.54	$-0.66\cdot10^{-6}$	$35.85\cdot10^{-6}$	2.44
CF/EP (V_f = *0.4*)	202	7.56	0.31	2.61	0.59	$-0.28\cdot10^{-6}$	$50.97\cdot10^{-6}$	1.55
GF/EP (V_f = 0.6)	43.4	13.7	0.27	4.31	0.46	$6.86\cdot10^{-6}$	$32.2\cdot10^{-6}$	3.38

To calculate the ERR of the debond crack, VCCT was adopted. It has been well documented that for an interface crack between two dissimilar materials (here: debond), Mode I and Mode II components of the ERR are not well defined [33-36]. As a result, the calculated ERR modes here depend on the size of the near tip element. In the current study, the size of the near tip element is $r_f \cdot d\theta$, where $d\theta$ = 0.5°, as shown in Fig.2. Due to the lack of available data, the validation of the current FE model was conducted by comparing the debond crack ERR obtained by using the current FE model with those obtained by Sandino et al [26] for a single-fiber glass/epoxy composite using the BEM model . In order to model the single-fiber composite using the current FE model, the material properties of neighboring fibers and the homogenized composite were replaced with matrix properties. The validation results are presented in Fig.3. As displayed in Fig.3, the ERR calculated by both numerical models are practically the same.

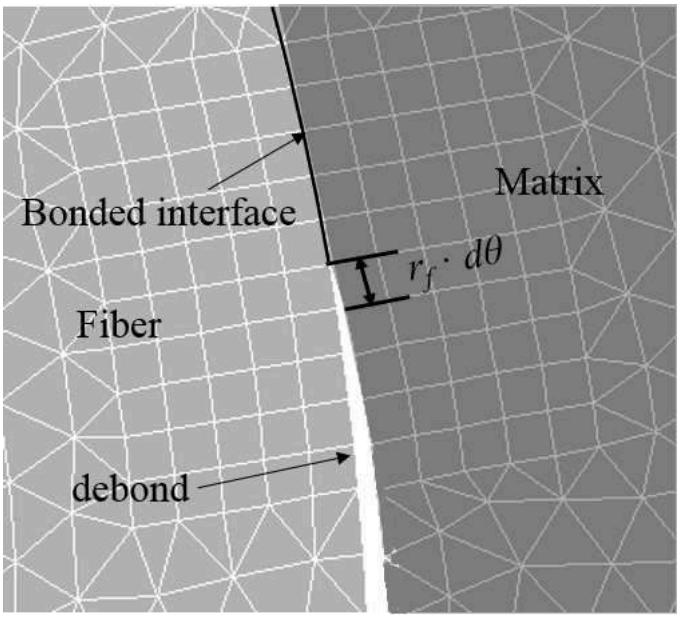

Fig.2 Details of mesh near debond tip

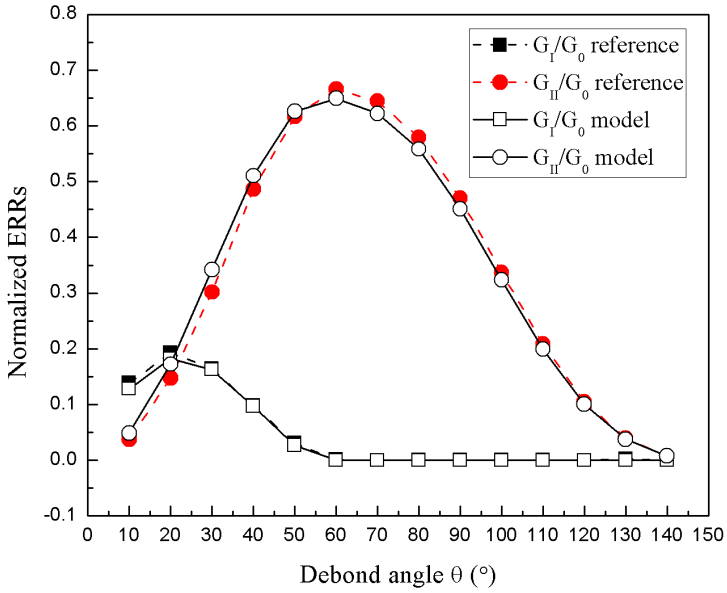

Fig.3. Comparison of obtained ERR results for a single fiber composite with numerical model in reference [26].

3.1 Carbon fiber/epoxy composite, $V_f = 0.6$

We first analyze the case of carbon fiber/epoxy composite with $V_f = 0.6$. Figure 4 shows the obtained ERR normalized with respect to G_0 (Table 1) for mechanical

loading only (ε_x = 0.5%). The initial debond was varied from the smallest value of θ = 2° and V_f^{loc} was selected at three values 0.66, 0.72 and 0.78. As seen from the figure, debond growth is in mixed-mode for all V_f^{loc} cases. For debond angles slightly greater than θ = 2° and until θ ≈ 70°, both ERR components G_I and G_{II} increases initially with the debond angle, attaining a maximum and then decreasing. Beyond θ ≈ 70° G_I is practically zero and the debond growth is driven by G_{II}. The G_I component attains a maximum at θ ≈ 20°, for all cases, while, the maximum value of G_{II} occurs at θ ≈ 50°. The debond growth becomes Mode II dominated at θ ≈ 30° and at θ ≈ 70°, where G_I = 0, a physically relevant finite contact zone where corresponding contact element status changed from open to contact was detected. Therefore, θ =70° is considered as a transition angle (denoted θ_t) beyond which debond grows in pure Mode II.

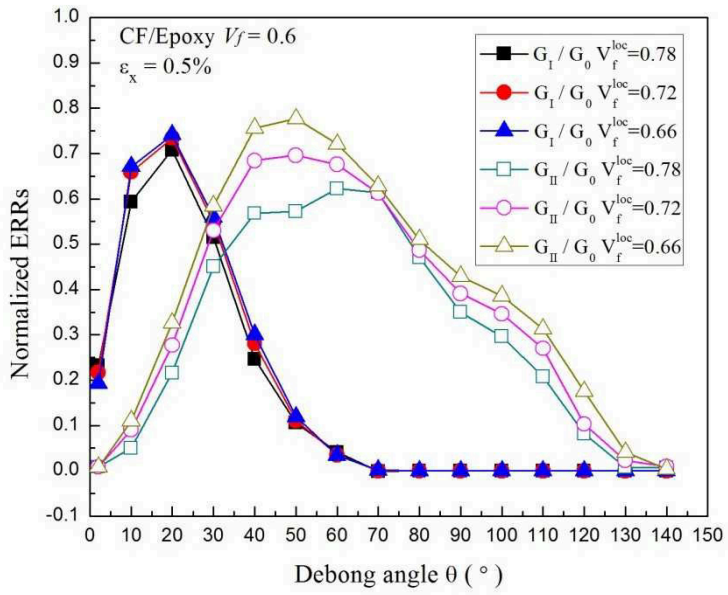

Fig.4. Normalized ERR with respect to debond angle for CF/EP UD composites under mechanical loading. ε_x = 0.5%. V_f = 0.6

It can be seen from Fig. 4 that as V_f^{loc} increases, i.e., as the fully bonded fibers get closer to the debonded fiber, the ERR of the debond crack decreases. However, exception is for G_I at θ = 2° where the opposite trend is seen. Thus, between the computed G_I values at θ = 2° and at θ = 10° there is a switchover in the effect of the surrounding fibers on the debond growth. To confirm this, the radial opening of the debond crack along its length (debond angle) is plotted for θ = 2° in Fig. 5 (a) and for θ = 10° in Fig. 5 (b).

The switchover effect is indicated by the crack opening, confirming the behavior seen in G_I. In Fig. 6 (a) and 6 (b) the radial normal stress on the interface ahead of the debond crack is plotted for the two cases. Once again, the trend in G_I is confirmed by these results.

The ERR results in Fig. 4, and the switchover in the G_I trend with inter-fiber distance at small debond angles described above, illustrate the interplay between the so-called "enhancement" and "shielding" effects on the debond crack tip stress field due to the proximity of the surrounding fibers. As other studies [23, 26] have found, the enhancement effect dominates when the line joining two adjacent fibers is aligned with the transverse loading direction, and the shielding effect depends on how much the line is rotated with respected to the loading direction.

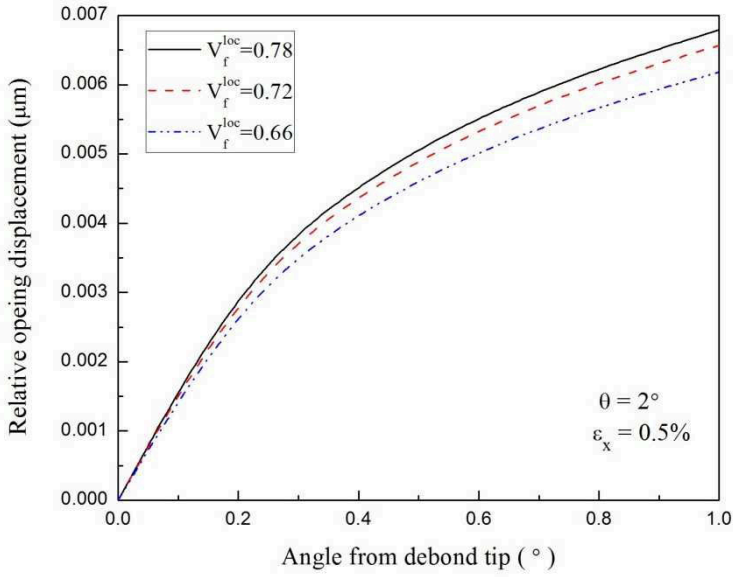

Fig. 5 (a) Debond opening near the debond tip. Debond angle θ = 2°, ε_x=0.5%.

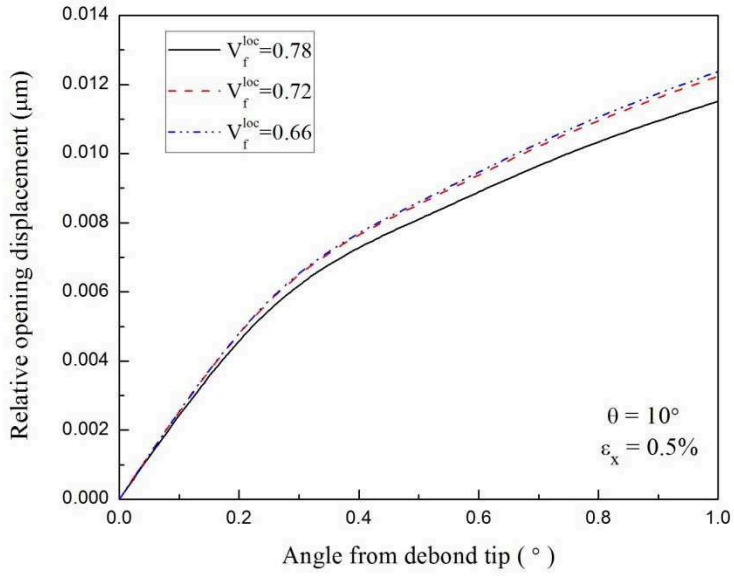

Fig. 5 (b) Debond opening near the debond tip. Debond angle θ = 10°, ε_x=0.5%

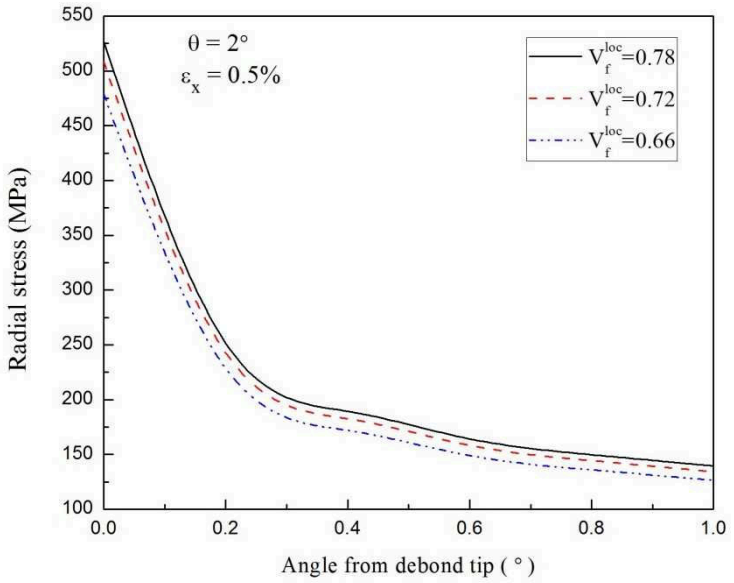

Fig. 6 (a) Radial stress distribution along the bonded interface ahead of the debond tip. Debond angle θ = 2°, ε_x=0.5%

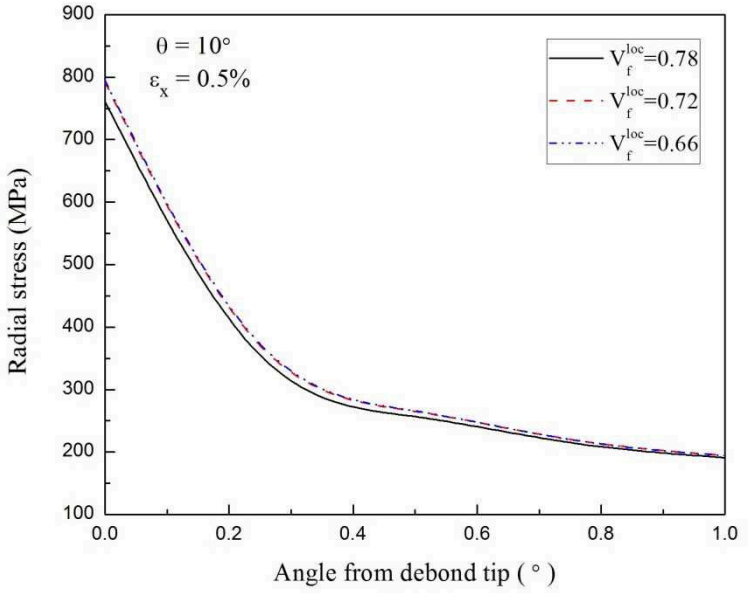

Fig. 6 (b) Radial stress distribution along the bonded interface ahead of the debond tip. Debond angle θ = 10°, ε_x=0.5%

3.1.1 Thermal cooldown effects

Since processing of carbon/epoxy composites often involves cooldown from the curing temperature, we investigate the effect of the local thermal stresses generated by the cooldown temperature ΔT = -100°C. This temperature change was applied uniformly to the model (Fig. 1) and was followed by a uniform displacement at $x = W$ to result in the mechanical strain $\varepsilon_x = 0.5\%$. The residual stress field induced by chemical shrinkage due to curing was, however, not included directly. As shown in [37], the thermal cool-down is the main contributor to the development of residual stresses and in a linear thermo-elastic analysis the effect of chemical shrinkage can be formally included as a part of thermal stress by taking a higher stress free temperature [38]. Fig. 7 displays the ERRs calculated for different V_f^{loc}. As can be seen, for all V_f^{loc} cases considered, the presence of thermal stress does not significantly alter the overall behavior of the ERR for debond growth compared to the mechanical loading case, except for small debond angle (θ < 5°) where now the trend seen in the mechanical loading case (Fig. 4) with respect to the influence of V_f^{loc} is absent. This behavior can be attributed to the compressive radial stress on the fiber surface caused by thermal cooldown. To clarify this effect, in Fig. 8 we plot this stress on the central bonded fiber

in the hexagonal fiber configuration along the interface for the three case of V_f^{loc}. In accordance with the observed effect in [39, 40], the magnitude of the compressive stress on the interface near the symmetry plane ($\theta_f = 0°$ in Fig. 8) increases with increasing V_f^{loc}. Comparing the ERR results in Fig. 4 and Fig. 7, we see that the presence of thermal stress reduces both ERR components, and that the reduction on Mode I component is more significant. That is due to the overall radial compressive stress field developed during thermal cool-down. This finding is similar to that in the single fiber composite case [21] where the authors found that thermal residual stress has a protective effect on debond growth. A closer look at Fig. 7 shows that there are local perturbations in G_{II} values in certain positions along the interface. These perturbations, although not significant (as G_{II} has passed the maximum), display the effect of the local micro-structure on the local stress field.

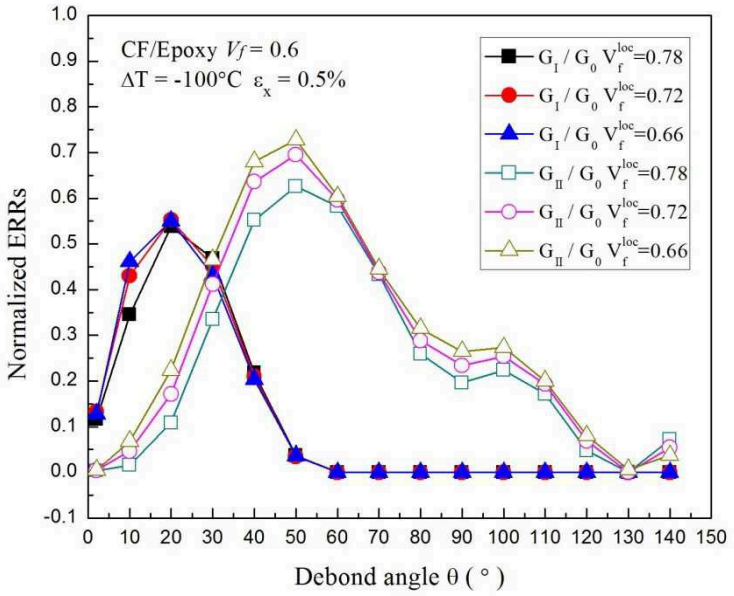

Fig.7. Normalized ERR with respect to debond angle for CF/EP UD composites under thermo-mechanical loading. V_f = 0.6 , ΔT=-100°C, ε_x=0.5%

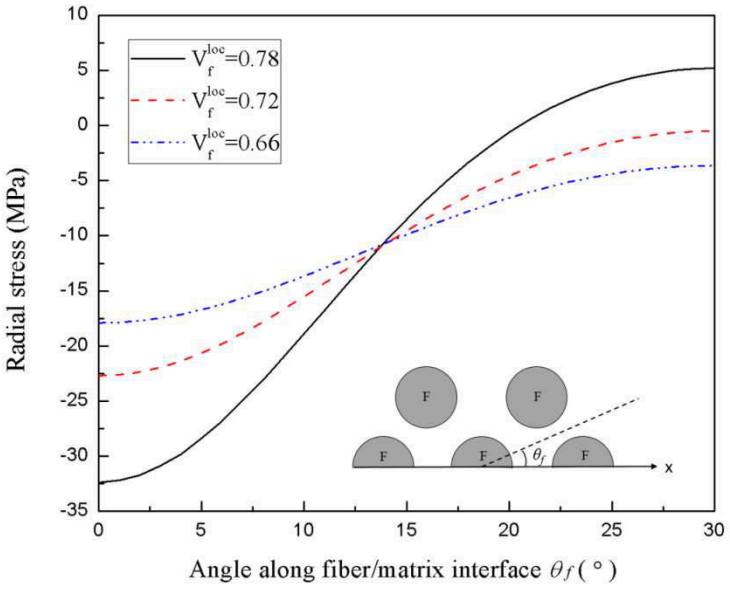

Fig. 8. Radial stress distribution along bonded fiber/matrix interface due to thermal cool-down, ΔT=-100°C.

3.1.2 Laminate constraint effect

The thermo-mechanical analysis described above was for a UD composite where on the macroscale the material is free to contract during the thermal cool-down. If the UD composite is within a multidirectional laminate, its contraction in a given direction will be different from its free contraction due to the mutual constraint induced by the differing thermal expansion coefficients of the layers in a laminate direction. The most extreme case of the constraint is for the 90^0 layer in a cross-ply laminate where the thermal expansion coefficient differs most from the adjacent 0^0 layer. In fact the value of the thermal expansion coefficient of the carbon/epoxy in the axial direction is very small (Table 1). Since the 0-layer in this direction is also very stiff, it will not allow the 90-layer to contract in this direction during the cool-down. Thus, as an approximation, $\varepsilon_x = 0$ (x is the 90^0 direction) for the cross-ply laminate on thermal cooldown. For the 90-layer in the laminate the strain induced by thermal cooldown is $\varepsilon_{x1} = -\varepsilon_{th}$, the negative of the free thermal contraction, i.e. a tensile strain. In addition to this strain we apply, as before, $\varepsilon_{mech} = 0.5\%$ to the laminate. This is the same as applying $\varepsilon_x = -\varepsilon_{th} + 0.5\%$ to the thermally contracted layer. For the considered composite at ΔT = -100°C we thus have $\varepsilon_x = 0.36\% + 0.5\% = 0.86\%$ and with this as the applied mechanical strain we calculate the ERR for a 90-layer within a cross-ply laminate.

Fig. 9 shows the obtained ERR for debond growth in 90° ply of a cross-ply laminate calculated with $\varepsilon_x = 0.86\%$. The trends in both Mode I and Mode II components with respect to the debond angle are the same as those for the UD composite under thermomechanical loading (Fig. 7) but the ERR values are higher. This suggests that the presence of mesoscale thermal stresses promotes the debond growth in transverse plies of a laminate. This effect might ultimately aid the formation of transverse cracks by coalescence of debonds and can be a likely explanation of transverse cracks seen on thermal cooldown, as reported e.g. in [41-44].

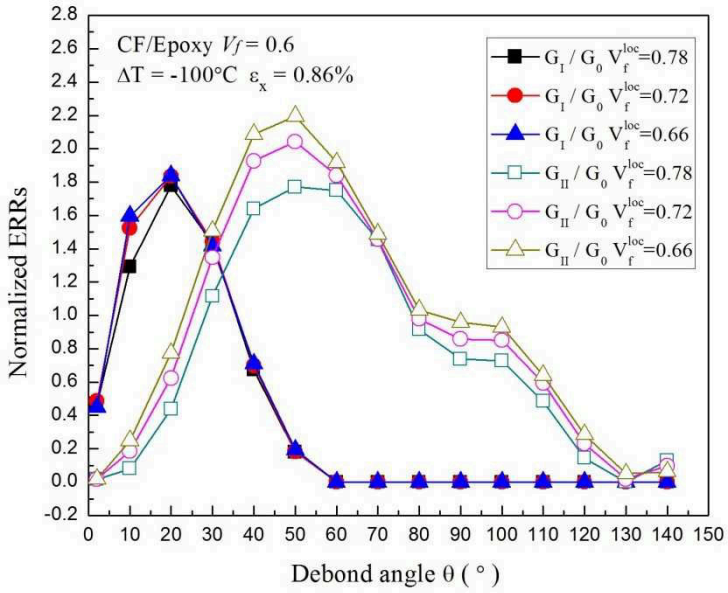

Fig. 9. Normalized ERR with respect to debond angle for CF/EP UD plies, equivalent to 90-layers of CF/EP cross-ply laminate under thermo-mechanical loading. V_f = 0.6, ΔT=-100°C, ε_x=0.86%

3.2 Carbon fiber/epoxy composite, V_f = 0.4

We now study the debond ERR for the same CF/EP composite as above, but with a lower fiber volume fraction, V_f = 0.4 in order to get some insight into the effect of the global fiber volume fraction. Figures 10 and 11 show the obtained ERR normalized with G_0 calculated using composite properties for this case (Table 1), for mechanical loading only (Fig. 10) and for thermo-mechanical loading (Fig. 11). It can be seen that

the trends for Mode I and Mode II component in this case are very similar to those for $V_f = 0.6$ case (Figs. 4 and 7). Comparing Fig. 4 and Fig. 10 we see that the normalized ERR components are very similar, which indicates that the debond stress field is indeed affected mostly by the local geometry. However, the G_0 is approximately 50% larger for $V_f = 0.6$, which means that the real values of ERR are also about 50% larger, which in turn means that the strain levels for debond growth in $V_f = 0.6$ are lower. When comparing the results in Figs. 10 and 11, it's found that the presence of the thermal stresses reduces ERR, and the effect is larger for $V_f = 0.4$ than for $V_f = 0.6$, as the UD composite contracts transversely more due to higher transverse thermal expansion coefficient at $V_f = 0.4$ than at $V_f = 0.6$.

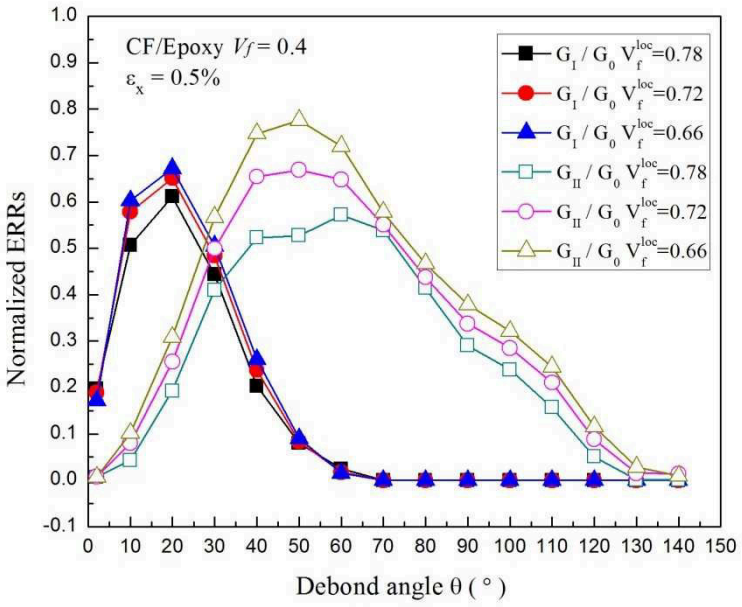

Fig.10. Normalized ERR with respect to debond angle for CF/EP UD composites under mechanical loading. $V_f = 0.4$, $\varepsilon_x = 0.5\%$

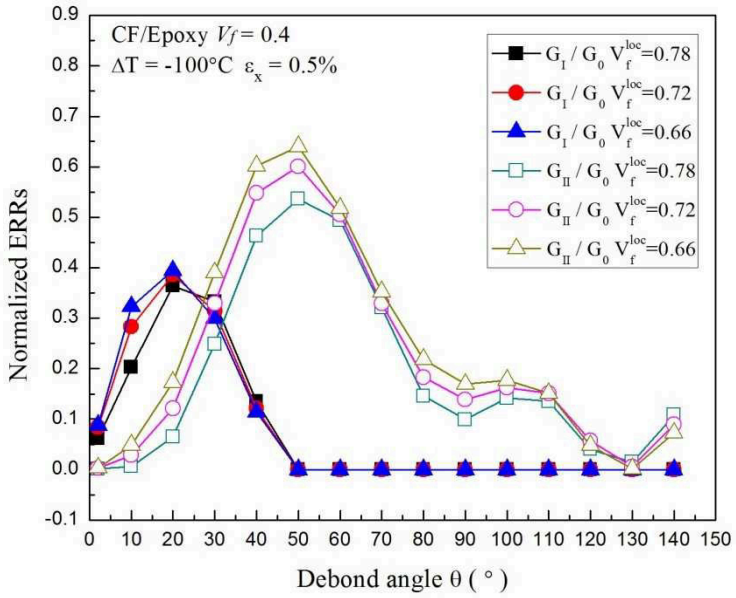

Fig. 11. Normalized ERR with respect to debond angle for CF/EP UD composites under thermo-mechanical loading for V_f = 0.4, ΔT=-100°C, ε_x=0.5%

3.3 Glass fiber/epoxy composite, V_f = 0.6

Finally, we study one case of UD glass fiber/epoxy composite (GF/EP) with V_f= 0.6 in order to understand the influence of the fiber stiffness. The results for the normalized ERR under pure mechanical loading are displayed in Fig. 12. Again, G_0 in this case is based on glass fiber composite properties listed in Table. 1. As shown in Fig. 12, the overall behavior of debond growth at each debond angle is similar to that in CF/EP discussed above. The transition angle $\theta_t \approx 60°$ in this case and is lower than that in CF/EP composite with the same V_f ($\theta_t \approx 70°$) but very close to that in a single-fiber composite (Fig. 3). The presence of thermal stress reduces the ERR and results also in a smaller transition angle for pure Mode II debond growth ($\theta_t \approx 50°$), as shown in Fig. 13.

In general, for applied mechanical loading, in all composite cases considered here the normalized ERR in Mode I is much larger than in a single fiber composite: the maximum normalized values of Mode I and Mode II ERR are approximately of the

same magnitude in composites whereas in the single-fiber case the normalized Mode I value is less than 30% of the Mode II maximum value (Fig.3).

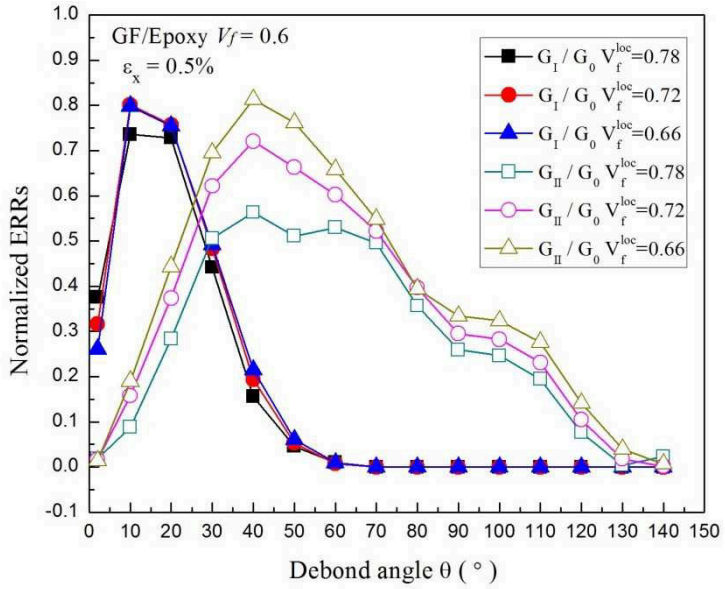

Fig.12. Normalized ERR with respect to debond angle for GF/EP UD composites under mechanical loading. V_f= 0.6, ε_x=0.5%

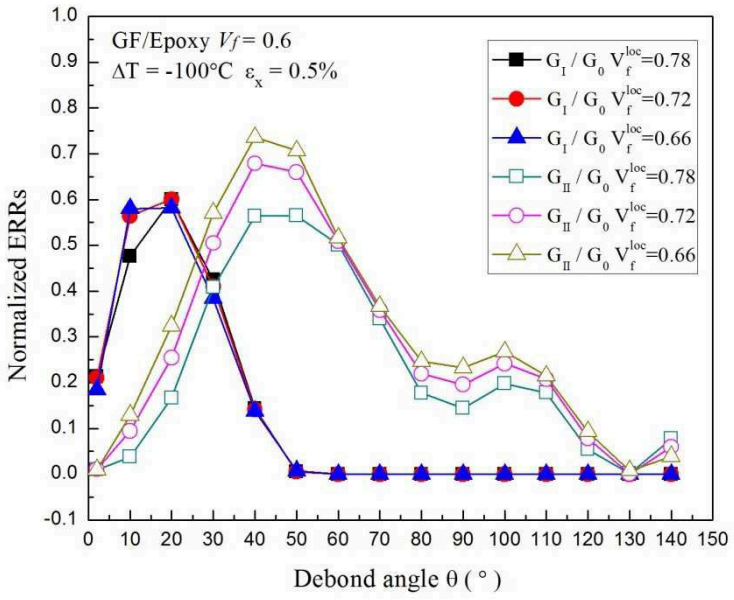

Fig.13. Normalized ERR with respect to debond angle for GF/EP UD composites under thermo-mechanical loading for V_f= 0.6, ΔT=-100°C, ε_x=0.5%

3.4 Transition angle θ_t for pure Mode II debond growth

Based on the results described above, at debond angles $\theta > \theta_t$, the crack faces in the crack tip region are in contact and Mode I ERR is zero. The debond growth then changes from mixed mode to pure Mode II. This transition angle is of interest in view of the finding in Paris et al [20] that in a single-fiber composite the debond crack is most likely to kink out of the interface into the matrix at an angle very close to this angle. As a result, for a single-fiber composite, smaller transition angle will likely result in an earlier kinking out of the debond crack. The kinking out process in a UD composite is likely more complex and will be fully investigated in a future study. Here we focus only on the transition angle and summarize our findings with respect to that in Table 2 and have the discussions below:

Table 2. Summary of transition angle θ_t for different cases

	Mechanical loading			Thermo-mechanical loading		
Composites	CF/EP (V_f=0.6)	CF/EP (V_f=0.4)	GF/EP (V_f=0.6)	CF/EP (V_f=0.6)	CF/EP (V_f=0.4)	GF/EP (V_f=0.6)
θ_t (°)	70	65	60	60	50	50

Under mechanical loading, the transition angle θ_t for the composites analyzed here is found to have the following values. a) For CF/EP composite, $\theta_t \approx 70°$ at V_f =0.6, and $\theta_t \approx 65°$ at V_f =0.4. Thus, in both cases θ_t is not sensitive to the local fiber volume fraction. b) For GF/EP composite, $\theta_t \approx 60°$ at V_f =0.6 , which is slightly lower than in CF/EP composite with the same V_f ($\approx 70°$), and is practically the same for a single-fiber composite. Therefore, we conclude that the transition angle is rather insensitive with respect to the constituent properties, the average fiber content V_f and the local fiber content V_f^{loc}.

In thermo-mechanical loading the transition angle is found to be smaller: $\approx 60°$ for $V_f = 0.6$; $\approx 50°$ for $V_f = 0.4$ for CF/EP composites and $\approx 50°$ for GF/EP composite with $V_f = 0.6$.

3.5 Applicability of the principle of linear superposition

In the previous sections we have shown that the presence of thermal stress leads to the reduction of ERR in a UD composite and the level of reduction depends on the applied temperature change (ΔT = -100°C in the current paper). Usually in linear elasticity the stress state in combined thermal and mechanical loading can be obtained as a superposition of the stress state in purely mechanical loading and the stress state from purely thermal loading. Theoretically speaking this principle is not applicable in the debond growth analysis performed in this paper. The reason is that the zone where the matrix and the fiber are in contact is different in the thermal, the mechanical and the mixed thermo-mechanical cases. This means that the interface conditions in these three cases are different, so they are three different types of elasticity problems and superposition is not possible. The implication of this situation is that for each new combination of the mechanical and thermal load (different temperature) new FEM calculations are required.

Since these calculations and data analysis are time consuming, a reasonable question arises: even if it is theoretically incorrect, how big is the error if we use the superposition?

Linear superposition would mean that for any combination of mechanical and thermal loads the ERR can be written

$$\frac{G_I}{G_0} = (C_1(\theta)\varepsilon_x + D_1(\theta)\Delta T)^2 \tag{3}$$

$$\frac{G_{II}}{G_0} = (C_2(\theta)\varepsilon_x + D_2(\theta)\Delta T)^2 \tag{4}$$

The $\theta -$ dependent C_1 and C_2 can be calculated from ERR data in purely mechanical loading

$$C_1(\theta) = \frac{1}{\varepsilon_x}\sqrt{\frac{G_I^{mech}(\theta)}{G_0}} \qquad C_2(\theta) = \frac{1}{\varepsilon_x}\sqrt{\frac{G_2^{mech}(\theta)}{G_0}} \tag{5}$$

To find $D_1(\theta)$ and $D_2(\theta)$ FEM calculations for one thermo-mechanical case are required (for example using the same ε_x as in the mechanical loading and selecting value ΔT_1). From (3) and (4) follows

$$D_1(\theta) = \frac{1}{\Delta T_1}\left[\sqrt{\frac{G_I^{th-mech}(\theta)}{G_0}} - C_1(\theta)\varepsilon_x\right] \quad D_2(\theta) = \frac{1}{\Delta T_1}\left[\sqrt{\frac{G_{II}^{th-mech}(\theta)}{G_0}} - C_2(\theta)\varepsilon_x\right] \quad (6)$$

As an example we consider CF/EP composite with $V_f = 0.6$ and local fiber content $V_f^{loc} = 0.72$. The two loading cases used to determine $C_i(\theta)$ and $D_i(\theta)$, $i = 1,2$ are: a) purely mechanical loading $\varepsilon_x = 0.5\%$; b) thermo-mechanical loading with $\varepsilon_x = 0.5\%$ after application of $\Delta T_1 = -150℃$. The ERR values for these cases are given in Table 3.

Table 3. ERR in thermo-mechanical loading at two different cool-down temperatures and in pure mechanical loading. (CF/EP composite with $V_f = 0.6$, $V_f^{loc} = 0.72$, $\varepsilon_x = 0.5\%$)

	ΔT_1=-150°C		Mechanical	
θ (°)	G_I / G_0	G_{II} / G_0	G_I / G_0	G_{II} / G_0
2	0.098	0.003	0.217	0.009
10	0.334	0.030	0.659	0.090
20	0.471	0.128	0.735	0.277
30	0.406	0.358	0.549	0.530
40	0.179	0.612	0.281	0.685
50	0.010	0.695	0.111	0.696
60	0.00	0.555	0.035	0.676
70	0.00	0.354	0.00	0.613
80	0.00	0.195	0.00	0.487
90	0.00	0.176	0.00	0.391
100	0.00	0.220	0.00	0.346
110	0.00	0.189	0.00	0.270
120	0.00	0.062	0.00	0.103
130	0.00	0.00	0.00	0.022
140	0.00	0.085	0.00	0.010

The obtained parameters were used in (3) and (4) to predict ERR for thermo-mechanical loading with $\varepsilon_x = 0.5\%$ and $\Delta T = -100℃$. The predictions and the FEM calculations for this case are shown in Fig 14.

Fig. 14 shows that the agreement is excellent, showing that even being theoretically inapplicable the principle of superposition can be used. It is not too surprising because results presented in this paper show that the transition angle for pure Mode II (onset of large contact zone) depending on the loading case is between 60° and 70°. In this debond size region we should expect problems applying the superposition whereas for much smaller or much larger debond angles the calculated ERR should be acceptable. We can see in Fig. 14 that even in the transition angle region the predictions are good but it is only because the values of G_I/G_0 are small (the error in % can be large).

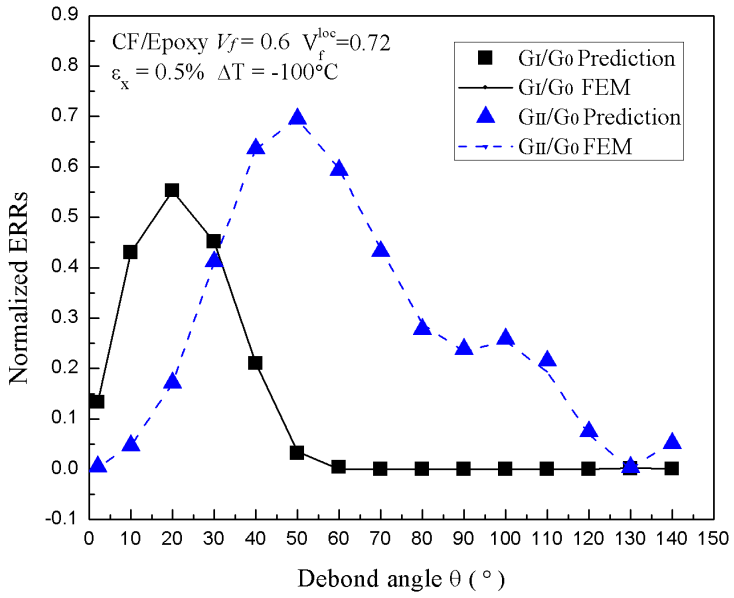

Fig. 14. Comparison of obtained ERR using linear supposition and FEM. $V_f = 0.6$, ΔT=-100°C, ε_x=0.5%, $V_f^{loc} = 0.72$

4. Conclusions

This study has examined the fiber clustering effects on fiber-matrix debond growth in UD composites subjected to transverse tension. To systematically study these effects, a hexagonal packing arrangement of fibers with a centrally placed debonded fiber was taken. The ERR of the debond crack was studied by varying the interfiber spacing of

the fibers (quantified by the local fiber volume fraction). The Mode I and Mode II components of the ERR were calculated by the VCCT for CF/EP and GF/EP composites at different global fiber volume fractions. From the findings of the study, the following conclusions are drawn.

(1). Both Mode I and Mode II components increase first with increasing debond angle and then decreases after reaching maximum at different debond angles. Debond growth is Mode I dominated at the early stage and switches to Mode II dominated growth until debond surfaces come into contact, at which point the growth is in pure Mode II.

(2). For all the cases considered in this paper, the presence of the neighboring fibers is found to increase the ERR when debond angle is small ($\theta < 5°$ in this paper), primarily due to the enhancement caused by the neighboring fiber aligned with the loading direction. However, at larger debond angles the ERR is lowered by the close presence of the neighboring fibers, indicating a protective effect with debond growth. This effect is similar to what was found in a two-fiber composite [26].

(3). Residual stress due to thermal cooldown has a protective effect on debond growth due to the local compressive stress. However, if the UD composite is placed as 90° plies within a multi-directional composite laminate, the same thermal cool-down will enhance the debond growth.

(4). Under transverse stress, the transition angle beyond which the debond growth becomes purely Mode II has been found to be relatively insensitive to the constituent properties (glass or carbon fibers, fiber volume fraction) and the local fiber volume fraction. The transition angle has been found to decrease by a few degrees when thermal cooldown of 100^0C is taken into account.

(5). The principle of linear superposition for thermal and mechanical loading, which theoretically does not apply to the debond problem, has been found to give accurate results for the ERR calculated here.

5. Ackownledgements

Linqi Zhuang would like to thank European DocMASE program for the financial support. Funding from the strategic innovation programme LIGHTer provided by VINNOVA (Sweden) is greatly acknowledged

References

[1] Aveston, J., and Kelly, A., 1973, "Theory of multiple fracture of fibrous composites," Journal of Materials Science, 8(3), pp. 352-362.
[2] Parvizi, A., and Bailey, J., 1978, "On multiple transverse cracking in glass fibre epoxy cross-ply laminates," Journal of Materials Science, 13(10), pp. 2131-2136.
[3] Bailey, J., Curtis, P., and Parvizi, A., "On the transverse cracking and longitudinal splitting behaviour of glass and carbon fibre reinforced epoxy cross ply laminates and the effect of Poisson and thermally generated strain," Proc. Proceedings of the Royal Society of London A: Mathematical, Physical and Engineering Sciences, The Royal Society, pp. 599-623.
[4] Hashin, Z., 1985, "Analysis of cracked laminates: a variational approach," Mechanics of materials, 4(2), pp. 121-136.
[5] Talreja, R., 1985, "Transverse cracking and stiffness reduction in composite laminates," Journal of composite materials, 19(4), p. 355.
[6] Nairn, J. A., 1989, "The strain energy release rate of composite microcracking: a variational approach," Journal of composite materials, 23(11), pp. 1106-1129.
[7] Berglund, L. A., Varna, J., and Yuan, J., 1992, "Transverse cracking and local delamination in [04/90n] s and [90n/04] s carbon fiber/toughened epoxy laminates," Journal of reinforced plastics and composites, 11(6), pp. 643-660.
[8] Varna, J., Berglund, L., Talreja, R., and Jakovics, A., 1993, "A study of the opening displacement of transverse cracks in cross-ply laminates," Int. J. Damage Mech., 2(3), p. 272.
[9] Bailey, J. E., and Parvizi, A., 1981, "On fibre debonding effects and the mechanism of transverse-ply failure in cross-ply laminates of glass fibre/thermoset composites," Journal of Materials Science, 16(3), pp. 649-659.
[10] Gamstedt, E., and Sjögren, B., 1999, "Micromechanisms in tension-compression fatigue of composite laminates containing transverse plies," Composites Science and Technology, 59(2), pp. 167-178.
[11] Asp, L. E., Berglund, L. A., and Gudmundson, P., 1995, "Effects of a composite-like stress state on the fracture of epoxies," Composites Science and Technology, 53(1), pp. 27-37.

[12] Asp, L., Berglund, L. A., and Talreja, R., 1996, "Prediction of matrix-initiated transverse failure in polymer composites," Composites Science and Technology, 56(9), pp. 1089-1097.
[13] Asp, L., Berglund, L. A., and Talreja, R., 1996, "A criterion for crack initiation in glassy polymers subjected to a composite-like stress state," Composites Science and Technology, 56(11), pp. 1291-1301.
[14] Toya, M., 1974, "A crack along the interface of a circular inclusion embedded in an infinite solid," Journal of the Mechanics and Physics of Solids, 22(5), pp. 325-348.
[15] París, F., Cano, J., and Varna, J., 1990, "The fiber-matrix interface crack—a numerical analysis using boundary elements," Int. J. Fract., 82(1), pp. 11-29.
[16] Varna, J., Berglund, L., and Ericson, M., 1997, "Transverse single-fibre test for interfacial debonding in composites: 2. Modelling," Composites Part A: Applied Science and Manufacturing, 28(4), pp. 317-326.
[17] Zhang, H., Ericson, M., Varna, J., and Berglund, L., 1997, "Transverse single-fibre test for interfacial debonding in composites: 1. Experimental observations," Composites Part A: Applied Science and Manufacturing, 28(4), pp. 309-315.
[18] Ageorges, C., Friedrich, K., Schüller, T., and Lauke, B., 1999, "Single-fibre Broutman test: fibre–matrix interface transverse debonding," Composites Part A: Applied Science and Manufacturing, 30(12), pp. 1423-1434.
[19] Martyniuk, K., Sørensen, B. F., Modregger, P., and Lauridsen, E. M., 2013, "3D in situ observations of glass fibre/matrix interfacial debonding," Composites Part A: Applied Science and Manufacturing, 55, pp. 63-73.
[20] París, F., Correa, E., and Mantič, V., 2007, "Kinking of transversal interface cracks between fiber and matrix," Journal of Applied Mechanics, 74(4), pp. 703-716.
[21] Correa, E., Mantič, V., and París, F., 2011, "Effect of thermal residual stresses on matrix failure under transverse tension at micromechanical level: A numerical and experimental analysis," Composites Science and Technology, 71(5), pp. 622-629.
[22] Carraro, P. A., and Quaresimin, M., 2014, "Modelling fibre–matrix debonding under biaxial loading," Composites Part A: Applied Science and Manufacturing, 61(0), pp. 33-42.
[23] Bouhala, L., Makradi, A., Belouettar, S., Kiefer-Kamal, H., and Fréres, P., 2013, "Modelling of failure in long fibres reinforced composites by X-FEM and cohesive zone model," Composites Part B: Engineering, 55, pp. 352-361.

[24] Távara, L., Mantič, V., Graciani, E., and París, F., 2016, "Modelling interfacial debonds in unidirectional fibre-reinforced composites under biaxial transverse loads," Composite Structures, 136, pp. 305-312.
[25] Kushch, V. I., Shmegera, S. V., Brøndsted, P., and Mishnaevsky Jr, L., 2011, "Numerical simulation of progressive debonding in fiber reinforced composite under transverse loading," International Journal of Engineering Science, 49(1), pp. 17-29.
[26] Sandino, C., Correa, E., and París, F., 2016, "Numerical analysis of the influence of a nearby fibre on the interface crack growth in composites under transverse tensile load," Engineering Fracture Mechanics, 168, Part B, pp. 58-75.
[27] Zhuang, L., and Pupurs, A., "Effect of neighboring fibers on energy release rate during fiber/matrix debond growth," Proc. 16th European Conference on Composite Materials, ECCM 2014.
[28] Zhuang, L., Pupurs, A., Varna, J., and Ayadi, Z., 2016, "Fiber/matrix debond growth from fiber break in unidirectional composite with local hexagonal fiber clustering," Composites Part B: Engineering, 101, pp. 124-131.
[29] Zhuang, L., Pupurs, A., Varna, J., and Ayadi, Z., 2016, "Effect of fiber clustering on debond growth energy release rate in UD composites with hexagonal packing," Engineering Fracture Mechanics, 161, pp. 76-88.
[30] 2016, "ANSYS Academic Research, Release 16.0,"Canonsburg, Pennsylvania.
[31] Hashin, Z., 1983, "Analysis of composite materials—a survey," Journal of Applied Mechanics, 50(3), pp. 481-505.
[32] Christensen, R., and Lo, K., 1979, "Solutions for effective shear properties in three phase sphere and cylinder models," Journal of the Mechanics and Physics of Solids, 27(4), pp. 315-330.
[33] Sun, C. T., and Jih, C. J., 1987, "On strain energy release rates for interfacial cracks in bi-material media," Engineering Fracture Mechanics, 28(1), pp. 13-20.
[34] Raju, I. S., Crews, J. H., and Aminpour, M. A., 1988, "Convergence of strain energy release rate components for Edge-Delaminated composite laminates," Engineering Fracture Mechanics, 30(3), pp. 383-396.
[35] Sun, C., and Manoharan, M., 1989, "Strain energy release rates of an interfacial crack between two orthotropic solids," Journal of Composite Materials, 23(5), pp. 460-478.

[36] Krueger, R., 2004, "Virtual crack closure technique: History, approach, and applications," Applied Mechanics Reviews, 57, p. 109.
[37] Wisnom, M., Gigliotti, M., Ersoy, N., Campbell, M., and Potter, K., 2006, "Mechanisms generating residual stresses and distortion during manufacture of polymer–matrix composite structures," Composites Part A: Applied Science and Manufacturing, 37(4), pp. 522-529.
[38] Pupurs, A., Goutianos, S., Brondsted, P., and Varna, J., 2013, "Interface debond crack growth in tension–tension cyclic loading of single fiber polymer composites," Composites Part A: Applied Science and Manufacturing, 44, pp. 86-94.
[39] Fiedler, B., Hojo, M., Ochiai, S., Schulte, K., and Ochi, M., 2001, "Finite-element modeling of initial matrix failure in CFRP under static transverse tensile load," Composites Science and Technology, 61(1), pp. 95-105.
[40] McLendon, W. R., and Whitcomb, J. D., 2016, "Influence of thermally induced microstress and microstructural randomness on transverse strength of unidirectional composites," Journal of Composite Materials, 50(11), pp. 1467-1481.
[41] Park, C. H., and McManus, H. L., 1996, "Thermally induced damage in composite laminates: Predictive methodology and experimental investigation," Composites Science and Technology, 56(10), pp. 1209-1219.
[42] Adams, D. S., Bowles, D. E., and Herakovich, C. T., 1986, "Thermally induced transverse cracking in graphite-epoxy cross-ply laminates," Journal of reinforced Plastics and composites, 5(3), pp. 152-169.
[43] Varna, J., Zrida, H., and Fernberg, P., "Microdamage analysis in thermally aged CF/polyimide laminates," Proc. IOP Conference Series: Materials Science and Engineering, IOP Publishing, p. 012050.
[44] Varna, J., Joffe, R., Akshantala, N. V., and Talreja, R., 1999, "Damage in composite laminates with off-axis plies," Composites Science and Technology, 59(14), pp. 2139-2147.

Paper E

Growth and interaction of debonds in local clusters of fibers in unidirectional composites during transverse loading

Growth and interaction of debonds in local clusters of fibers in unidirectional composites during transverse loading

Janis Varna [1, a], Linqi Zhuang[1,2,3,b], Andrejs Pupurs[1,c] and Zoubir Ayadi[3,d]

[1]Lulea University of Technology, SE 97187 Lulea, Sweden

[2]Texas A&M University, 77843-3141 College Station, USA

[3]Universite de Lorraine, 54010 Nancy, France

[a]Janis.Varna@LTU.SE, [b]Zhuanglinqi8808@tamu.edu, [c]Andrejs.Pupurs@LTU.SE, [d]Zoubir.Ayadi@univ-lorraine.fr

Keywords: Unidirectional composite, transverse failure, fiber/matrix debonding, energy release rate.

Abstract. Fiber/matrix debonding in transverse tensile loading of a unidirectional composite is analyzed calculating energy release rate (ERR) for interface crack propagation. Non-uniform fiber distribution (local hexagonal fiber clustering) is assumed in the model. The matrix region containing the central fiber with the debond and the 6 surrounding fibers is embedded in a large block of homogenized composite which has the same fiber content as the region analyzed explicitly. Some of the fibers surrounding the central fiber may also have a debond. The effect of the local clustering and of the presence of other debonds on magnification of the ERR is analyzed.

Introduction

A commonly accepted scenario analyzing initiation of transverse failure in unidirectional (UD) composites or in composite laminates containing 90° plies assumes that the macro crack is formed by coalescence of fiber/matrix debonds on the microscale, see [1, 2] as examples. Single fiber composite has been widely adopted to investigate the debond growth in the hoop direction using mostly numerical methods, see [3] for application of BEM. Recently, several studies have been performed to investigate the progressive debonding behavior of one fiber using numerical models containing multiple fibers [4,5]. However, limited progress has been made on understanding of the effects of the local micro-structure in composites on energy release rate (ERR), which is typically considered as the driving force for the debond growth. Sandino et al [5] investigated the influence of a nearby perfectly bonded fiber on debond

growth around the second fiber in a two fiber composite subjected to transverse loading. The bonded fiber was placed in different positions near the central fiber with debond and the effect of location parameters on the ERR was investigated. They found that the neighboring fiber has a protective effect on debond growth at all positions except at the location that is aligned to the loading direction. However, the two fiber composite model is still not an entirely adequate representation of a typical fiber clustering in unidirectional composite. The influence of neighboring perfectly bonded fibers on the debond growth around the central fiber in transverse loading of a UD composite was studied in [6]. A fiber with an initial debond, see Fig.1, was placed in the center of a UD composite with local hexagonal fiber packing. Only 6 fibers near to the central fiber with debond were modeled explicitly. The inter-fiber distance between the central fiber and the perfectly bonded neighbors was varied in order to account for local fiber clustering. The rest of the hexagonally packed UD composite was represented by a homogenized effective composite material with thermo-elastic properties calculated using micromechanics. It was found that the debond growth is Mode I dominated at early stage and then it switches to Mode II dominated growth until the debond surfaces come into contact and the further growth is in pure Mode II. It was shown tha the distance to the neighboring fibers does not affect the ERR significantly.

Composite model with debonded fibers.

The model shown in Fig. 1 was described in the Introduction. Due to symmetry, only the upper part of the composite is modeled. The debond arc length is represented by "debond angle" θ. In calculations the fiber radius r_f = 4 μm. The fiber content in the matrix area is equal to the fiber volume fraction, V_f in the effective composite. In the model $L = 20 \cdot RMO$ and $W = 40 \cdot RMO$. We will use the normalized inter-fiber distance $IDn = ID/r_f = 0.15; 0.25\ and\ 0.35$ to represent the local volume fraction V_f^{loc} (0.66, 0.72, 0.78). For the global V_f=0.6 used in this paper, $ID/r_f = 0.46$. Symmetry conditions are applied on the left side of the model and uniform displacement (0.5% strain) is applied at x=W. For relatively small debond angles, 2-D quadratic plane strain elements with pure Lagrange multipliers on normal and tangential contact were generated on the debond surface to model the contact behavior with minimal interpenetration. Penalty based contact elements were generated to ensure quicker

convergence for debonds with θ > 90°. The ERR is considered as the driving force for debond growth and it was calculated by the Virtual Crack Closure Technique (VCCT) using Finite Element (FE) software ANSYS. The size of the near tip element was $r_f \cdot d\theta$ where $d\theta = 0.4°$.

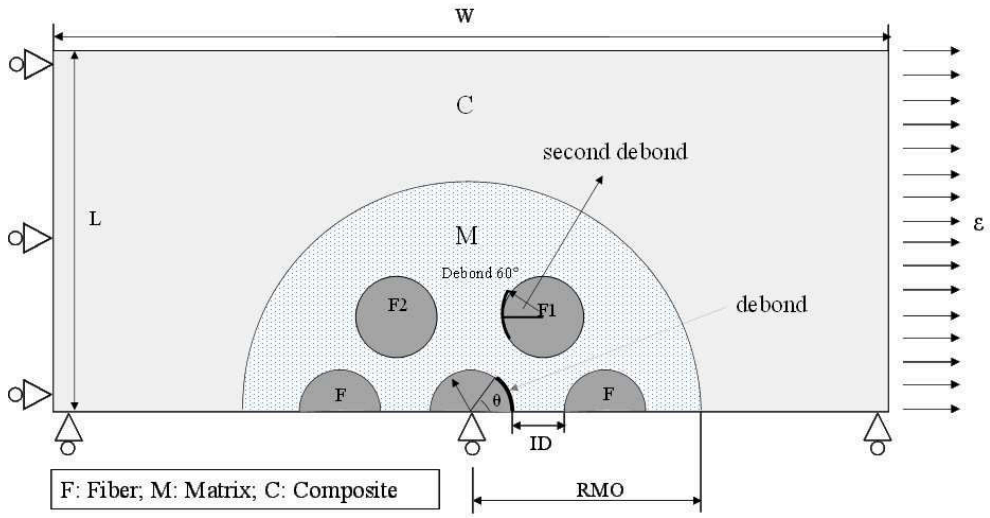

Figure 1. Schematics of the model used for debond growth analysis around the central fiber showing explicitly the central fiber and the 6 closest fibers. One of them may have a Semi-angle of 60° debond on one side. The fiber/matrix unit is embedded in a homogenized composite.

Results and analysis

Results are presented for carbon fiber/epoxy (CF/EP) composite with V_f=0.6. Thermo-elastic properties of materials are: for fiber E_{1f}=500 GPa, E_{2f}=30 GPa, υ_{12f} =0.2, G_{12f} =20 GPa, υ_{23f}=0.45; for matrix E_m=3.5 GPa, υ_m =0.4, G_m=1.25 GPa. Elastic constants of the homogenized composite are E1=301.4 GPa, E2=11.04 GPa, υ_{12} =0.27, G_{12} =4.06 GPa, υ_{23} =0.54 The elastic constants of the homogenized composite were calculated using the Hashin's Concentric Cylinder Assembly model [7] and the self-consistent scheme suggested by Christensen [8] (for the out-of-plane shear modulus).

Three cases of the composite with microdamage have been analyzed:

Case 1: The central fiber has a debond angle θ. Remaining fibers are perfectly bonded.

Case 2: The central fiber has a debond angle θ. Fiber F1 has Semi-angle of 60° debond on the left side.

Case 3: The central fiber has a debond angle θ. Fiber F2 has 60° debond on the right side.

The Case 1 is the same as analyzed in [6]. Results presented for Case 1 and Case 2 in Fig. 2 can be used to analyze the effect on ERR of the second 60° degrees debond on the left side of fiber F1. In Case 1, for small debond angles the G_I is larger than G_{II} , the G_I reaching maximum at about 20°. After that, G_I decreases and for large debonds (θ>60°) where the crack faces are in contact it turns to zero. The maximum value of G_{II}, which is similar to the G_I maximum value, is reached at about 60°. If thermal stresses are also included in the analysis ($\Delta T \approx -100℃$ due to cooling down to room temperature after manufacturing) the Mode I ERR is about 20% lower as an effect of compressive radial thermal stresses due to larger thermal expansion coefficient of the resin. The maximum value of G_{II} and its position remains almost unaffected by the temperature change. The main conclusion from Fig. 2 is that the presence of the F1 fiber debond significantly magnifies the ERR for debond propagation around the central fiber. For Mode I propagation in Case 2 there are even two local maxima: one has a similar location as for the Case1 when all the surrounding fibers are perfectly bonded. However, the G_I ERR is magnified more than two times comparing with Case 1. The second peak in G_I is for debond angle close 60°, where the line connecting the central fiber with F1 fiber goes directly through a) the debond crack tip of the central fiber and b) the middle of the F1 fiber debond (30°) which is open. The value of the second peak is lower than the value of the first peak but it becomes more significant with increase of IDn (higher local fiber content). It is expected that reducing the interfiber distance even more, this second local maximum would become the most important. It means that for a debond, created and growing in dominant Mode I, the growth which is unstable in the very beginning would slow down and an increasing load would be necessary for it to grow to 60° size when it becomes unstable again due to interaction with the F1 fiber which has 60° debond. The large value of G_{II} in this debond angle region would contribute to accelerated growth of the debond. The maximum value of G_{II} in Case 2 is almost five times higher than in Case 1and the maximum is shifted to larger debond angle (close to 70°). Looking in more details, one can notice an entirely different effect of the normalized interfiber distance, IDn on the ERR. In Case 1 the interfiber distance has a marginal effect with slightly lower ERR for cases with small IDn. More detailed analysis can be found in [6]. Due to the presence of the second debond in Case 2, the

trends are opposite: a) the ERR is much more sensitive to the IDn value; b) the ERR is significantly higher if the surrounding fibers (including the F1 fiber with Semi-angle of 60° debond) are close to the central fiber.

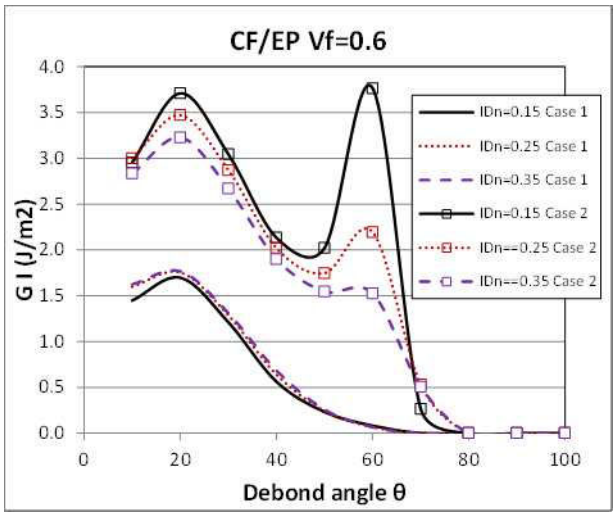

(a)

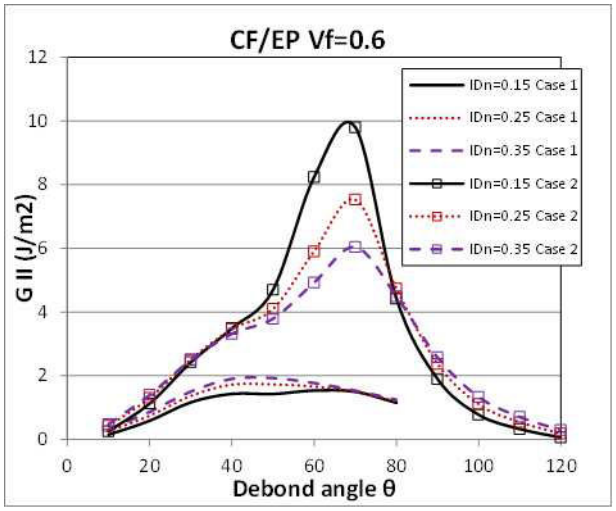

(b)

Figure 2. Energy release rate versus debond length and Case 1 and Case 2 for different values of interfiber distance: a) Mode I: b) Mode II.

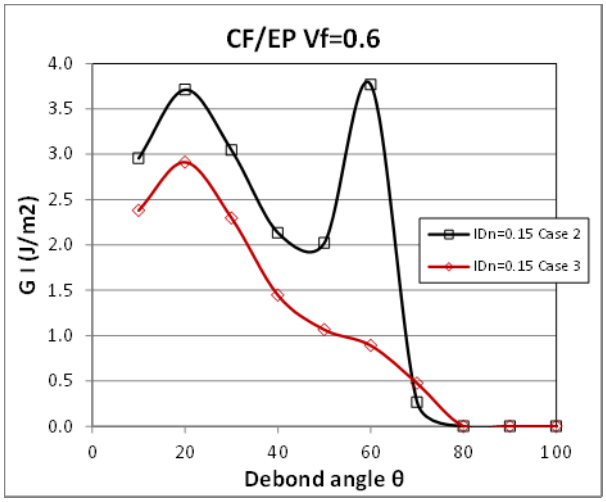

(a)

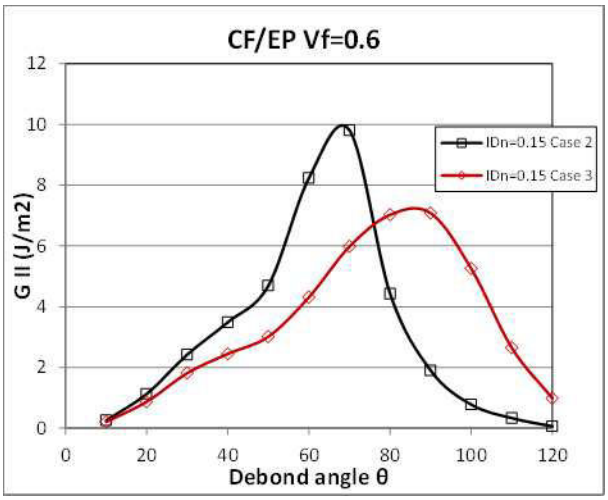

(b)

Figure 3. Energy release rate versus debond length and Case 2 and Case 3 for interfiber distance IDn=0.15: a) Mode I: b) Mode II.

In Fig.3 results for an alternative scenario for the location of the second debond are presented as Case 3: Instead of being on the left side of the F1 fiber the 60° debond is now on the right side of the fiber F2. Results show that in this case the effect of the second debond on the ERR magnification is significantly smaller than in Case 2 and there is no second peak for G_I. The maximum of G_{II} is shifted closer to 120°, which is the angle connecting the central fiber with the second debonded fiber F2

Summary

Energy release rate (ERR) calculations for debond growth around a central fiber in a hexagonal fiber cluster surrounded by homogenized composite show that the distance to surrounding fibers has a relatively small effect on the ERR if the surrounding fibers are perfectly bonded to the matrix. If one of the surrounding fibers also has a relatively large debond, the ERR for the central debond growth can be magnified two or more times and the dependence on the interfiber distance is strong. The magnitude and the shape of the ERR magnification due to the presence of a second debond depends on the position of the second debonded fiber.

References

[1] Bailey, J. E., and Parvizi, A., Journal of Materials Science, 16(3), (1981), p. 649-659.

[2] Gamstedt, E., and Sjögren, B., Composites Science and Technology, 59(2), (1999), p. 167-178.

[3] París, F., Cano, J., and Varna, J., Int. J. Fract., 82(1), (1990), p. 11-29.

[4] Távara, L., Mantič, V., Graciani, E., and París, F., Composite Structures, 136, (2016), p. 305-312.

[5] Sandino, C., Correa, E., and París, F., Engineering Fracture Mechanics, 168, Part B, (2016), p. 58-75.

[6] Zhuang L., A. Pupurs, J.Varna, R.Talreja, Z. Ayadi Submitted to Composites: Part A, (2017).

[7] Hashin, Z., Journal of Applied Mechanics, 50(3),(1983), p. 481-505.

[8] Christensen, R., and Lo, K., Journal of the Mechanics and Physics of Solids, 27(4), (1979), p. 315-330.

Summary

Effects of nonuniform fiber distribution on fiber/matrix interface crack propagation in polymeric composites

Keywords
Non-uniform fiber distribution, Composite, Crack propagation

In the presence thesis, the growth of fiber/matrix interface debond of a UD composite with hexagonal fiber packing under longitudinal and transverse tensile loading was investigated numerically, with the special focus on the influence of neighboring fibers on its growth. In the current study, energy release rate (ERR) is considered as the driving force for debond growth and was calculated based on J Integral and Virtual Crack Closure Technique (VCCT) using finite element software ANSYS. In the present thesis research, we started with investigating the influence of neighboring fibers on ERR of a debond emanating from a fiber break in longitudinal loading condition. In longitudinal loading case, debond growth is mode II dominated. As the starting point for the research, an axisymmetric model consisting 5 concentric cylinders that represent broken fiber with debond, surrounding matrix, neighboring fibers, surrounding matrix and effective composites was generated. It's found that there are two stages of debond growth, the first stage is when debond length is short, the ERR decreases with increasing debond angle, and the presence of neighboring significantly increase the ERR of debond. For relatively long debond, the debond is in a steady state growth region when ERR is almost constant regardless of debond length. In steady state of debond growth, the presence of neighboring fibers have little effect on the ERR. In the later research, a 3-D model was generated with broken fiber and its 6 nearest fibers in a hexagonal packed UD composite were modelled explicitly, surrounded by the homogenized composite. Based on the obtained results, it's shown that ERR is varying along debond front, and has its maximum at the circumferential location where the distance between two fiber center is the smallest. This indicates the debond front is not a circle. For steady state debond, the presence of fibers have little effect on ERR that averages along debond front. For short debond, the presence of fibers increases the averaged ERRS, and that the increase is more significant when inter-fiber distance are the smallest. When we conclude our investigation on fiber/matrix debonding under longitudinal loading, we began studying the growth of a fiber/matrix debond along fiber circumference under transverse loading. It's found that debond growth is mixed-mode, and both mode I and mode II ERR components increase with increasing debond angle and then decreases. Debond growth is mode I dominated for small debond angle and then switch to mode II dominated. The presence of neighboring fibers have an enhancement effect on debond growth up to certain small debond angle and then changes to a protective effect. Finally, the interaction between two arc-size debond under transverse loading is investigated. It's found that when two debonds are close to each other, the interaction between two debond becomes much stronger, and that interaction leads to the increase of ERR of each debond significantly, which facilitates further debond growth for both debond.

Les effets de la répartition nonuniforme des fibres sur la propagation des fissures á l'interface fibre/matrice dans les matériaux composites

mots clés
Distribution de fibres non uniforme, Composite, propagation d'une fissure

Dans ces travaux, nous avons étudié numériquement la croissance du décollement de l'interface fibre / matrice d' un composite UD avec garnissage hexagonale de fibre sous charge longitudinal et transversal. Nous avons mis l'accent en particulier sur l'influence des fibres voisines sur sa croissance. Dans la présente étude, le taux de libération d'énergie (ERR) est considéré comme la force motrice de la croissance du décollement et a été calculé sur la base de Integral J et de la technique de fermeture virtuelle de fissures (VCCT) à l'aide du logiciel de calcul par éléments finis ANSYS. Dans la présente recherche de thèse, nous avons étudier d'abord l'influence des fibres voisines sur ERR d'une décohésion émanant d'une rupture de fibre en condition de chargement longitudinal. Dans le cas du chargement longitudinal, la croissance du décollement est gouvernée par le mode II. Comme point de départ l'étude, nous avons mis place un modèle axisymétrique composé de 5 cylindres concentriques représentant la fibre endommagée, la matrice environnante, les fibres voisines, la matrice environnante et le composite effectif généré. On constate qu'il y a deux stades de croissance, la première étape correspond à une longueur courte du décollement, l'ERR diminue à mesure que l'angle du décollement augmente, et la présence de voisins augmente significativement la décohésion de l'ERR. Pour une décohésion relativement longue, le décollement se situ dans une région de croissance en état stationnaire lorsque l'ERR est pratiquement constant quelle que soit la longueur du décollement. A l'état stationnaire de la croissance du défaut, la présence de fibres voisines n'a que peu d'effet sur l'ERR. Les travails ultérieurs, nous avons mis en place un modèle 3-D (explicite) avec la fibre endommagée et ses 6 fibres les plus proches dans un composite UD compacté hexagonal, entourées par le composite homogénéisé. Sur la base des résultats obtenus, nous avons montré que l'ERR varie le long de la face frontale et a son maximum à l'endroit circonférentiel où la distance entre deux centres de fibre est la plus petite. Cela indique que le front du décollement n'est pas circulaire. Pour l'état stable du décollement, la présence de fibres a peu d'effet sur l'ERR qui progresse le long du front du décollement. Pour un décollement court, la présence de fibres augmente l'ERRS moyenné, et cette augmentation est plus significative lorsque la distance entre fibre est la plus petite. Après l'étude du la décollement fibre / matrice en charge longitudinale, nous avons commencé à étudier la croissance du décollement fibre / matrice le long de la circonférence de la fibre sous charge transversale. On constate que la croissance de la du décollement est en mode mixte, et les composants ERR du mode I et du mode II augmentent avec l'augmentation de l'angle de déformation puis diminuent. La croissance du décollement démarre principalement en mode I pour les petits angles de décollement et se poursuit en mode II. La présence de fibres voisines a un effet d'accroissement sur la croissance du décollement jusqu'à certains petits angles et change ensuite en effet protecteur. En fin, nous avons étudié l'interaction entre deux décollement sous chargement transversale. Nous avons constaté que lorsque deux décollements sont proches l'un de l'autre, l'interaction entre devient beaucoup plus forte et conduit à l'augmentation significative de l'ERR de chaque décollement, ce qui facilite la croissance du décollement.